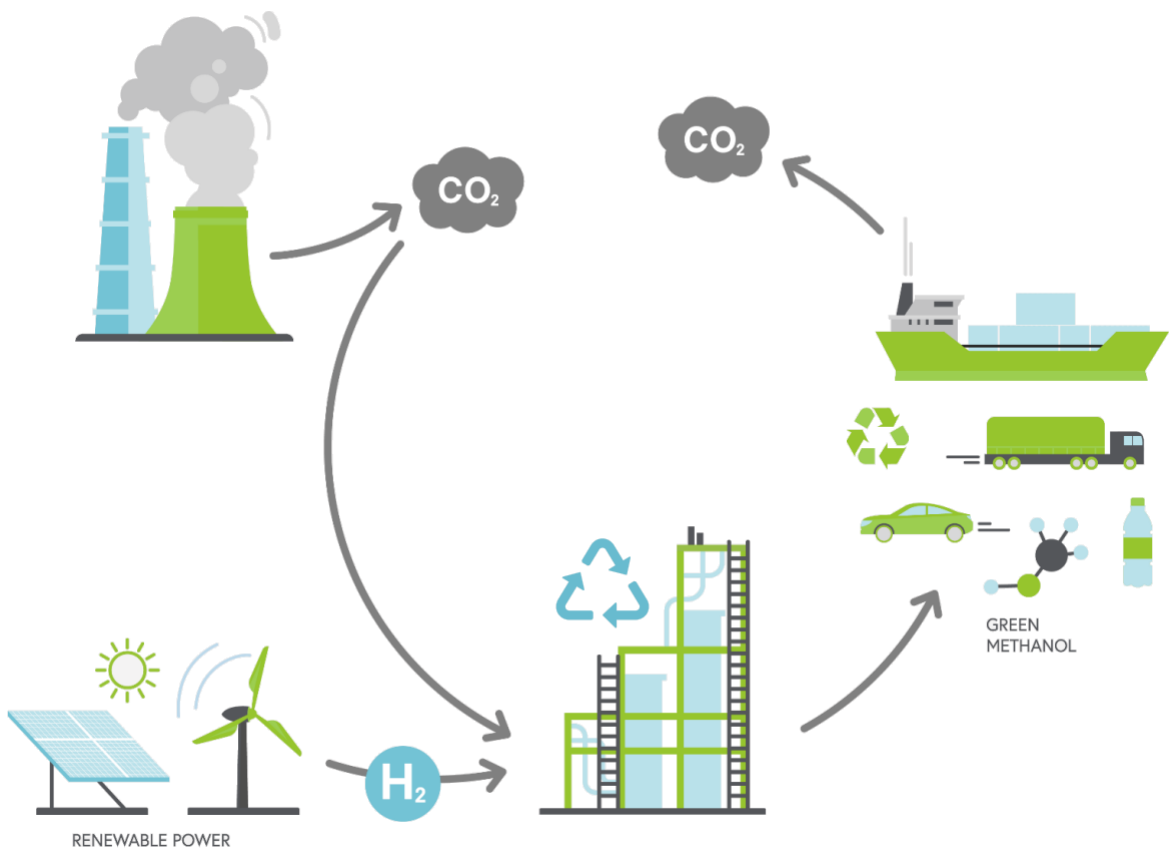


Methanol production from renewable sources

A techno-economic assessment



Ioannis Karountzos

METHANOL PRODUCTION FROM RENEWABLE SOURCES

A TECHNO-ECONOMIC ASSESSMENT

by

Ioannis Karountzos

Student number:	5149266
Project duration:	November 2020-December 2021
Faculty:	Electrical Engineering, Mathematics & Computer Science
Supervisors:	Dr. Ir. Laura Ramirez Elizondo EEMCS, TU Delft
Thesis committee:	Prof. Pavol Bauer EEMCS, TU Delft
	Dr. Ir. Laura Ramirez Elizondo EEMCS, TU Delft
	Dr. Hesam Ziar EEMCS, TU Delft

SUMMARY

The urgency of taking actions against climate crisis is unprecedented. The human-produced CO₂ is the largest contributor to global warming, which drives the climate change. Many countries around the world have committed to net-zero greenhouse gas emissions in the next coming decades. Power-to-X (PtX) technologies in combination with carbon capture technologies might contribute to a carbon-neutral future, since they can convert electricity and captured carbon to synthetic gases (e.g. hydrogen, methane), chemicals (e.g. propylene, ethylene) and liquids (e.g. methanol).

This thesis aims to research the techno-economic potential of a system that is able to produce methanol at industrial scale via a PtX scheme, which is coupled with carbon capture technologies. The system of this thesis consists mainly of PV panels, an alkaline water electrolyzer, a polymer electrolyte membrane (PEM) CO₂ electrolyzer and a single-stage Lurgi quasi-isothermal methanol reactor. The feedstocks for this system are water and carbon dioxide (captured from the flue gases of a cement plant).

The whole production process of this system has been designed and modelled in such a way, that both electrolyzers can follow the intermittent power supply from the PV panels. The electrolyzer's dynamic operation is controlled by a deterministic control logic, which takes into account the variable energy efficiencies of the electrolyzers and the intermittent power output of the PVs. Moreover, it has been decided that the methanol synthesis is based on the CO₂ hydrogenation process, which converts syngas (i.e. a mixture of CO, CO₂ and H₂) into methanol with the use of the methanol reactor. Hydrogen is produced by the water electrolyzer and the captured CO₂ is reduced to CO by the CO₂ electrolyzer.

As far as the sizing and production results are concerned, the system is able to produce 3.999 kT of methanol per year, consuming 2,147 tons of CO₂ per year and requiring an energy input of 30.3 GWh/year. The installed peak PV power is equal to 18 MWp and 99.60% of their energy yield is exploited by the system (the rest is dumped). Due to the implemented control logic, the operating energy efficiency range for the CO₂ electrolyzer is 45.07-55.32% and for the H₂O electrolyzer is 75.83-81.71%.

In terms of economic analysis, the proposed system requires a total capital investment (TCI) of 195.7 M€ and its operational expenditures are equal to almost 2 M€ per year. The performed cash flow analysis showed that the system has an annual gross profit of € 855,535 per year. Despite the yearly profit, it was found that the system's net present value (NPV) is negative and equal to -179.5 M€ at the end of its lifetime (i.e. 20 years). Also, the levelized cost of methanol (LCOM) was found to be equal to 4.44 €/kg, which is almost 10 times higher than the current market price of methanol. Therefore, such an investment would be economically unfeasible, despite its environmental benefit, because it would result in a net loss of capital.

CONTENTS

Summary	v
List of Figures	xi
List of Tables	xiii
1 Introduction	1
1.1 Motivation	1
1.2 Thesis scope and goals	5
1.3 Research questions	6
1.4 Research approach and methodology	7
1.5 Thesis outline	9
2 Literature Review	11
2.1 Alternatives to fossil fuels	11
2.1.1 Methanol	12
2.1.2 Methane	14
2.1.3 Ethylene	15
2.1.4 Conclusion.	16
2.2 Main technologies for methanol production using renewable energy	17
2.2.1 CO ₂ electrochemical reduction	18
2.2.2 CO ₂ hydrogenation	18
2.2.3 Methanol reactor.	19
2.3 H ₂ O electrolysis.	21
2.3.1 Alkaline Electrolysis (AEL)	22
2.3.2 Polymer Electrolyte Membrane Electrolysis (PEM)	23
2.3.3 Solid Oxide Electrolysis (SOEC)	24
2.3.4 Comparison	25
2.4 CO ₂ electrolysis	27
2.4.1 Solid Oxide Electrolysis (SOEC)	27
2.4.2 Molten Carbonated Electrolysis (MCEC)	29
2.4.3 Low-Temperature Electrolysis in H-cell Configuration	30
2.4.4 Low-Temperature Electrolysis with Gas Diffusion Electrode (GDE) as Cathode	31
2.4.5 Polymer Electrolyte Membrane	32
2.4.6 Conclusion.	34
2.5 Influence of rectifiers on electrolysis systems	35

3	System Design and Model	37
3.1	Product Specifications	37
3.2	Carbon Specifications and Effect of Impurities in the CO ₂ Feed	38
3.3	Plant Location	41
3.4	System Overview	41
3.5	Solar Energy	43
3.6	Control Logic	44
3.7	CO ₂ Electrolyzer	48
3.7.1	Design	49
3.7.2	Reactions	50
3.7.3	Operating Conditions	51
3.7.4	Performance Parameters	51
3.7.5	Structure Design	52
3.7.6	Model Implementation	53
3.8	H ₂ O Electrolyzer	54
3.8.1	Design	54
3.8.2	Reactions	55
3.8.3	Operating Conditions	55
3.8.4	Performance Parameters	56
3.8.5	Structure Design	57
3.8.6	Model Implementation	58
3.9	Auxiliary Equipment	59
3.9.1	Compressor	59
3.9.2	Cooling Units	61
3.9.3	Buffer Tanks	62
3.9.4	DC-DC Converter	63
3.9.5	Power Supply	64
3.10	Methanol Synthesis Process	65
3.11	Methanol Reactor	66
4	System Sizing and Production Results	71
4.1	Sizing Approach	71
4.2	Estimations of Energy Requirements and Production Output	72
4.3	PV Panels	76
4.4	DC-DC Converters	77
4.5	CO ₂ Electrolyzer	77
4.6	H ₂ O Electrolyzer	80
4.7	Methanol Reactor and Buffer Tanks	81
4.7.1	Activation Step of the Methanol Converter	83
4.8	Compressors	85
4.9	Cooling Units	86
4.10	Dump Energy	88
4.11	Summary	88

5	Economic Analysis	91
5.1	Equipment Prices Estimation	91
5.1.1	PV panels	91
5.1.2	DC-DC Converters	92
5.1.3	CO ₂ Electrolyzer	92
5.1.4	H ₂ O Electrolyzer	93
5.1.5	Methanol Reactor and Buffer Tanks	93
5.1.6	Compressors	94
5.1.7	Cooling Units	95
5.2	Sales, Dump Energy and Feedstock Prices Estimation.	95
5.3	Capital Expenditures Estimation	96
5.4	Operational Expenditures Estimation.	98
5.5	NPV Results	99
5.6	LCOM Results	103
5.7	Environmental Benefit	103
5.8	Summary	103
6	Conclusions and Recommendations	105
6.1	Conclusions.	105
6.2	Recommendations for future research	110
	Bibliography	113
A	Data on plant location	131
B	Methods used for the PVGIS calculations	133
C	MATLAB script	137
D	Simulink models	143
E	Reaction kinetics of the Lurgi quasi-isothermanl methanol reactor	153
F	Economic analysis	155

LIST OF FIGURES

1.1	Possible routes for Power-to-X and X-to-Power schemes [10]	3
1.2	System overview of Power-to-X scheme with carbon capture, storage and utilisation [10]	5
1.3	Methodology block diagram for the thesis development	7
2.1	Illustration of a combustion chamber, with methanol injection valve [19]	12
2.2	Overview of a PtG plant with a H ₂ O-electrolyzer and a methanation sub-system for converting H ₂ and CO ₂ into CH ₄ and H ₂ O [31]	15
2.3	Adiabatic methanol reactors and corresponding methanol yield vs. temperatures profiles (conversion profiles with red-blue sawtooth pattern and equilibrium profiles with black solid curve) [43]	20
2.4	Isothermal methanol reactor and corresponding methanol yield vs. temperature profile (conversion profile with red solid curve and equilibrium profile with black solid curve) [43]	21
2.5	Technologies for water electrolysis [16]	22
2.6	Technologies for carbon dioxide electrolysis [52]	28
2.7	Simplified structure of a gas diffusion electrode (GDE) [53]	31
2.8	Schematic diagram of a low-temperature electrolyzer with cathode GDE, catholyte, anolyte and ion-exchange membrane [53]	32
2.9	Schematic diagram of a polymer electrolyte membrane (PEM) flow cell for CO ₂ electrolysis [53]	33
3.1	Horizon and sun path in the selected plant location, according to Global Solar Atlas v2.4 [92]	41
3.2	Graphic design of the main system	42
3.3	Monthly solar irradiation for the selected plant location in 2016, from PVGIS [94]	44
3.4	Average daily irradiance per month for the selected plant location in 2016, from PVGIS [94]	45
3.5	Control logic of the system	46
3.6	Structure of the APE cell for CO ₂ electrolysis [96]	50
3.7	Experimental J-V curve, related to the cell performance of the APE CO ₂ electrolyzer, at an operating temperature of 60°C [96]	51
3.8	Experimental energy efficiency (EE) and Faradaic efficiencies of CO and H ₂ production (FE _{CO} and FE _{H₂} , respectively), related to the cell performance of the APE CO ₂ electrolyzer, at an operating temperature of 60°C [96]	52
3.9	Experimental I-V curve for the AEL water electrolyzer H ₂ IGen 300/1/25, in relation to pressure and for an operating temperature of 65°C [100]	56

3.10	Experimental J - V_{cell} curve for the AEL water electrolyzer of this project, for the operating conditions of 65°C and 10 bar	57
3.11	Specific energy consumption (left) and energy efficiency (right) for the AEL water electrolyzer, in relation to pressure and for an operating temperature of 65°C [100]	57
3.12	Experimental J -EE curve for the AEL water electrolyzer of this project, for the operating conditions of 65°C and 10 bar	58
3.13	Energy efficiency of the DC-DC converter with the switching technology of Infineon CoolMOS IPW60R045CP MOSFET in relation to input power, using a DAB topology with triangular modulation[116]	64
3.14	Typical syngas compositions for industrial applications along with the stoichiometric line [121]	66
3.15	Flow diagram of a single-stage Lurgi quasi-isothermal reactor [123]	68
4.1	Dynamic operation of the CO ₂ electrolyzer's stacks	79
4.2	Dynamic operation of the CO ₂ electrolyzer's stacks, in the interval 2000-2300	79
4.3	Dynamic operation of the H ₂ O electrolyzer's stacks (no limit in the amount of stacks with red and limit of 100 stacks with blue)	81
4.4	Percentage change of the H ₂ and CO buffer tanks capacities	83
4.5	Percentage change of the H ₂ and CO buffer tanks capacities, in the interval 2040-2140	84
5.1	Cost centers shares of TPEC per equipment type	98
5.2	Cost centers shares of TAMC per equipment type	101
5.3	Cumulative NPV over the project lifetime (20 years)	102
A.1	Plant location on Google Maps	131
A.2	Screenshot of the platform PVGIS	132
D.1	Model of APE CO ₂ electrolyzer in Simulink	144
D.2	Model of AEL H ₂ O electrolyzer in Simulink	145
D.3	Model of Compressor in Simulink	146
D.4	Model of Cooling Units in Simulink	147
D.5	Model of DC-DC Converter in Simulink	148
D.6	Model of Power Supply to Auxiliary Equipment in Simulink	148
D.7	Model of Control Logic in Simulink	149
D.8	Model of Control Logic for the CO ₂ electrolyzer in Simulink	150
D.9	Model of Control Logic for the H ₂ O electrolyzer in Simulink	151

LIST OF TABLES

2.1	Hazard statements for fuels and chemicals [21], [26], [27]	14
2.2	Comparison between different technologies for water electrolysis	26
3.1	Production specifications for methanol	38
3.2	Summary of metrics for CO ₂ capture technologies of interest	39
3.3	Specifications for carbon capture	40
3.4	Parameters for the download of hourly radiation data from PVGIS 5.1	44
3.5	Specifications of the APE CO ₂ electrolyzer	49
3.6	Specifications of the AEL water electrolyzer	55
3.7	Parameters values and descriptions for equations 3.22 and 3.23	60
3.8	Specifications of the buffer tanks	63
3.9	Main features of the methanol synthesis process	67
3.10	Specifications of the methanol reactor	69
4.1	Parameters of the system sizing approach	72
4.2	Estimated energy requirements and production output data for the whole system	76
4.3	Sizing data and production results of the PVs	77
4.4	Sizing data and production results of the CO ₂ electrolyzer	78
4.5	Sizing data and production results of the H ₂ O electrolyzer	81
4.6	Sizing data and production results of the methanol converter and the buffer tanks	84
4.7	Sizing data and production results of the compressors	86
4.8	Sizing data and production results of the cooling units	88
5.1	Cost data for the PVs	92
5.2	Cost data for the DC-DC converters	92
5.3	Cost data for the CO ₂ electrolyzer	93
5.4	Cost data for the H ₂ O electrolyzer	94
5.5	Cost data for the methanol reactor	94
5.6	Prices for revenues, dump energy and feedstock expenses	96
5.7	Worksheet for the total equipment cost of the project	97
5.8	List of direct and indirect costs for the estimation of fixed capital investment [141]	98
5.9	Worksheet for the total capital investment of the project	99
5.10	Worksheet for the operational expenditures of the project	100
5.11	Parameters for cash flow analysis	101

E.1	Parameters values and descriptions for equations E.1 and E.2 (obtained from [123])	154
F.1	MACRS depreciation scheme over 10 years [143]	155
F.2	Cash Flow Analysis	156

1

INTRODUCTION

This chapter provides the background information for the thesis project. The motivation behind this project is explained in section 1.1. The scope of this thesis and its goals are explained in section 1.2, while the research questions that have been formulated and need to be answered are presented in section 1.3. The adopted approach and methodology for tackling the main target of this project is presented in section 1.4. Finally, section 1.5 presents the outline and the structure of this thesis.

1.1. MOTIVATION

GLOBAL warming is one of the most important challenges that our world faces today. It affects our daily lives, from sea levels and weather conditions to business and the food we eat. Global warming is mainly caused by the human-driven increases in Earth's temperature [1], [2]. Human activities, which include burning of fossil fuels, cutting down forests and farming livestock, increase the Earth's temperature, because all these activities increase the heat-trapping greenhouse gas concentrations in Earth's atmosphere [1], [2]. Apart from human activities, the climate change is also caused by natural processes (e.g. volcanic activity and changes in the Sun's energy output) [1].

In 2019, the global average temperature increased by 1.1°C above the pre-industrial levels and it currently continues increasing by a rate of 0.2°C per decade [1], [2]. In 2016 the Paris Agreement on climate change came into force and 191 countries have currently ratified it [3], [4]. The goal of this agreement is the limitation of global warming, by preventing the global temperature from increasing more than 2°C (preferably 1.5°C) above the pre-industrial levels [3]. This target can be achieved by reducing (or making more efficient) the energy consumption, decarbonising the electricity generation and decarbonising the industrial & service sectors.

The most important heat-trapping greenhouse gases are carbon dioxide (CO₂), methane, nitrous oxide and fluorinated gases [2]. But, the human-produced CO₂ gas is the

largest contributor to global warming, since its concentration in the atmosphere increased by 48% in 2020, compared to pre-industrial levels [2]. The man-made CO₂ gas is emitted into the atmosphere due to the combustion of fossil fuels and the production processes of heavy industries (such as cement, iron, steel and aluminium plants). Therefore, the climate change could be mitigated by capturing, utilising and storing the emitted carbon.

According to the EU Climate & Energy Framework, the EU aims to reduce the greenhouse gas emissions by at least 40% in 2030 and by 80-95% in 2050, with 1990 as a reference year [5], [6]. In the EU Energy Roadmap 2050, different scenarios explore possible routes towards a low-carbon energy system, providing energy security, stability and certainty [6]. The achievement of these targets has the potential to lead Europe into a net-zero greenhouse gas economy. These targets could be reached, if the annual average reduction of CO₂ emissions was equal to 130 ton_{CO₂}/year from 2017 to 2050 [7]. However, the value of 130 ton_{CO₂}/year is an ambitious target, because the annual reduction of CO₂ emissions was equal to 50 ton_{CO₂}/year from 1990 to 2016 (4300 ton_{CO₂} in this year) [7].

Two of the main strategies of the EU Energy Roadmap 2050 are related to (i) the maximization of the renewables' deployment and of the electricity use and (ii) the decarbonisation of the power generation and industrial sectors towards a circular economy [6]. Based on the aforementioned scenarios from EU for 2050, the carbon capture and storage (CCS) technologies will have to be implemented in 7-32% of the power generation sector, which relies on the combustion of fossil fuels [6]. Apart from CCS technologies, carbon capture and utilisation (CCU) technologies will also have to be implemented in the power and industrial sectors of the EU, for reaching the targets of 2050 in a cost-effective way [6], [7]. Therefore the handling of CO₂ is going to be an important part of the EU strategies and play an important role for the energy transition in the EU.

CCU technologies

CCU processes are able to capture CO₂ and recycle it for further usage. Such processes convert the captured CO₂ into more valuable substances or products (i.e. C₁ or C_n molecules), through (i) the synthesis of chemicals and materials (e.g. methanol, carbonates, formic acid), (ii) the synthesis of fuels (e.g. methane, kerosene) and (iii) the direct use in applications based on CO₂ physico-chemical properties [8]. Another application of CCU processes is the storage of renewable energy, by using the surplus of electrical energy for the CO₂ conversion into an H₂ carrier (through the CO₂ reduction and H₂O splitting) [8].

CCU technologies have the potential to delay and reduce CO₂ emissions and to reduce fossil fuels depletion [8], [9]. In CCU processes, the captured CO₂ is first released by the use or combustion of CO₂-based product (e.g. oil). As it can be seen, CCU processes aim to retain carbon neutrality in the overall product chain. However, in terms of total CO₂ emissions reduction, the amount of captured and utilized CO₂ is not exactly the same as the amount of avoided CO₂ [9]. In case of a CCU plant, more CO₂ emitted is avoided (i.e. it is not emitted) than the CO₂ that is captured and utilized [8]. The

CCU plant reduces its original feedstock consumption (i.e. fossil fuels) and prevents the emissions associated to the use of this feedstock, because the plant synthesizes a specific product through the CCU processes [8]. Therefore, there might be financial incentives for heavy industries and power sector to invest in CCU technologies.

Power-to-X and X-to-Power technologies

Power-to-X (PtX) technologies allow the conversion of electricity into synthetic gases (e.g. hydrogen, methane), chemicals (e.g. propylene, ethylene) and liquids (e.g. methanol) [10]. In this way, the electricity can be stored in the form of chemical energy carriers, which can subsequently be exploited for time-shifted power delivery (i.e. the reverse scheme of PtX, known as X-to-Power [XtP] scheme) and/or cover the non-electrical energy demand in heating, transportation and industrial sectors [10]. In Figure 1.1, the possible routes of PtX and XtP schemes can be seen, in which the electricity can be supplied by the grid or the renewables.

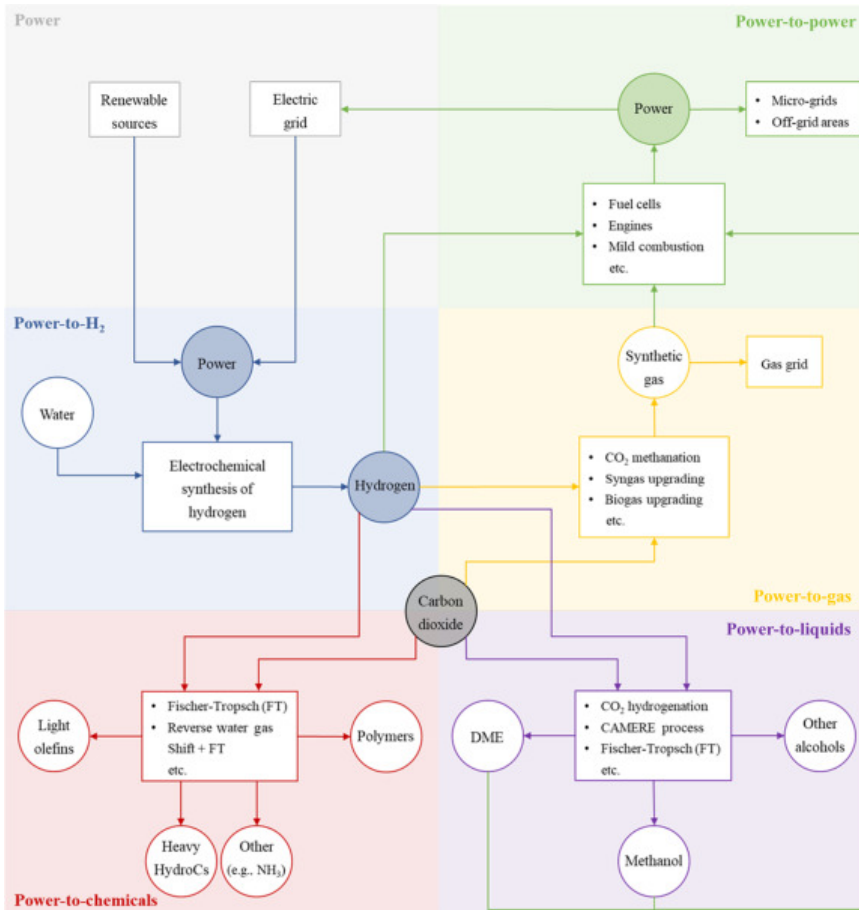


Figure 1.1: Possible routes for Power-to-X and X-to-Power schemes [10]

The exploitation of XtP schemes offers the potential for reconvertng the chemical energy carriers, which were synthesized through PtX schemes, back to electricity. This is how the energy is stored, before it is reconverted back to electricity. These schemes might provide a long-term alternative storage solution to batteries (not suitable for long-term storage) and pumped hydroelectric (topographically constrained) [10]. Applications of such PtX and XtP schemes include the use of methanol, methane (or synthetic gas) and hydrogen (see Figure 1.1).

The synthesized chemical energy carriers of the PtX schemes might be an exploitable feedstock for the heating, transport and industrial sectors [10]. The chemical energy demand of these sectors could be covered totally or partially by the aforementioned energy carriers (i.e. integrating into or replacing the existing feedstock of these sectors) [10]. This is how these sectors could reduce their environmental footprint. For example, light olefins (such as ethylene or propylene) could be produced via PtX processes with captured CO₂ and subsequently be supplied to the chemical industry as important raw materials. Another example could be the production of methanol in a similar way, providing a liquid fuel for transport sector.

System overview of Power-to-X scheme with CCU or/and CCS technologies

The production of chemical energy carriers via PtX schemes requires carbon (i.e. CO₂ or CO). Based on that, the integration of CCS and/or CCU technologies into PtX schemes is possible (see Figure 1.2). In the system overview of this Figure, it can be seen how these technologies can be integrated into PtX schemes and combined with renewables:

- The required electricity for the whole system's operation can be supplied from renewables.
- CO₂ can be captured from flue gases (or from the atmosphere with direct air capture technologies).
- Water and CO₂ can be reduced to H₂, O₂ and CO via electrolysis.
- The products of electrolysis can be used for the synthesis of the final products of PtX schemes (e.g. methane, methanol).
- Subsequently, the synthesized final products can be used for power generation or other applications (e.g. fuel for transport, feedstock to industry, heating).

Conclusion

The PtX schemes with CCS and/or CCU technologies may offer carbon-neutral alternatives to fossil fuels, only if these schemes are powered by renewables and the CO₂ is captured from flue gases. It is worth mentioning that if the CO₂ is captured from the atmosphere (with direct air capture technologies), then it would be possible to have a net-negative system [10], [11]. Moreover, these alternatives (e.g. methanol, methane) could use the existing infrastructure of fossil fuels for distribution and storage and be used by the existing machinery (without fundamental changes). As far as the long-term storage of renewable energy is concerned, these schemes seem very attractive, because captured CO₂ and the electricity surplus of renewables can be converted into chemical energy carriers (i.e. C₁ or C_n molecules). Therefore, these schemes (including CCS

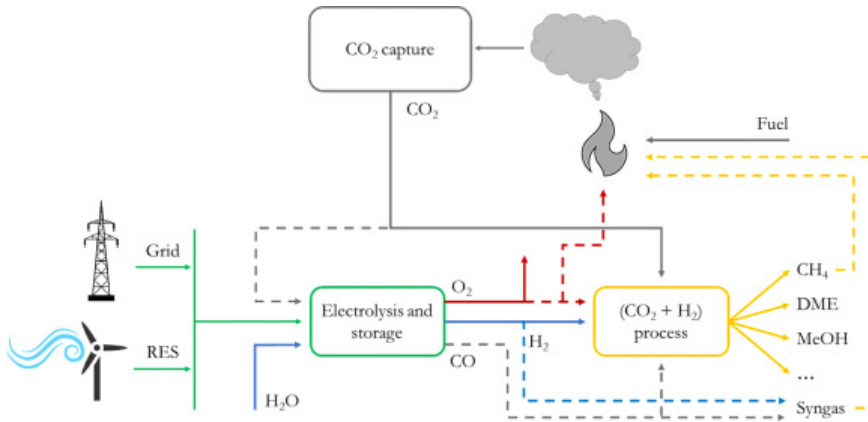


Figure 1.2: System overview of Power-to-X scheme with carbon capture, storage and utilisation [10]

and/or CCU) could be part of a circular economy, where carbon is recycled and reused over a long-time scale.

The potential of PtX schemes for the production of methanol is addressed and investigated in this thesis. Such PtX schemes are expected to enhance the resilience of our future (renewable) energy system and methanol could be a carbon-neutral alternative to fossil fuels.

1.2. THESIS SCOPE AND GOALS

THIS thesis aims to research the potential of methanol production via a PtX scheme, which will use H_2O and CO_2 as raw materials, be powered by solar panels and be coupled with CCU technologies. The production process of such a system will be analyzed and its techno-economic feasibility will also be evaluated in an industrial scale. Moreover, this thesis aims to draw realistic conclusions on the potential role of the aforementioned system in the decarbonisation and competitiveness of methanol production.

Recent papers have dealt with this topic, exploring and comparing different routes, in terms of electricity source, carbon source (captured from the atmosphere or from flue gases) and the use of CO_2 or CO in the methanol synthesis [8], [12]. In the paper of Smith et al. [12] in 2019, the electrolysis process was powered by solar panels and used for the water splitting and the reduction of CO_2 to CO . In the same paper, the following assumptions were also made [12]:

- The downstream synthesis of methanol was continuous and the operation of H_2O and CO_2 electrolyzers were independent of the intermittent power of solar panels.
- Both electrolyzers were running constantly at an overall efficiency of 70%.

In literature, it was also found that electrolyzers are assumed to work under constant-

efficiency conditions. However, this assumption is not valid for the case in which the power supply of the electrolyzers is intermittent and not constant. For this reason, in this thesis, the dynamic operation of electrolyzers is going to be taken into account. Therefore, this thesis will tackle the following knowledge gaps:

- The dynamic operation of H₂O and CO₂ electrolyzers in a load-following process, taking into account:
 - their variable energy efficiencies
 - their integration with the intermittent power supply from PV panels.
- The effect of this dynamic operation on the economic feasibility of the methanol synthesis process.

1.3. RESEARCH QUESTIONS

THE scope and the goals of this thesis can be tackled, by working on the main research question and its sub-questions, which can be expressed as follows:

- Main research question:

Is it economically feasible to produce methanol at a plant level, using the intermittent power output of PV panels, captured CO₂ from flue gases and dynamically operating electrolyzers under variable efficiency conditions?
- Sub-questions:

- *How can the whole process for methanol production be modelled and designed at industrial scale, when the system is connected to renewables?*

In such a system, PV panels, H₂O and CO₂ electrolyzers, methanol converter and utilities equipment are required. So, this equipment needs to be designed and modelled.

- *How can the intermittent power output of PV panels be integrated in such a production process?*

The grid can supply a constant power to the production system, which subsequently will be in constant operation. However, in case of PV panels, their power output is intermittent and the whole system will not be in constant operation.

- *What is the techno-economic performance of the intermittent production process and how can it be compared to the existing market of methanol?*

The intermittent production process needs to be assessed, in terms of capital and operational costs, production results and equipment size. This assessment is important for drawing the proper conclusions on the feasibility potential of the methanol production (as it was stated in the main research question).

1.4. RESEARCH APPROACH AND METHODOLOGY

THIS section gives an overview of the methodology and research approach, which have been conducted in this thesis for tackling the research questions of the previous section. Figure 1.3 shows the methodology steps that have been followed.

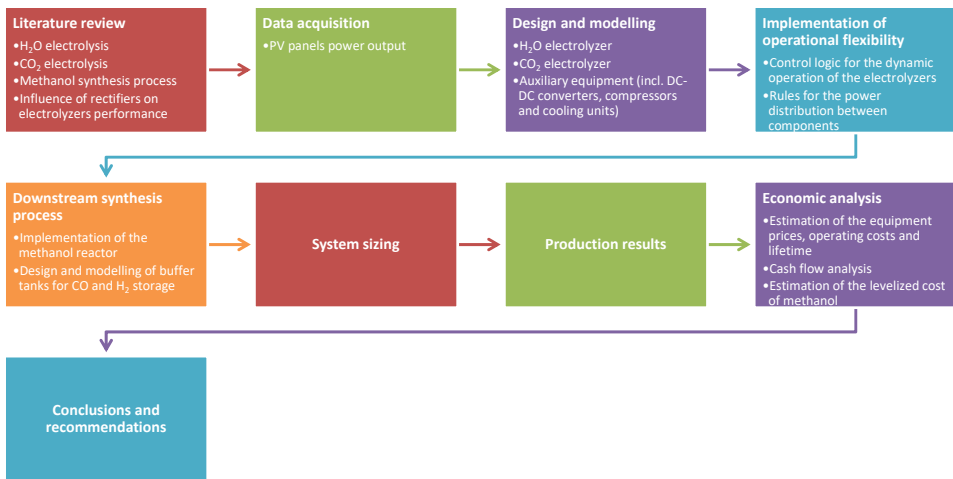


Figure 1.3: Methodology block diagram for the thesis development

The first step of the research approach is related to literature review, which has been carried out for the methanol synthesis process using renewable energy. Literature review has also been conducted for the various technologies of H₂O and CO₂ electrolysis, since such electrolyzers are parts of the aforementioned process. Taking into account the intermittent power output of PV panels, the influence of the rectifiers on the electrolyzers' performance had to be reviewed in literature, as well, because the electrolyzers will be in dynamic operation (i.e. under variable efficiency conditions).

Based on the findings of the literature review, it was decided that the methanol would be produced through the CO₂ hydrogenation process. Also, the required system's components were defined, according to the aforementioned synthesis process. Another prerequisite for the system design and modelling is the estimation of the PV panels' power output. That's why; the platform Photovoltaic Geographical Information System (PVGIS) 5.1 of the EU Science Hub has been used for the relevant data acquisition.

The system's H₂O and CO₂ electrolyzers have been designed and modelled by scaling

up the alkaline water electrolyzer H₂ IGen 300/1/25 and the cell of an alkaline polymer electrolyte membrane CO₂ electrolyzer, respectively. Both scaling-ups were based on the performance parameters of the aforementioned electrolyzers (found in literature) and built in MATLAB/Simulink. The system's DC-DC converter was also designed and modelled in MATLAB/Simulink, based on the performance characteristics of the Infineon CoolMOS IPW60R045CP MOSFET converter (found in literature). Compressors and cooling units had to be also designed and modelled in MATLAB/Simulink, since the H₂ and CO (i.e. electrolysis products) must be fed to the methanol converter at specific temperature and pressure.

As it has been mentioned, both types of electrolyzers will be in dynamic operation, since they will follow the intermittent power output of the PV panels. In other words, the electrolyzers operating efficiency will not be constant. Therefore, a system's control logic that controls the electrolyzers operation (inside their efficiency range) had to be designed and modelled in MATLAB/Simulink. This control logic is a deterministic method (based on a set of rules) and responsible for the system's operational flexibility. The power distribution between the system's components is also controlled by the same control logic.

The last step of the system's design and modelling in MATLAB/Simulink is related to the methanol converter. The design and model of the methanol reactor is based on the simulation results of a study that has been based on the selected methanol synthesis process (i.e. using the same converter's catalysts and feeding gases' compositions). Contrary to electrolyzers, it has been decided that the methanol converter will operate constantly and continuously, without following the intermittent power output of the PV panels. That's why; buffer tanks for the H₂ and CO storage had to be designed and modelled in MATLAB/Simulink. These buffer tanks will ensure the continuous and constant operation of the methanol converter.

As soon as the system has been designed and modelled, it was sized by doing an empirical analysis of the various system parameters and not by using an optimisation tool. A backward approach was followed for the system sizing. Various simulations were conducted in Simulink and many sizing calculations were done in Excel (according to the simulation results). In this way, the system parameters (such as the power split between the H₂O and CO₂ electrolyzers, the buffer tanks capacity, the feeding rates of H₂ and CO, etc.) were empirically analysed and tested, so that a system equilibrium could be reached. The system's equilibrium was defined as the minimization of the system size and the maximization of the system efficiency, by producing the desired amount of methanol.

Subsequently, the model simulation was run in Simulink and its final results were acquired. Those results were used for the assessment of the economic potential and the environmental benefit of the proposed system. Therefore, the system's equipment prices, operating costs and lifetime were estimated, based on the relevant sizing data and literature review. The system's economic potential was assessed, according to a cash

flow analysis (i.e. determining the end-of-life net present value, NPV, of the system) and the levelized cost of methanol.

Finally, conclusions have been drawn, according to the production and economic results of the proposed system. Also, recommendations for future research work could be made based on the findings of this thesis.

1.5. THESIS OUTLINE

THE previous sections have already mentioned the potential of PtX schemes for the production of methanol, which could be a carbon-neutral alternative to fossil fuels. More specifically, this thesis aims to investigate the technical and economical potential of such a system, which mainly consists of PV panels, H₂O and CO₂ electrolyzers and is in dynamic operation. This scope can be tackled by forming and working on research questions, which have been presented and further explained. This section presents the thesis outline, which can be provided as follows:

- **Chapter 2** presents the literature review for the system of this thesis. First, the use of methanol is described and compared to alternative fuels (e.g. methane). Then, various technologies for the methanol production using renewable energy have been reviewed and presented. In the next two sections of this chapter, the various technologies for H₂O and CO₂ electrolysis are discussed. The last section presents the influence of rectifiers on the electrolyzers' performance (operating in dynamic operation).
- **Chapter 3** refers to the design and modelling of this thesis system. First, the product (i.e. methanol) and captured CO₂ (from flue gases) specifications are given. Then, the plant location and the system's configuration are presented. Next, the data acquisition method for the PV panels' power output is described. The design and modelling of CO₂ and H₂O electrolyzers are described in this chapter. The system's control logic that controls the dynamic operation of the electrolyzers is included in this chapter, as well. Finally, the design and modelling of the auxiliary equipment and the selected downstream synthesis process of methanol (including the methanol reactor) are described.
- **Chapter 4** provides the sizing approach, sizing data and production results of the proposed system. The sizing approach is described in the first section of this chapter. Then, the system's energy requirements are initially estimated, according to the desired production output of each equipment. Next, the PV panels were sized, according to the initial energy requirements. Finally, using the aforementioned parameters, the sizing data and production results of each equipment are estimated and presented.
- **Chapter 5** is dedicated to the assessment of the economic potential and the environmental benefit of the proposed system. This chapter describes the estimation method for the equipment prices, operating costs and lifetime. Also, it includes

the market prices of methanol and feedstocks. Then, the capital and operational expenditures are estimated and presented, based on the aforementioned prices. Finally, the system's environmental benefit is presented and its economic potential is assessed, according to a cash flow analysis (i.e. determining the end-of-life net present value, NPV, of the system) and the levelized cost of methanol.

- **Chapter 6** includes the conclusions and recommendations for this thesis. The research questions are answered, based on the results of the proposed system, and recommendations for future research work are provided.

2

LITERATURE REVIEW

The use of fossil fuels is extremely important in our modern world, since it affects the transportation of people and goods. Unfortunately, fossil fuels contribute to global warming, environmental pollution and problems with air quality. Pollutant and carbon emissions can be decreased by consuming alternative fuels instead of fossil fuels. However, the use of alternative fuels is not totally feasible, due to their limited availability, high cost and limited energy density.

The literature review for the methanol use and production is presented in this chapter. The use of methanol is compared to alternative fuels (such as methane and ethylene) in section 2.1. In section 2.2, various technologies for methanol production using renewable energy are presented. The H₂O and CO₂ electrolyzers are discussed in sections 2.3 and 2.4 respectively. In the last section, the influence of rectifiers on the performance of electrolyzers, which are in dynamic operation, is reviewed.

2.1. ALTERNATIVES TO FOSSIL FUELS

SOLAR energy is a renewable alternative to fossil fuels, despite the fact that it is characterised by fluctuations. These fluctuations can be overcome by energy storage systems that store surplus energy in many ways (e.g. in batteries, compressed air, molten salt, synthetic fuels etc.) and make it available at a later time as needed. Synthetic fuels might be an ideal solution for long-term energy storage and for the carbon-neutral heating, industrial and transportation sector. The generated electricity of the solar panels can be converted to:

- hydrogen or methane (using power-to-gas technologies),
- liquids like methanol (using power-to-liquid technologies)
- or chemicals like ammonia, propylene or ethylene (using power-to-chemicals technologies).

Using carbon utilization technologies, CO₂ can be electrochemically reduced to many products (such as CO). By combining CO₂ or its products with H₂, the production of chemicals, fuels and other materials (such as methanol, methane, ethylene etc.) is possible.

2.1.1. METHANOL

Methanol (CH₃OH) can be synthesized from syngas (i.e. synthesis gas) that is produced from biomass and fossil fuels (natural gas leads to a cheaper methanol production compared to coal) [13], [14]. Also, syngas can be produced from renewable energy sources in schemes, which capture and utilize carbon and thus the methanol production from renewables is possible [13], [14]. The renewable electricity is used to power the CO₂-electrolyzers for the reduction of CO₂ to CO and the H₂O-electrolyzers for the reduction of water to H₂ and O₂. Methanol can also be formed from CO₂ via heterogeneous catalysis, homogeneous catalysis, electrochemical reduction and hydrogenation [15], [16].

The world's first CO₂-to-methanol plant is the George Olah plant, located in Svartengi, Iceland [17]. This plant is operational since 2012 and its production capacity is 4000 tons of methanol per year, utilizing 5500 tons of CO₂ per year [17]. The carbon dioxide is captured from the flue gas that is released by an adjacent geothermal power plant [17]. The hydrogen is generated by water electrolysis (using electricity from renewable sources) and reacts with CO₂ for forming methanol [17], [18]. According to SGS Germany (an inspection and certification company), this plant has received an ISCC certificate, because its methanol production process can reduce CO₂ emissions by 90% when compared to the use of gasoline or diesel [17].

Currently, methanol is a widely traded chemical in the world, because it can be used as a transport fuel or a feedstock for many industrial processes. As far as its use as a fuel is concerned, methanol can be used as a blend component or in pure form, in internal combustion engines (ICEs) or in direct methanol fuel cells (DMFCs) [20]. It is worth mentioning that 40% of the total 80 million metric tons of methanol (global sales in 2018) was used as fuel and energy source [21]. Apart from the aforementioned methanol uses, methanol is the largest chemical feedstock for the plastics industry, mainly via methanol-to-olefin (MTO) processes [20], [22]. Methanol fuel is an attractive alternative to fossil fuels, because it can also be used as an energy carrier for storing and distributing energy, due to its liquid state at ambient temperature and pressure and its high specific energy.



Figure 2.1: Illustration of a combustion chamber, with methanol injection valve [19]

Methanol could extensively be used in marine industry as a blend component, by being directly injected in the combustion chamber of the vessels' ICEs (see Figure 2.1). The marine sector has shown a great interest in methanol as an alternative fuel, due to the tightening emissions legislation [23]. As far as the automotive industry is concerned, methanol is commercially blended into gasoline at various locations around the world, since 1980 [24]. The mixture of methanol and gasoline provides a cleaner fuel when it is burnt (i.e. lower vehicle exhaust emissions) [24]. For example, in China, the methanol consumption in fuel products was approximately 250 thousand barrels per day in 2010, but it was more than 500 thousand barrels per day in 2016 [24]. Another example is India and Israel, which allowed the use of methanol M15 as a blend component in 2019 and 2016 respectively [24]. As it can be seen, there is currently a growing interest in methanol as an alternative fuel worldwide.

The following is a list with a few attributes of methanol, when it is consumed in fuel products by ICEs:

- High specific energy ratio (e.g. methanol M85 has a specific energy density of 19.7 MJ/kg and 15.6 MJ/l)
- High flame speed, leading to higher ICE efficiency
- Low combustion temperature, leading to better fuel vaporisation
- Being liquid at ambient temperature and pressure
- High hydrogen-to-carbon ratio, leading to lower carbon intensity fuel
- High octane and oxygen content (e.g. methanol M85 has 112 octane), leading to improved fuel combustion and smoother fuel burning [20], [21], [24], [25].

Despite the interesting and beneficial characteristics of methanol, there are concerns about its toxicity and safety. The major issue that methanol has to face is its toxicity in terms of ingestion, inhalation, skin or eye contact. Although methanol is dangerous and toxic, this is true for all fuels such as gasoline and diesel substitutes [20]. According to Methanol Institute, the following health and physical hazards have been defined for methanol in Table 2.1.

With regard to fire safety, another significant hazard is that methanol flames are practically invisible in sunlight [20]. This issue could be addressed by the use of additives or methanol-gasoline blends [20]. On the other hand, the advantage of pure methanol is that its fires can be extinguished with water [20]. Methanol also outperforms gasoline in terms of fire risk and safety, because methanol evaporates more slowly, has a lower vapor density and a lower heat release rate than gasoline [21], [22].

In case of spills, methanol has a lower environmental impact than gasoline. According to the European Chemicals Agency (ECHA), the registered dossiers for methanol, diesel, and gasoline report the lethal LC50 dose in water (i.e. the concentration in water, at which half the population died within specified test duration) to be 15400 mg/l, 65 mg/l and 8.2 mg/l, respectively [21], [22]. Another interesting property of methanol is its

Table 2.1: Hazard statements for fuels and chemicals [21], [26], [27]

Methanol	Methane	Ethylene
H225: Highly flammable liquid and vapour	H220: Extremely flammable gas	H220: Extremely flammable gas
H301: Toxic if swallowed	H280: Contains gas under pressure; may explode if heated	H280: Contains gas under pressure; may explode if heated
H311: Toxic in contact with skin	-	H336: May cause drowsiness or dizziness
H331: Toxic if inhaled	-	-
H370: Causes damage to organs	-	-

rapid biodegradation (a few days), since any spill of methanol quickly disperses due to its infinite solubility in water and then biodegrades simply [20]. This fact could be very interesting to the marine sector, taking into account the consequences of a hydrocarbon fuel spillage in the marine environment.

2.1.2. METHANE

Methane (CH_4) can be produced from biomass by either thermal gasification or biological gasification [28]. The latter process is a low-temperature process ($<70\text{ }^\circ\text{C}$) that converts wet or dry feeds and is commonly referred to as anaerobic digestion [28], [29]. According to Sabatier reaction, methane can be also produced by combining CO and H_2 (CO methanation process) or CO_2 and H_2 (CO_2 methanation process) at high pressure and temperatures above $250\text{ }^\circ\text{C}$ [29]. Both catalytic processes are basically exothermic, whose educts are CO/ CO_2 and H_2 and their products are CH_4 and H_2O [29].

The electricity from renewables could be used to power the CO_2 -electrolyzers for the reduction of CO_2 to CO and the H_2O -electrolyzers for splitting the water into H_2 and O_2 . Renewable sources and the aforementioned electrolyzers constitute a Power-to-Gas (PtG) plant for producing synthetic natural gas (SNG), i.e. methane. An overview of a PtG plant can be seen in Figure 2.2, where the SNG can be fed into the natural gas network or used for other final processes. Most of the worldwide existing PtG plants were launched from 2009 onwards and the Audi e-gas plant in Werlte (Germany) is the largest PtG plant in the world (6 MW_e) [30]. The Audi e-gas plant is in operation since 2013 and it produces carbon-neutral SNG via the catalytic methanation of H_2 and CO_2 [30].

Methane is a chemical compound and the main constituent of natural gas, which is used nowadays in many industrial chemical processes, power plants and homes (for cooking and heating) [32]. Due to the existing massive distribution infrastructure of natural gas in many countries worldwide, this gas (and consequently methane) affects significantly their economies, being an important energy carrier to the industry, energy and transportation sector. In comparison with H_2 , SNG (predominantly CH_4) faces less re-

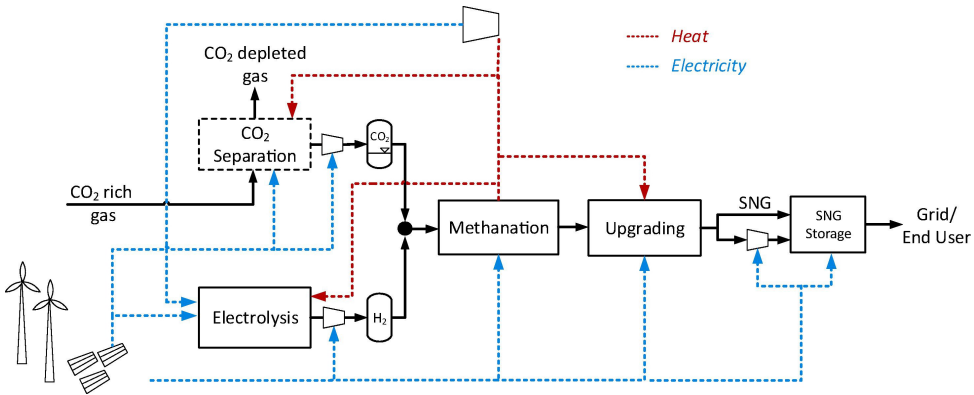


Figure 2.2: Overview of a PtG plant with a H₂O-electrolyzer and a methanation sub-system for converting H₂ and CO₂ into CH₄ and H₂O [31]

restrictions in terms of infrastructure, because it can be directly fed into the existing natural gas grid for energy transportation (both gases allow the storage of renewable energy) [31]. It is worth mentioning that the grid capacity of natural gas in 2018 was equal to 1131 TWh across EU28 and it can deliver up to 22 TWh of natural gas per day [33]. In Europe, the 21% of annual natural gas consumption can be represented by the grid storage capacity [33]. This enormous storage capacity could be used for storing methane as a renewable energy carrier in a cheap and easy way, over long periods of time.

As far as the health safety matters are concerned, methane is a nontoxic gas, but extremely flammable (see Table 2.1) [26]. In case of spills, methane has a similar environmental impact as diesel and heavy fuel oil. According to ECHA, the registered dossiers for methane, diesel, and heavy fuel oil report the lethal LC₅₀ dose in water to be 49.9 mg/l, 65 mg/l and 79 mg/l, respectively [21].

2.1.3. ETHYLENE

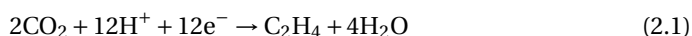
Nowadays, ethylene (C₂H₄) is mainly produced by the thermal cracking (also known as steam cracking) of ethane, propane, butane, oil or naphtha with steam at high temperatures [34], [35]. The process of steam cracking accounts for the 95% of the global ethylene production and ethane is the most common feedstock in this process, accounting for the 30% of the total ethylene production [34], [35]. Other production processes of ethylene are the fluidized-bed cracking, catalytic pyrolysis (e.g. pyrolysis of waste plastics), methanol to olefins (MTO) and Fischer-Tropsch synthesis [34], [35].

Besides the aforementioned production processes that use fossil fuels or waste plastics, ethylene can be also produced by renewable sources and feedstocks. Biomass can be used as a feedstock in the process of catalytic pyrolysis for the ethylene production [35]. Another way of using biomass in the ethylene production is the dehydration of bio-ethanol over acidic catalysts [35]. The latter process is characterized by high atom efficiency and it has been implemented in Braskem, Brazil, where the first ethylene pro-

duction plant based on renewable sources opened in 2010 [35]. This plant consumes 462 million liters of bio-ethanol annually (produced from sugarcane) and produces 200 kton/year of ethylene [35].

The dehydration of bio-ethanol is a feasible technology for the production of ethylene, only if the biomass (e.g. sugarcane) is vastly available at a low cost. This production route cannot be applied in Europe, due to the unavailability and high prices of sugarcane. For example, a feasibility study, which was done in cooperation with Dow Chemical Company (2013), showed that the production of 200 kton/year of bio-ethylene from bio-ethanol (using sugar beets as a feedstock) was not commercially viable for the company's plant in Terneuzen, the Netherlands, resulting in a negative Net Present Value (NPV) [36].

Another production route for ethylene is the electrochemical CO₂ reduction, which can be powered by renewable sources (the half-reaction of the cathode for this process is listed below) [15]. The CO₂ reduction in the CO₂ electrolysis cells often leads to the formation of byproducts such as gases (e.g. H₂, CH₄ and CO) and liquids [15], [37]. That's why; the effective separation between liquids and gases is vital for decreasing the overpotential and improving the conversion efficiency and selectivity towards C₂₊ products (such as ethylene) [15], [37].



Ethylene is used as a feedstock for the production of various chemical products such as plastics (e.g. polyethylene), resins, fibers, packaging materials and polymers (e.g. polyester and polystyrene) [34]. Ethylene is one of the most important raw materials in the chemical industry, because it is one of the most important petrochemically derived monomers and the largest contributor to the olefin market [34]. It is worth mentioning that 183 million tons of ethylene were produced worldwide in 2019 and 60% of this capacity was used in the production of polyethylene [34], [38]. As it can be understood, the applications of ethylene affect many industries such as packaging, transportation, automotive, construction, plastics, adhesives etc.

As it can be seen in Table 2.1, exposure to ethylene has no significant toxic potential in humans, but ethylene is an extremely flammable gas [27]. Also, ethylene is a volatile substance, slightly soluble in water, soluble in most organic solvents, noncorrosive and colorless at room temperature [34]. It can be concluded that environmental pollution can unlikely be caused by ethylene (if properly handled) and toxic exposure to humans can be considered low as well.

2.1.4. CONCLUSION

In conclusion, the main advantage of methanol against methane and ethylene is the methanol's wide range of application, including energy carrier (liquid at ambient temperature and pressure), feedstock to the petrochemical industry (e.g. via MTO processes) and direct use as a pure fuel or blend component (added to conventional fossil fuels like gasoline). Methanol is a chemical that can be processed as an intermediate to other

chemicals and fuels. For instance, the plastics production could be carbon-negative, if methanol was used as a chemical feedstock to the petrochemical industry via MTO processes, because the main raw material would be the CO₂ of the atmosphere and not fossil fuels.

The use of methanol as a fuel is a more eco-friendly option than the use of methane, because methanol has a lower environmental impact than methane. Also, methane and methanol have a higher hydrogen-to-carbon ratio than gasoline and ethylene. Thus, the use of methanol as a fuel can lead to 7% lower CO₂ emissions than the use of gasoline (on an energy specific basis, CO₂/MJ) [20]. Shipping and automotive industries have shown great interest in methanol, because methanol can be burned by ICEs without fundamental changes to the existing machinery. Methanol could be an intermediate and temporary alternative to fossil fuels for the transportation sector, until the electrification of this sector or the use of hydrogen in this sector is successful in the long term.

Since methanol is a liquid at ambient temperature and pressure, it can be transported and stored easily, offering a high value of energy as an energy carrier. Methanol allows large scale storage of the excess renewable energy, so that it can be used when there is not sufficient power from renewables. As a result of its liquid state, existing transport and storage infrastructure such as vessels, terminals, gas stations, tanks and pipelines could be used with little or no alterations.

2.2. MAIN TECHNOLOGIES FOR METHANOL PRODUCTION USING RENEWABLE ENERGY

THE main technologies that incorporate the electricity of renewable sources in the production of methanol will be reviewed in this section. One pathway to methanol production is the CO₂ electrochemical reduction, but the most direct way is the CO₂ hydrogenation [16]. Traditionally, the industrial production process of methanol consists of the three following steps:

- production of syngas
- catalytic conversion of syngas into methanol
- distillation of the reactor effluent [13], [39].

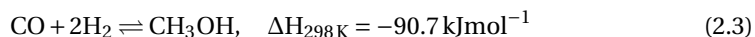
Syngas is a mixture of CO, CO₂ and H₂ gases and is characterized by its stoichiometric number (SN), which is a measure of the reduction potential of the gas mixture [13], [16]. Based on the components of syngas, it can be produced using the electricity from renewables for running the CO₂ and H₂O electrolyzers.

$$SN = \frac{H_2 - CO_2}{CO + CO_2}, \quad \text{in mol or mol\%} \quad (2.2)$$

The value of SN is equal to 2 for the production of methanol under ideal conditions [13], [39]. However, the optimal SN value is slightly larger than 2 (i.e. 2.05) for commercial applications [13], [14], [39]. It can be understood that an SN value lower than 2 means hydrogen deficiency, while an SN value larger than 2 shows surplus of hydrogen [39].

2.2.1. CO₂ ELECTROCHEMICAL REDUCTION

The CO₂ electrochemical reduction is an effective, simple and scalable technology for producing CH₃OH [14], [16]. This technology is a sustainable approach to CH₃OH production, when the electricity from renewables is used. The main advantages of this technology are the ambient reaction conditions and use of renewable energy [14]. However, the main challenge of this technology is the development of proper catalysts, which selectively produce methanol [16]. The CO₂ electrochemical reduction produces also by-products such as formaldehyde and formic acid (which in turn can be reduced to CH₃OH) [16], [39]. The exothermic reaction from syngas is given by the following equation and shows the hydrogenation of CO [13], [14], [16], [40]:



Among various materials, copper (Cu) and copper-based electrodes are one of the most promising materials, because they have a very good performance, when they are used as catalysts in the electrochemical reduction of CO₂ into CH₃OH [16], [41]. For industrial applications, oxidized Cu-based electrodes are used as catalysts for the production of CH₃OH, because the reported current densities (i.e. up to 33 mA/cm²) and Faradaic efficiencies (i.e. greater than 100%) are among the highest ones [41].

2.2.2. CO₂ HYDROGENATION

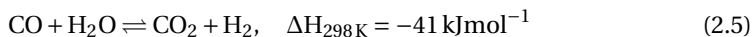
The most direct way for producing methanol is the CO₂ hydrogenation process, which does not require the preliminary reduction of CO₂ to CO [16], [40]. The exothermic reaction takes place at 250-300 °C and 50-100 bars and is given by the following equation [16], [40], [42]. Usually for commercial applications, copper-zinc oxide catalyst with aluminium oxide (CuO/ZnO/Al₂O₃) catalysts are used for these reaction conditions [16], [39], [40], [42].



As it can be seen in the above equation, water is a by-product in this reaction (a third of the H₂ is converted to water). This reaction leads to a decrease in the number of molecules present and thus it can be more efficient, if it takes place at high pressure and low temperature [40]. But, if the temperature of this process is lower than 250 °C, then the CuO/ZnO/Al₂O₃ catalysts exhibit poor activity [40].

The challenge of this process is the catalyst deactivation, which occurs due to the contained water (i.e. the by-product of the reaction) and affects negatively the productivity of the whole process [13], [39], [40]. The water causes the crystallization of Cu and ZnO in the catalyst, which in turn causes the deactivation and sintering of the catalyst

[39], [40]. This challenge can be overcome by the presence of CO, which will react with the water in order to form CO₂ and H₂ [13], [40]. The reaction between CO and H₂O is exothermic and is called water-gas shift (WGS) reaction (see the following equation) [13], [40]:



2.2.3. METHANOL REACTOR

Methanol reactor comprises the exothermic chemical reactions of the methanol synthesis and thus it is the most important piece of equipment in the whole downstream process. Since the generated heat by the reactions needs to be removed and recovered (if possible), the reactor's temperature can be efficiently controlled and the process economics can be optimized [39]. Adiabatic and isothermal gas phase reactors are the two main types of reactors, which are used for the methanol synthesis [39], [43]. Liquid phase reactors are not so commonly used for the methanol synthesis, but they are considered as the future of methanol industry, because the reactions' heat can be efficiently removed and the reactor's temperature control is more tight [39], [43]. Liquid phase reactors are outside the scope of this thesis.

Market share of methanol reactors' manufacturers

The most commonly used reactors in industry are mainly developed by Lurgi (27 %), Johnson Matthew/Davy (25 %), Haldor Topsøe (16 %), followed by Mitsubishi Gas Chemical Company (MGC) and Linde [44].

Adiabatic reactors

The adiabatic reactors commonly consist of one single pressurized vessel, which includes multiple fixed adiabatic beds in series [39], [43]. The adiabatic beds are catalysts that in some designs are separated by gas cooling devices [39], [43]. In Figure 2.3, the two main categories of the adiabatic reactors, i.e. indirect cooled and quench reactors, can be seen [43]. The temperature profile of both types have a sawtooth pattern (see the red-blue line of Figure 2.3) and their operating temperature increases linearly in the heat removal section [43]. This section is defined as the area left of the equilibrium profile, which is presented by the black line of Figure 2.3 [43].

In Figure 3.27, the schematic diagram of an adiabatic quench reactor can be seen. Quench reactors are one of the simplest and most reliable system configurations for methanol synthesis [39], [43]. Syngas is not fully fed into the top of the reactor, but only a portion of it is preheated and fed into the reactor's top [43]. The rest of the syngas is cold and fed stepwise along the catalysts' volume [43]. The preheated syngas is converted into methanol, as it flows from the top to the bottom part of the reactor and thus the overall reactor's operating temperature increases [43]. However, the cold syngas reduces the overall reactor's operating temperature and increases the conversion rate [43]. Thus, the reactor's temperature is controlled by the irregular syngas flow distribution and without external cooling units [39], [43].

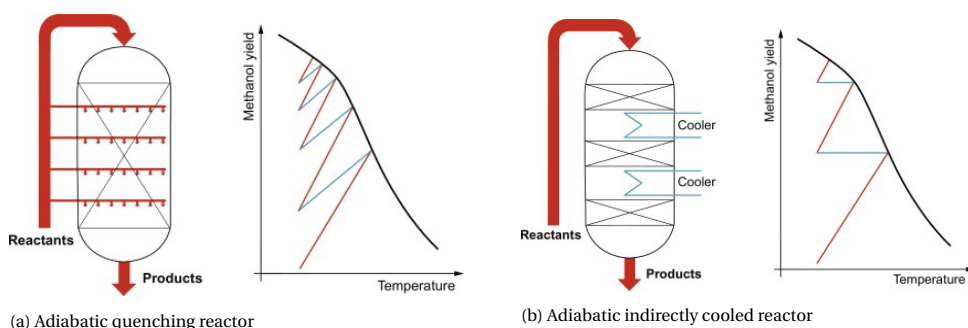


Figure 2.3: Adiabatic methanol reactors and corresponding methanol yield vs. temperatures profiles (conversion profiles with red-blue sawtooth pattern and equilibrium profiles with black solid curve) [43]

Quench reactors usually operate at 50-100 bar and 270°C, with a production capacity up to 3000 tons/day [39]. Although the reactor's temperature can be easily controlled, the catalysts are not fully exploited, since the syngas is not uniformly distributed across the whole catalysts' volume [39], [43]. Therefore, the catalysts' temperature is not uniform across their volume and hot and cold zones can be found across them [39]. Cold zones lead to low reaction rate and hot zones lead to byproducts formation or catalysts deactivation (i.e. catalysts' lifetime is reduced) [39].

In Figure 3.28, the schematic diagram of an adiabatic indirect cooled reactor can be seen. This type of reactor is one of the most commonly used in methanol industry and the syngas is fed only into the top of the reactor [43]. In this reactor, the use of external coolers is necessary for removing and reducing the operating temperature of the process stream [43], [45]. The external coolers separate the catalysts, which are connected in series, from each other [43]. High productivity of methanol can be achieved by such reactors and the reactor's temperature can be efficiently controlled by the external cooling units [43]. Indirect cooled reactors are characterized by a constant methanol fraction, compared to the quench reactors [43].

In general, the advantages of adiabatic reactors are the high production capacity, low installation cost, simplicity in construction and good reliability [39], [43]. On the other hand, their disadvantages are the low conversion for each cycle, high recycle ratio, high dilution of reagents and high volume of catalysts [39], [43].

Isothermal reactors

Compared to the adiabatic reactors, the isothermal reactors are continuously cooled using water or gas [43]. In Figure 2.4, the schematic diagram of an isothermal reactor and its temperature profile can be seen. The shape of this Figure's reactor is similar to the shape of a tube shell heat exchanger, in which the coolant (i.e. water) flows on the shell side, while the catalysts are installed on the tube side [43]. The aim of such reactors is to keep their operating temperature constant at a low level (through cooling), so that an isothermal axial temperature profile can be achieved.

Isothermal reactors usually operate at 50-100 bar and 230-265°C (with a high recycle ratio), requiring a low volume of catalysts [43], [46]. In such system configurations, the catalysts are usually surrounded by the coolant and the reactors' operating temperature can be simply controlled by varying the coolant pressure [43], [46]. Under these operating conditions, a high conversion rate can be achieved, since the isothermal downstream process makes the reaction trajectory as optimal as possible [43]. Another advantage of isothermal reactors is the longer lifetime of their catalysts, due to the lower operating temperatures and optimal reaction trajectory [43], [46]. Despite the ease of management of such reactors and their advantages over the adiabatic ones, isothermal reactors require higher capital expenditures, more materials and more space, due to the tubes and the large shell [43].

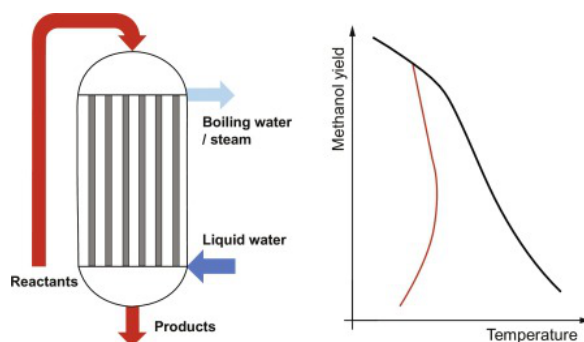


Figure 2.4: Isothermal methanol reactor and corresponding methanol yield vs. temperature profile (conversion profile with red solid curve and equilibrium profile with black solid curve) [43]

2.3. H₂O ELECTROLYSIS

WATER electrolysis is an electrochemical process for producing hydrogen and oxygen, by splitting water using electricity. The water is dissociated to high-purity H₂ (up to 99.999 vol.%) and O₂ by applying a direct electric current [47]. Since this process can produce high-purity hydrogen, it will play an important role in the conversion of renewable electricity to chemicals and fuels (as it was briefly stated in section 2.1).

The main technologies for water electrolysis are classified, according to their electrolyte, into: alkaline electrolysis (AEL), polymer electrolyte membrane electrolysis (PEM) and solid oxide electrolysis (SOEC) (see Figure 2.5) [16]. As it can be seen in this figure, the direct electric current flows in an outside circuit and between the electrodes [16]. The electrodes are separated from each other and immersed in an electrolyte, which conducts ions and is impermeable to electrons [16]. The electrons leave the anode, polarizing this electrode positively, and the oxidation half-reaction takes place [16]. Then, the electrons flow to the cathode, polarizing this electrode negatively, and the reduction half-reaction takes place [16]. So, the oxygen is generated at the anode, the hydrogen at

the cathode and the global electrolysis reaction can be seen below [16]:

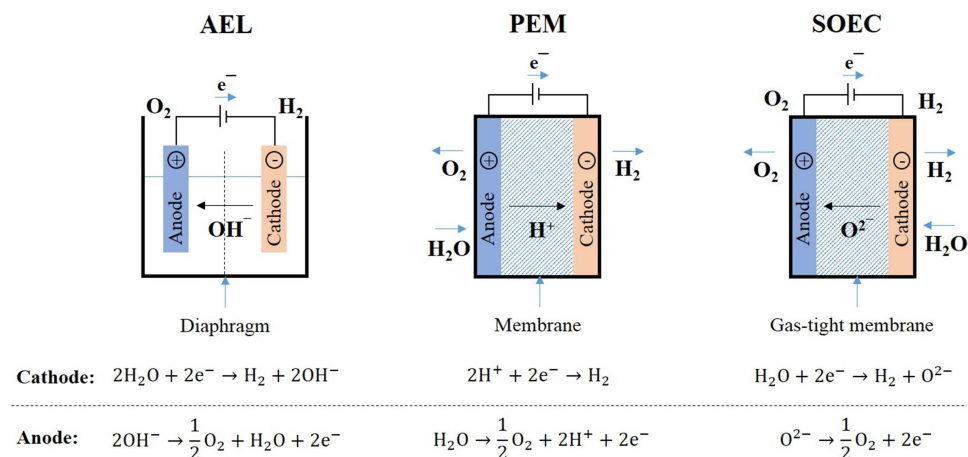


Figure 2.5: Technologies for water electrolysis [16]

2.3.1. ALKALINE ELECTROLYSIS (AEL)

Alkaline electrolysis is a mature, reliable and safe technology, which is widely used in many large scale applications since 1920 [16], [48]. For example, the Audi e-gas plant in Germany (the world's biggest PtG plant) uses three AEL electrolyzers with a total power of 6 MW [16], [30]. In the AEL technology (see Figure 2.5), two electrodes are immersed in a liquid alkaline electrolyte (usually KOH or NaOH solution) and separated by a diaphragm (so that the product gases are not mixed) [16]. The electrolyte concentration usually varies from 20 to 40 wt.% and the purity of the generated H_2 and O_2 is more than 99% [16], [48]–[50]. The AEL electrolyzers operate at low temperatures (60–80 °C) and at pressures between 1 and 30 bars [16], [48], [49]. These electrolyzers can operate at higher pressures (up to 690 bars), producing pressurized H_2 , whose process has a higher energy efficiency than the H_2 pressurization after production [16]. Nevertheless, when these electrolyzers operate at such high pressures, they produce lower purity H_2 , the risk of formation of hazardous gas mixtures increases and their efficiency drops [16], [47].

The main advantages of AEL electrolyzers are their durability (up to 90,000 hours), readily availability and application in large-scale projects [16], [48]. Also, this type of electrolyzers exhibit low capital costs (because no noble metals are used and the stack components are relatively mature) and low maintenance costs (2–3% of the annual investment expenditure) [16], [48].

Despite being a mature technology, AEL has some disadvantages, such as low current density (up to 0.4 A/cm²) and low partial load range [16], [49]. These drawbacks negatively affect the system size and the production costs of H₂ [16], [48]. An important disadvantage of AEL electrolyzers is that they have a limited dynamic operation and a slow loading response [16], [48], [49]. That's why; it is difficult for them to be adapted to renewable energy sources, due to the intermittent power output of these sources [16], [48], [49]. Usually, these electrolyzers are used with a steady power input, otherwise the system efficiency and the generated gas purity decrease [16], [48], [49].

2.3.2. POLYMER ELECTROLYTE MEMBRANE ELECTROLYSIS (PEM)

Polymer electrolyte membrane electrolysis is a very promising technology for H₂ production and many companies such as Siemens, General Electric, Air Liquide, Hydrogenics etc. have invested in this technology since 1960s [16], [47]. For example, Air Liquide has built the world's largest PEM electrolyzer in Quebec, Canada with a total power of 20 MW [51]. This electrolyzer is supplied with renewable energy and now produces 8.2 tonnes of H₂ per day [51].

In this type of electrolyzers (see Figure 2.5), there is a proton exchange membrane that is most commonly made of Nafion polymer and separates not only the two half-cells (i.e. the anode and the cathode) but the generated gases as well [16], [47], [50]. This membrane has a very small thickness (less than 0.2mm) and is gas-tight with a strongly acid character and cross-linked structure [47]. The polymeric membrane limits the gas crossover, provides high proton conductivity and allows high pressure operation (up to 200 bar) [16], [48]. High purity H₂ (up to 99.99%) can be produced, because of the limited gas crossover in this type of electrolyzers [16], [47], [48]. Due to the low ionic resistances of PEM electrolyzers, high current densities (up to 2 A/cm²) can be also achieved [47], [48], [50]. The maximum operating temperature of these electrolyzers is 80°C due to the presence of the polymeric membrane [47], [48]. Moreover, the electrodes of these electrolyzers are made of noble metals, such as platinum, ruthenium, rhodium or iridium, because they need to resist low pH conditions [16], [47], [50].

The main advantage of PEM electrolyzers is their flexible operation, due to their fast response to the power input (i.e. the proton transport H⁺ responds quickly to the power fluctuations); hence they can be used over a wide range of power supply [16], [47]–[49]. That's why; this type of electrolyzers can work under variable power input and be coupled with renewable energy sources [16], [47]–[49]. Another advantage of PEM electrolyzers is the H₂ production at 35 bar, while the O₂ is produced at atmospheric pressure, avoiding the hazard of handling O₂ at high pressures [47]. The low gaseous permeability of the polymeric membrane offers another advantage, which is the low risk of formation of flammable mixtures [47]. High power efficiency and compact design are also some of the advantages of these electrolyzers [16], [49].

The main disadvantage of PEM electrolyzers is their high capital cost (around 2,000 €/kW_{e1}) and high maintenance cost (3-5% of the annual investment expenditure) [16], [48]. The expensive polymeric membranes and noble metals increase the investment

cost of these electrolyzers [16], [47]–[49]. Other disadvantages of PEM electrolyzers are their water purity requirements (water electric conductivity must be less than $1 \mu\text{S}/\text{cm}$) and high system complexity, due to their operation at high pressure [47], [48].

2

2.3.3. SOLID OXIDE ELECTROLYSIS (SOEC)

Solid oxide electrolyzers is an advanced concept of electrolysis, which can use water or steam as feedstock and can operate at high temperatures, from 500°C to 1000°C [16], [47]–[49]. In this technology, part of the electrical energy required to split water is replaced with thermal energy [50]. For example, in case of steam electrolysis (at $1,000^\circ\text{C}$), up to 40.1% of the energy required to produce H_2 can be theoretically supplied as heat at that temperature [47]. The higher the operating temperature, the lower the cell voltage and the higher the rate of the electrochemical reactions [47], [49]. Due to the high temperatures, the electrolyzers efficiency increases, because the overpotentials at the anode and cathode, which cause power losses in electrolysis, decrease and the ionic conductivity of the electrolyte increases [47], [50].

These electrolyzers are able to operate at so high temperatures, because their electrolyte is made of solid ion-conducting ceramics, such as zirconia-based materials and rare-earth oxides [16], [47], [48]. The aforementioned materials offer good ionic conductivity and mechanical properties, when they are under so high temperatures [16]. As far as the electrodes are concerned, their materials consist of mixed oxides with perovskite structure, like yttria-stabilized zirconia (Ni-YSZ) and lanthanum strontium manganite (LSM) [16], [48], [50]. These electrode materials offer good ionic and electronic conducting, allowing the migration of O^{2-} and facilitating electron and mass transport [16].

The advantages of the operation at so high temperatures are the lower cell voltage (up to 1.5 V), less electricity demand ($\text{kW}_{\text{el}}/\text{m}^3$ of H_2) and higher energy efficiency (more than 90%, when the heat utilization is included), compared to AEL or PEM electrolyzers [16], [47]–[49]. Another advantage of the SOEC electrolyzers is that they can be integrated with a high-temperature heat source (e.g. geothermal energy) for steam electrolysis [47]. The process of steam electrolysis is less energy intensive and its operational cost is lower, compared to liquid water electrolysis [47]. The flexible operation of the SOEC electrolyzers as solid oxide fuel cells (SOFCs) in reverse mode is another advantage of this technology [16], [47], [48]. SOEC systems also offer the possibility of co-electrolysis of CO_2 and steam for syngas production [16], [48].

The main drawbacks of this technology are the fast material degradation, low thermal stability of the materials and sealing issues, due to high operating temperatures and high current densities (more than $1 \text{ A}/\text{cm}^2$) [16], [47]. That's why; these electrolyzers are not currently suitable for large scale projects and long-term operation [16]. The materials degradation in the SOEC electrolyzers (such as electrolyte aging, cracking and electrode deactivation) is faster than in SOFCs [47]. Another disadvantage of SOEC electrolyzers is their high capital cost (higher than $2,000 \text{ €}/\text{kW}_{\text{el}}$), because their materials are expensive and there is a mixture of water vapor and H_2 at the cathode's stream that requires further processing in order to obtain high purity hydrogen [47]–[50]. Finally, this

technology is not yet widely commercialized, because it is currently under development and on laboratory scale (many companies like Toshiba and Sunfire have invested in its development) [47]–[49].

2.3.4. COMPARISON

Table 2.2 presents the main advantages and disadvantages of each technology as well as their operational parameters and main characteristics. More analytically, the following comparisons can be made:

- PEM electrolyzers can be better adapted to the intermittent power output of renewable sources, compared to AEL and SOEC electrolyzers [16], [47]–[49]. In AEL electrolyzers, the ionic transport shows a greater inertia compared to PEM electrolyzers [47].
- PEM and SOEC electrolyzers operate at higher current densities, have higher efficiency and produce H₂ at a slightly higher purity, compared to AEL electrolyzers [16], [47]–[49].
- In comparison with PEM and AEL electrolyzers, SOEC electrolyzers require less electrical energy and can operate as fuel cells or in co-electrolysis mode of CO₂ and steam [16], [48].
- PEM electrolyzers have a shorter lifetime than AEL electrolyzers do [47], [48]. Since SOEC is not a mature technology, these electrolyzers have an extremely short lifetime [47], [48].
- PEM and SOEC electrolyzers are more expensive than AEL electrolyzers, due to their precious materials, fabrication methods and polymeric membranes [47]–[50].

Table 2.2: Comparison between different technologies for water electrolysis

	AEL	PEM	SOEC
Feedstock	H ₂ O + electricity [50]	H ₂ O + electricity [50]	H ₂ O + electricity + heat [50]
Electrolyte	Aq. potassium hydroxide (20–40 wt% KOH) [48]	Polymer membrane (e.g. Nafion) [48]	Yttria stabilised Zirconia (YSZ) [16], [48]
Cathode	Ni, Ni-Mo alloys [48]	Pt, Pt-Pd [48]	Ni/YSZ [16], [48]
Anode	Ni, Ni-Co alloys [48]	RuO ₂ , IrO ₂ [48]	LSM ¹ /YSZ [16], [48]
Current density [A/cm ²]	0.2-0.4 [48]	0.6-2.0 [48]	0.3-2.0 [48]
Cell Voltage [V]	1.8-2.4 [48]	1.8-2.2 [48]	0.7-1.5 [48]
Gas Purity [%]	>99.5 [48]	99.99 [47], [48]	99.99 [48]
T _{operating} [°C]	60-80 [48], [49]	50-80 [47], [48]	500-1,000 [16], [47]–[49]
P _{operating} [bar]	<30 [48]	<200 [48]	<25 [48]
Stack Lifetime	60,000-90,000 [48]	20,000-60,000 [48]	<10,000 [48]
Efficiency [%]	59-79 [16], [49]	62-82 [16], [49]	>90 [16], [49]
Maturity	Mature and Commercial [48], [49]	Near-term Commercial [48], [49]	Laboratory Scale [48], [49]
Capital Cost [€/kW _{el}]	1,000-1,200 [48]	1,860-2,320 [48]	>2,000 [48]
Advantages	Low capital cost, relatively stable, mature technology and possible application in large plant sizes [16], [49]	High power density, high pressure, rapid system response, no corrosive substances, compact design and high-purity H ₂ [16], [49]	High efficiency, possible integration of waste heat, lower energy demands and co-electrolysis of CO ₂ and steam [16], [49]
Disadvantages	Low current density, low dynamics, corrosive electrolyte, slow dynamics and gas permeation [16], [49]	High cost and fast degradation of membranes [16], [49]	Low long term cell stability, mechanically unstable electrodes (i.e. cracking) and not suited for fluctuating systems [16], [47]–[49]

¹Perovskite-type lanthanum strontium manganese [48]

2.4. CO₂ ELECTROLYSIS

THE electrochemical reduction of CO₂ to CO is a process that uses direct electric current. Rapid scientific and technological progress has recently been made in this field. Nowadays, carbon monoxide has a wide range of applications and is used as a pure compound or as a constituent in syngas (i.e. mixture of CO and H₂), for the production of chemicals and fuels. That's why; CO₂ electrolysis can play an important role in the conversion and storage of renewable energy via Power-to-X pathways (see section 2.1).

Like in water electrolysis, the cell for the CO₂ electrolysis consists of two electrodes and an electrolyte, which can be a liquid or a solid material. The operating temperature of the cell determines the material of the electrolyte and affects the ionic conductivity of the electrolyte [52]. The electrons flow from the anode to the cathode, when an external voltage is applied between the two electrodes [52]. The reduction half-reaction (e.g. CO₂ to CO) takes place at the cathode and the oxidation half-reaction (e.g. OH⁻ to O₂ and H₂O or O²⁻ to O₂) takes place at the anode [52]. The main technologies for CO₂ electrolysis are categorized as follows (see Figures 2.6, 2.8 and 2.9):

- Batch-type reactors
 - Low-temperature electrolyzers in H-cell configuration
- Flow cell reactors
 - Solid oxide electrolyzers (SOEC)
 - Molten carbonate electrolyzers (MCEC)
 - Low-temperature electrolyzers with gas diffusion electrode (GDE) as cathode
 - Polymer electrolyte membrane (PEM) electrolyzers [52], [53].

The difference between the batch-type and the flow cell reactors is that the electrolyte is in continuous flow in the flow cell reactors [53]. In the latter type of reactors, the catholyte and anolyte are continuously refreshed, but in some cases the anolyte may not be refreshed [53], [54]. The advantages of the flow cell reactors over the batch-type reactors are: increased mass transfer, higher faradaic efficiencies, higher current densities, more precise control of the reaction environment and better temperature and heat management [53], [55].

2.4.1. SOLID OXIDE ELECTROLYSIS (SOEC)

As it was previously stated in section 2.3.3, solid oxide electrolyzers (SOEC) operate at high temperatures (above 500°C) and their electrolyte is made of a solid ceramic material. As the operating temperature of the cell increases, the ionic conductivity of the electrolyte increases and the cell efficiency increases as well [47], [50], [52]. In case of CO₂ electrolysis, a SOEC cell typically operates at temperatures from 700°C to 900°C [52], [56]. The commonly used materials for the electrolyte of a SOEC cell are yttria stabilised

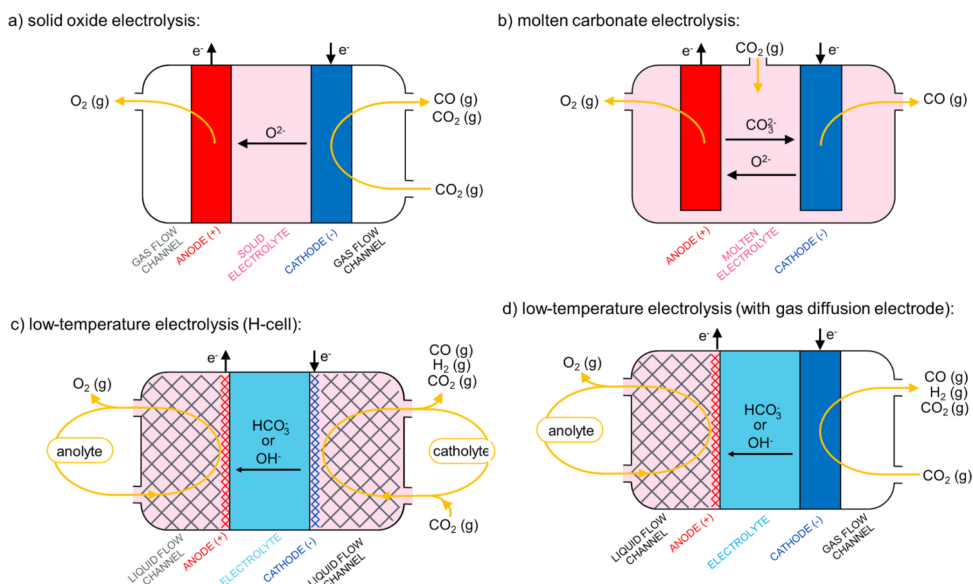
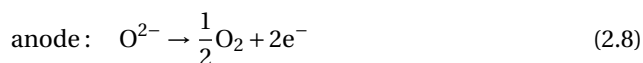
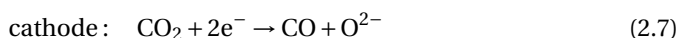


Figure 2.6: Technologies for carbon dioxide electrolysis [52]

zirconia (YSZ) and scandia-stabilized zirconia (ScSZ) [16], [48], [52]. These materials allow the ionic conduction and block the conduction of electrons and oxygen gas (these operating parameters are important for a SOEC electrolyte) [16], [48], [52].

In Figure 2.6a, a schematic illustration of a SOEC cell, which operates in dry CO_2 electrolysis is presented [52]. As it can be seen, the carbon dioxide is uniformly fed into the cathode of the cell via gas channels and the oxygen is formed at the anode of the cell [52]. The carbon dioxide is reduced to carbon monoxide at the porous cathode, using the electrons that are provided by an external power supply [52]. The oxide ions (O^{2-}) are transferred through the electrolyte to the anode, where the oxygen is formed [52]. The reactions taking place in this cell are shown in the following equation:



The advantage of SOEC cells is that they make the CO_2 electrolysis process more efficient and operate at higher current densities, compared to cells with aqueous electrolytes [56]. The operating current density of SOECs is high, because the activation of CO_2 becomes easy at high temperatures (above 600°C) [56]. Obviously, the high current densities positively affect the system size, CO production output and production costs [56]. Also, SOECs can integrate heat (e.g. waste heat of industrial processes) into operation and thus require less electrical energy input [57]. It is worth mentioning that NASA

has invested in this technology and a small CO₂ system based on SOECs will be tested on Mars, producing oxygen (for propellant oxidant) out of Martian atmosphere CO₂ [58].

Although this technology is very promising and has been attracted great interest, it is not mature and widely commercialized. The electrochemical reduction of CO₂ in SOECs is characterized by a few drawbacks such as materials degradation, difficulty in the sealing at high temperatures, current collector coarsening, impurities contamination and metal particles oxidation [56]. Another problem with the SOEC technology for CO₂ reduction is that it cannot be adapted to the intermittent power supply of the renewable energy sources, because the system degradation is rapid and the current density can be degraded almost 50% [57], [59]. This issue can be tackled, if the renewable energy-powered SOECs operate continuously and are integrated with thermal or/and battery storage systems (including complex thermal and electrical load management systems) [57], [59].

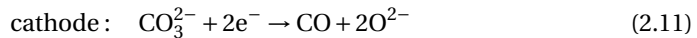
2.4.2. MOLTEN CARBONATED ELECTROLYSIS (MCEC)

Another advanced technology for CO₂ electrolysis is the molten carbonate electrolysis (MCEC), in which the electrolyte is carbonate melt [52]. The most promising results of this technology are given in case the MCEC cell consists of a titanium (Ti) cathode, a graphite anode and a combination of molten Li₂O/Li₂CO₃ electrolyte [52], [60]. MCEC cells operate at high temperatures (around 900°C) with current densities higher than 100 mA/cm² [60]. The process of this high-temperature electrolysis has a thermodynamic efficiency of at least 85% (at 100 mA/cm²) and a faradaic efficiency close to 100% [60].

In Figure 2.6b, a schematic illustration of a MCEC cell, which operates in CO₂ electrolysis, is presented [52]. As it can be seen, CO₂ is fed into the melt of the Li₂CO₃ electrolyte at 1 atm (for maintaining the stability of the electrolyte) [52], [60]. Since Li₂CO₃ is electrochemically converted into a solution of Li₂O in Li₂CO₃, the ratio of Li₂O/Li₂CO₃ increases in the melt. As the content of oxide ions (O²⁻) increases in the melt, new CO₂ is chemically formed and can be incorporated into the mixture. Thus Li₂CO₃ undergoes a reversible decomposition process, the rate of which depends on the applied current density and the pressure of CO₂ above the melt [52], [60].



At the cathode, the carbonate ions (CO₃²⁻) are reduced to CO and oxide ions (O²⁻), using the electrons that are provided by an external power supply [52], [60]. The oxide ions are transferred through the electrolyte to the anode, where they are oxidized to oxygen gas [52], [60]. The reactions taking place in this cell are shown in the following equation:



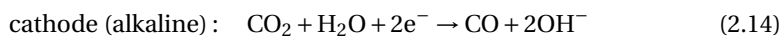
The main advantage of this technology is that pure CO and O₂ gases can be extracted, since they do not mix with the CO₂ feed [52], [60]. Since this technology is little affected by the content of SO₂ in the feed gas, flue gases of power stations can be used as input to the MCEC cells, for converting CO₂ to CO [52], [60]. Also, no precious metals are required for these cells and no hazardous or toxic by-products are produced by them [60].

Despite the interesting and beneficial characteristics of the MCEC cells, this technology is currently under development and on laboratory scale [61]. Another drawback of the MCEC electrolysis is that the performance and the stability of the cell and electrodes decrease in long-term operation (the duration of the longest reported tests varies from 100 to 120 hours) [52], [61].

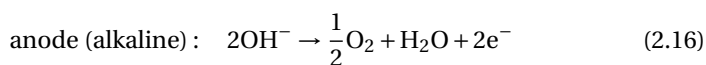
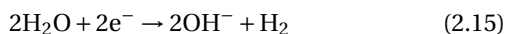
2.4.3. LOW-TEMPERATURE ELECTROLYSIS IN H-CELL CONFIGURATION

The most known and used lab-scale batch reactor for CO₂ reduction is the H-type cell, which operates at a lower temperature than SOEC and MCEC electrolyzers do [53], [62]. In the H-cell configuration, the cathode and anode are immersed in separate electrolyte solutions (i.e. catholyte and anolyte respectively) [52], [63]. Moreover, the cathodic and anodic compartments are usually connected through a circular channel and separated by the electrolyte (preventing the reduced products from oxidizing again) [53], [62]. This set-up provides the "H" shape of the cell. The electrolyte of an H-cell can be aqueous solutions (e.g. KHCO₃), solid ion-selective membranes (e.g. Sustainion, Nafion) or combinations of them [52], [64].

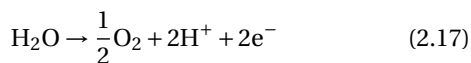
In Figure 2.6c, a schematic illustration of an H-cell with an anion-conducting electrolyte membrane, which operates in CO₂ electrolysis, is presented [52]. At the cathode, the CO₂ reduction reaction takes place and is accompanied by the H₂ evolution reaction (HER) [52], [62]. The HER reaction competes against the CO₂ reduction reaction and may lead to poor selectivity of the CO product [62]. At the anode, the oxygen evolution reaction takes place [52], [62]. The reactions taking place in such a cell are shown in the following equations [52]:



and



or



When an H-cell reactor is in operation, the CO₂ gas flows continuously into the cathodic compartment and thus the reactor must be gas tight (otherwise the reactor's faradaic efficiency may decrease) [53], [62]. Also in such systems with anion-conducting electrolyte membrane (see Figure 2.6c), the liquid products should be collected in both compartments, because negatively charged ions (e.g. bicarbonate HCO₃⁻ or carbonate

CO₃²⁻) may be formed at the cathode [52], [62]. Such negatively charged ions may diffuse through the anion exchange membrane and reach the anode, making the CO₂ evolution at the anode possible [52], [62].

The H-cell reactors are suitable for evaluating, quantifying and selecting electrocatalysts for the reduction of CO₂ to carbonaceous products (e.g. CO) in lab-scale [53], [62]. On the other hand, the H-cell reactors are not suitable for industrial applications, because electrolysis cells with lower resistance and higher mass transfer efficiency are required [62]. Another disadvantage of the H-cells is the low CO₂ conversion efficiency, because CO₂ cannot easily be dissolved and diffused in aqueous solutions (e.g. solubility of 33mM at 298 K and 1 atm) and the current density is usually very low in such systems (up to 35 mA/cm²) [52], [53], [62]. Only a small amount of the CO₂ fed in the reactor is converted to products [53], [62].

2.4.4. LOW-TEMPERATURE ELECTROLYSIS WITH GAS DIFFUSION ELECTRODE (GDE) AS CATHODE

The gas diffusion electrode (GDE) configuration is another technology for CO₂ electrolysis at low temperature. The GDE is a porous membrane electrode, consisting of a gas diffusion layer (GDL) and a catalyst layer (CL) on its top surface (see Figure 2.7a) [53], [62]. As it can be seen, the GDE is placed between the electrolyte and the gas flow field [53], [62]. Typically, the GDL has a dual-layer structure, consisting of a macroporous layer or substrate (MPS; a dense array of carbon fibers or carbon cloth) and a microporous layer (MPL; a more densely layer of carbon nanofibers or compressed carbon powder) [53], [55].

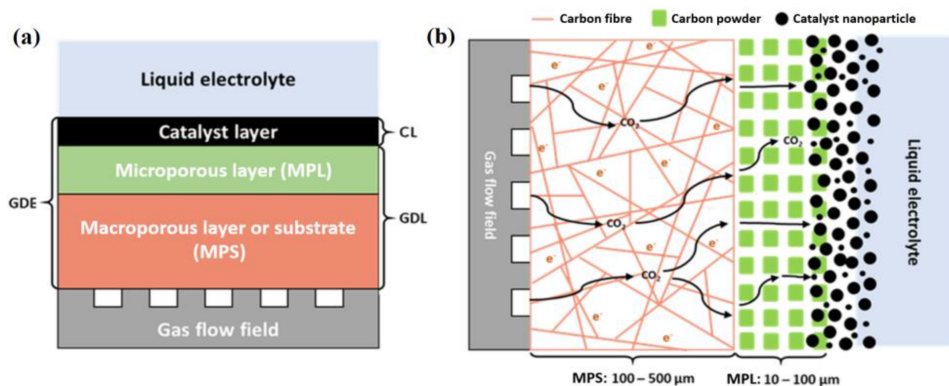


Figure 2.7: Simplified structure of a gas diffusion electrode (GDE) [53]

In Figure 2.7b, the purposes of the GDL are presented. The GDL physically supports the catalyst, allows the CO₂ gas transport to the CL and prevents the electrolyte from blocking its pores (the GDL is hydrophobic) [53]. Also, the electrons are carried by the GDL, from the current collector of the gas field to the CL [53]. It is worth mentioning that

MPL contains hydrophobic agents in order to control the electrolyte flooding as well [53].

Although GDEs can be installed in both electrodes [55], a schematic illustration of a cell with only a GDE cathode and an anion-conducting electrolyte membrane is presented in Figure 2.6d [52]. A broadly used configuration of a low-temperature electrolyzer with a GDE cathode is presented in Figure 2.8. In the latter configuration, the cell consists of 3 different compartments: CO₂ gas is fed into the 1st compartment, the 2nd compartment is filled with the catholyte and the 3rd compartment is filled with the anolyte [53]. An ion-exchange membrane separates the cathodic and anodic compartments [53]. The membrane can be cation-exchange or anion-exchange and prevents the crossover and the mixing between the products of the CO₂ reduction and the O₂ evolution [53]. The anolyte and catholyte are continuously refreshed, using separate pumps [53]. The CO₂ gas is fed into the back surface of the GDE, while the top surface of the GDE (i.e. its catalyst) is in contact with the catholyte [53].

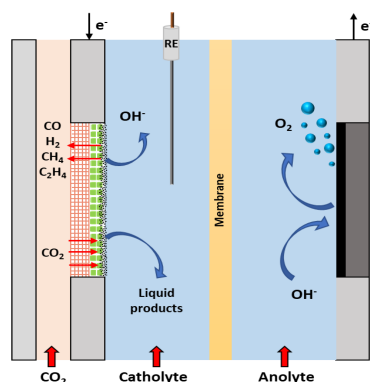


Figure 2.8: Schematic diagram of a low-temperature electrolyzer with cathode GDE, catholyte, anolyte and ion-exchange membrane [53]

In general, compared to H-cell configuration, the GDE configuration allows the cell to operate at higher current densities and does not limit the CO₂ mass transport between the electrocatalysts and the reactants at the electrode surface [52], [53], [62], [64]. The main reason for the higher current densities and the more efficient mass transport is that GDEs have a reduced diffusion length within the catalyst, provide high surface area and enable the prolonged contact between the electrocatalysts and the reactants [53], [55], [62]. That's why; when a GDE is installed at the cathode, the reaction of CO₂ reduction has a higher Faradaic efficiency (due to higher current densities) [55].

2.4.5. POLYMER ELECTROLYTE MEMBRANE

The polymer electrolyte membrane (PEM) electrolyzer is another type of flow cell reactor. The configuration of a PEM flow cell is similar to the configuration of a proton exchange membrane fuel cell (PEMFC) [53], [62]. The PEM flow cell can be considered as an evolution of the low-temperature electrolyzer, which consists of GDE cathode and liquid electrolyte (as it is presented in Figure 2.8) [53]. Compared to the latter type of electrolyzer, a PEM flow cell has GDE at both electrodes and no liquid electrolyte.

Typically, a PEM flow cell consists of GDE cathode, GDE anode, cathode flow plate, anode flow plate and polymer electrolyte membrane (see Figure 2.9) [53], [62]. As it can be seen, the CL of each GDE (highlighted in yellow) is in direct contact with the PEM ion-exchange membrane [53], [62]. A common setup of a PEM flow cell requires the input of CO₂ gas into the cathode and the input of concomitant water into the anode, for the production of CO gas [62]. As it was stated above, there is no aqueous electrolyte in the PEM flow cells and thus the H₂O needed for the CO₂ reduction is provided by the input of humidified CO₂ gas into the cathode [53], [65].

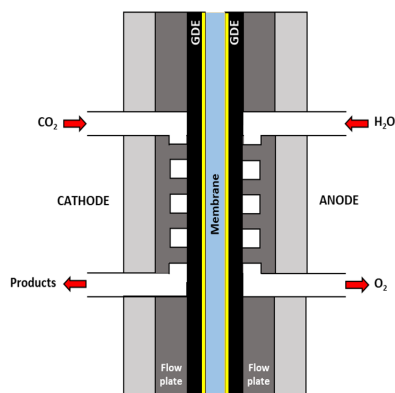


Figure 2.9: Schematic diagram of a polymer electrolyte membrane (PEM) flow cell for CO₂ electrolysis [53]

In PEM flow cells, the PEM membrane can be classified into three categories: cation-exchange membrane (CEM), anion-exchange membrane (AEM) and bipolar membrane (BPM) [53], [55], [62].

- In CEM (e.g. Nafion) configuration, protons or cations are transported through the membrane from anode to cathode [53]. Although this configuration is very good at protons transfer, precious metals are required for the anode catalysts (in order for the anode to become acidic and the OER to take place), increasing the cell cost [62]. Also, the H₂ evolution will dominate over the CO₂ reduction, because more protons are diffused from anode to cathode [53], [62].
- In AEM configuration, anions (such as OH⁻) are transported through the membrane from cathode to anode, encouraging the CO₂ reduction without the delivery of H⁺ ions to the cathode [53], [55], [62]. The use of AEM keeps the anode environment alkaline and no-precious metals are required for the anode catalysts, leading to lower cell cost [62]. Although the AEM shows a great stability at high current densities, the transfer of bicarbonate HCO₃⁻ or carbonate CO₃²⁻ ions from the cathode to the anode is possible [53], [55], [62]. If this happens, then the overall cell efficiency and anodic reaction are decreased, because CO₂ evolution may take place at the alkaline anode [52], [53], [55], [62]. That's why; the liquid products should be collected in both compartments of such systems, in order for a precise control over the cell reactions to be obtained [52], [62].
- In BMP configuration, anion and cation-exchange membranes are grouped and laminated together, enabling the water dissociation into OH⁻ (transported to the anode) and H⁺ (transported to the cathode) [55], [62], [66]. The advantages of this configuration are: high current densities (up to 200 mA/cm²) can be handled, good stability for the reaction of CO₂ reduction, no precious metals are required for both electrodes catalysts and a different pH on each cell compartment can be maintained constant (e.g. constant acidic cathode and constant alkaline anode)

[55], [62]. The BPM drawback is that higher applied voltage is required for the electrolysis process and thus the overall energy efficiency is reduced [55]. The split of water requires more energy, which is provided by the increased electrical voltage [55], [66]. In AEM and CEM, the CO₂ electrolysis has an onset potential of -1.6 V, but the onset potential is equal to -2.2 V in BPM [66].

As in H-type cells, the PEM electrodes are separated by the PEM membrane (i.e. solid state electrolyte) in order to prevent the mixing and the crossover of the products (only the ion transport through the membrane is possible) [53], [62]. Compared to H-type cells, the PEM electrodes are very close to each other, because the PEM membrane is very thin, leading to lower cell resistance [53], [62]. The problem of low CO₂ solubility in the liquid electrolyte of H-type cells does not exist in the PEM fuel cells, because there is no liquid electrolyte in them [53]. Since the GDL is placed at both electrodes, the achieved conversion rate of CO₂ and current densities are increased (for more information on the benefits of GDE flow cells, see the above subsection) [53], [62].

The proximity of electrodes might be advantageous for the PEM flow cells, because the cell resistance is decreased, but is one of their main disadvantages [53]. If the ion transport rates across the membrane exceeds an upper limit, then significant pH imbalance may be induced in the electrodes [53], [54]. For example, if the cathode becomes more acidic due to the high ion transport rates, then the H₂ evolution will dominate over the CO₂ reduction [53], [54]. This fact may make the balance control of the cell reactions more difficult. Another major disadvantage of the PEM flow cells is that if the ion exchange membrane dries, then the ion transport will negatively be affected [53], [65]. The last disadvantage of the PEM flow cells is that their membrane types need to be further studied, due to their vital effect on the CO₂ reduction and improvement on CO₂ PEM flow cells [53], [62]. PEM membrane is extremely important in these flow cells, because there is no catholyte, which provides the necessary local environment for the CO₂ reduction [53].

2.4.6. CONCLUSION

The different technologies for CO₂ electrolysis that have been presented in the previous subsections have to be examined in terms of industrial feasibility. For industrial applications, a CO₂ electrolyzer has to meet the following main requirements: long-term stability (up to 30,000 h), high current densities (>250 mA/cm²) and cell voltages below 3 V [53]. Taking into account these criteria, the following conclusions can be made:

- SOEC electrolyzers are very attractive, since they operate at very high current densities and high CO₂ conversion efficiencies. The main drawbacks of this technology are: not mature and widely commercialized, materials degradation and difficult adaptation to the intermittent power output of the renewables.
- Lots of research has to still be done for the MCEC electrolyzers, since they are currently on lab scale and under development. So far, their stability has examined up to 120 hours and their operating current densities have reached up to 100 mA/cm².

- H-cell reactors do not operate at current densities higher than 35 mA/cm^2 , due to their limited mass CO_2 transport and high cell resistance. Also, they have low CO_2 conversion efficiency, since CO_2 cannot easily be dissolved and diffused in aqueous solutions. However, they are commercialized and suitable for lab-scale applications.
- Low-temperature electrolyzers with GDE cathode can operate at current densities higher than 200 mA/cm^2 , because they do not present mass transport limitations.
- PEM electrolyzers (especially those with BPM membrane) can operate at current densities higher than 200 mA/cm^2 and offer good stability. Their drawbacks are: an increased electrical voltage is required for their operation and the PEM membranes are not allowed to get dried (otherwise the ion transport will decrease).

2.5. INFLUENCE OF RECTIFIERS ON ELECTROLYSIS SYSTEMS

THE influence of rectifiers on the performance of electrolysis systems, which are in dynamic operation, will be reviewed in this section. In PtX systems, the electrolyzers are the main energy consumers and the end product is the main energy carrier [67]. The electrolyzers require DC power and thus their operation depends on electric conditioning [67]. For the purposes of this section, thyristor-based rectifiers, transistor-based rectifiers and water alkaline electrolyzers are used.

Generally, if the provided current profile is characterized by fluctuations, then there are deviations from steady DC profile and the electrolyzers efficiency drops in turn [68]. In non steady DC profiles, the electrolyzers efficiency loss is affected by 3 parameters: the offset of the current waveform, its frequency and its ripple factor [68]. However, the type of the current waveform (e.g. sinusoidal, triangular, square and sawtooth current) does not affect the electrolyzers efficiency [68].

Energy consumption and efficiency

The ripple factor (RF) is an important parameter of rectifiers, because it describes the quality of rectification [69]. RF is affected by the effective current I_{RMS} and the mean current I_{mean} (see the following equation) [69]. This factor influences the electrolysis process and can be used as an indicator for the ohmic losses of this process [69].

$$RF = \sqrt{\frac{I_{\text{RMS}}^2 - I_{\text{mean}}^2}{I_{\text{mean}}^2}} \quad (2.18)$$

Moreover, the ohmic losses of an electrolyzer are caused by the provided current profile (from the rectifiers) and various components such as current conductors [69], [70]. The mean output current of the rectifier (I_{mean}) contributes to the electrolysis process, while the current ripple causes ohmic losses [68]–[70]. Normally, these losses are negligible in nominal operation, but they are significantly higher in low load operation due to the high current RF [69], [70]. It can be understood that, these losses affect negatively the energy consumption and efficiency of the electrolyzers.

Therefore, the higher the current ripple (i.e. the difference between the current peaks and the I_{mean}) is in low load stages, the higher the energy consumption is and the lower the energy efficiency is for the same amount of H_2 production [67]–[70]. For example, the electrical energy consumption of the electrolyzers increases up to 13%, for a high current ripple in low load operation of a six-pulse controlled bridge rectifier with commutating inductance (B6C) and a non controlled six-pulse bridge rectifier in series with a controlled thyristor based six-pulse bridge (W3M) [69]. Another study showed that the electrolyzers energy consumption increases up to 25% above their specifications value, for a high current ripple in low load operation of a three-phase half-controlled rectifier with thyristors and diodes and a three-phase thyristor voltage controller and diode full-bridge rectifier [70].

Gas quality

It has been shown that the gas quality of the electrolysis systems is negatively affected, when their operating load is below 25% of its nominal value [69]. The current ripples cause gas crossover through the electrolyzers membrane and thus the gas quality is decreased (i.e. H_2 is contaminated with excess O_2) [69]. In such cases, the H_2 gas product needs to be further processed (i.e. removing the impurities) and thus the capital cost of electrolysis systems increases.

In conclusion, transistor-based rectifiers are more suitable for electrolysis systems in dynamic operation, compared to conventional thyristor-based rectifiers [67], [69], [70]. For example, the electrolyzers efficiency may increase up to 10% when they are connected to transistor-based rectifiers in comparison with thyristor-based rectifiers [70]. Another study showed that transistor-based rectifiers offer up to 14% and 9% lower energy consumption (of the electrolyzers) than the 6-pulse and 12-pulse thyristor-based rectifiers offer respectively (as the current varies between 1000 and 5000 A) [67].

3

SYSTEM DESIGN AND MODEL

This chapter presents the design and modelling of this thesis system. The proposed system aims for a methanol production, whose product specifications are included in section 3.1. One of the main feedstocks for this production process is the CO₂, which will be captured from the flue gases of a cement plant. The CO₂ specifications and the effect of impurities in the CO₂ feed are presented in section 3.2. The plant location of this thesis system and its configuration are presented in section 3.3 and 3.4, respectively. The energy source of this system is solar energy and section 3.5 explains how the PVs power output data has been acquired. Section 3.6 explains how the system's control logic is implemented, so that the dynamic operation of the electrolyzers can be achieved. The design and modelling of CO₂ and H₂O electrolyzers are described in sections 3.7 and 3.8, respectively. Regarding the system's auxiliary equipment, compressors, cooling units, buffer tanks and DC-DC converters are required. The design and modelling of the auxiliary equipment is presented in section 3.9. The selected downstream production of methanol is described in section 3.10. Finally, the specifications and the modelling of the selected methanol reactor are presented in section 3.11.

3.1. PRODUCT SPECIFICATIONS

THIS thesis aims for a methanol production of approximately 4 kT/year. This target is equal to the production capacity of the George Olah plant (i.e. 4 kT/year), located in Svartsengi, Iceland [17]. This plant is the world's first CO₂-to-methanol plant and is operational since 2012 [17]. Therefore, the target of this thesis is feasible and reasonable, since it is already reached by an existing CO₂-to-methanol plant.

However, the target of this thesis is not close to the capacity of conventional commercial processes for LPM (low pressure methanol) synthesis, which is typically less than 3 kT/day [44]. Also, it is worth mentioning that large-scale plants have an even higher production capacity, exceeding 5 kT/day [44]. An example of a large-scale plant is the BioMCN plant in Delfzijl, the Netherlands, which operates two production lines with a

combined capacity of 900 kT/year (biomethanol and conventional methanol) [71], [72].

According to the Methanol Institute, the minimum required commercial purity of methanol is 99.85 %wt [73]. It is assumed that the system of this thesis will meet the aforementioned purity requirement. In Table 3.1, the production capacity and purity requirements can be seen.

Table 3.1: Production specifications for methanol

Specification	Value
Production capacity	4 kT/year
Minimum purity	99.85% wt% [73]

3.2. CARBON SPECIFICATIONS AND EFFECT OF IMPURITIES IN THE CO₂ FEED

CARBON capture and utilisation (CCU) is a new market for CO₂, because CO₂ can be used as a raw material in many production processes. For the purpose of this study, CO₂ is a raw material for the production of methanol and can be captured from the atmosphere or the flue gases of industrial plants. It is considered that CO₂ will be captured from the flue gases of a cement plant for the system of thesis (see Table 3.3).

Direct capture of CO₂ from the atmosphere

The technology for direct extraction of CO₂ from ambient air using sorbents is known as direct air capture (DAC) [74]. The obtained CO₂ through this process is very expensive, since this process requires lots of energy and the concentration of CO₂ in the atmosphere is extremely low (0.037% or roughly 400 ppm) [74], [75]. In Table 3.2, the minimum thermodynamic energy required and the capture cost for the DAC technology can be seen.

Capture of CO₂ from the flue gases of industrial plants

Compared to DAC technology, the CO₂ concentration in the flue gases of industrial plants is much higher (e.g. 350 times higher in coal-based flue gases) [74]. Among the different possibilities for carbon capture from flue gases, the options of cement plant, natural gas power plant and coal fired power plant are considered. In Table 3.2, the CO₂ concentration in the flue gases, the minimum thermodynamic energy required and the capture cost for each technology can be seen.

Flue gases from natural gas power plants

In case of natural gas power plants, the CCU technology has the cheapest application and it has been already implemented in many large-scale CCU facilities around the world [76]. For example, in natural gas combined cycle power plants, the post-combustion CCU technology (with amine scrubbing, using monoethanolamine solvent) provides high purity captured CO₂ (over 90%) [82], [83]. The flue gases of such plants are typically composed of nitrogen oxides (NO_x), carbon monoxide (CO), carbon dioxide (CO₂),

Table 3.2: Summary of metrics for CO₂ capture technologies of interest

Carbon Source	CO ₂ concentration in flue gases	Minimum thermodynamic energy required	Capture cost
DAC	0.037% [75]	250 kWh/tonCO ₂ [11]	500-700 \$ ₂₀₁₉ /tonCO ₂ [76], 600 \$ ₂₀₁₆ /tonCO ₂ [74], 200-1000 \$ ₂₀₁₈ /tonCO ₂ [11]
Natural Gas Power Plant	4% [74], 7-10% [77]	100 kWh/tonCO ₂ [11]	20-25 \$ ₂₀₁₉ /tonCO ₂ [76]
Cement Plant	up to 30% [78], 14-33% [77]	452.78-1130.56 kWh/tonCO ₂ [79]	42.5-83.5 € ₂₀₁₉ /tonCO ₂ [80]
Coal Power Plant	13-15% [74]	65 kWh/tonCO ₂ [11]	45 \$ ₂₀₁₉ /tonCO ₂ [76], 38.90 € ₂₀₁₆ /tonCO ₂ [81]

methane (CH₄), nitrous oxide (N₂O), volatile organic compounds (VOCs), sulfur dioxide (SO₂) and particulate matter (PM) [84]–[86].

Since an extremely high purity of captured CO₂ (e.g. over 98%) cannot be achieved, the impurities of SO₂ and NO_x cause a reduction in the Faradaic efficiency of the CO₂ electrolysis process of this thesis [86], [87]. The reductions of SO₂ and NO_x are more favorable than the reduction of CO₂ [86], [87].

Flue gases from cement plants

As far as the flue gases from cement plants are concerned, the variations in capture cost and minimum thermodynamic energy required rely on the implemented CO₂ capture technology. Such flue gases are also known as kiln-off gases and have a typical composition of 29.58 vol % CO₂, 11.20 vol % H₂O, 10.22 vol % O₂, 0.04 vol % SO₂, 0.01 vol % NO and 0.05 vol % CO [78]. More analytically, the main CO₂ capture technologies for cement plants are categorized as follows:

- Absorption with monoethanolamine (MEA)
- Oxyfuel process
- Chilled ammonia process (CAP)
- Membrane-assisted liquefaction (MAL)
- Calcium looping (CaL) Tail-End Configuration
- Integrated calcium looping configuration [79], [80].

The process of amine scrubbing (MEA) is a process of chemical absorption with amine solutions and is the most mature technology (extensively used in industry, including coal fired power plants, since 1930) [78]. Another advantage of this technology is the provision of high purity CO₂ and it is the easiest post-combustion technology to

be retrofitted in a cement plant [78], [79]. However, the disadvantages of this technology are its high energy demand (at least 2 GJ/ton_{CO₂} or 555.56 kWh/ton_{CO₂}) and the high capture cost of CO₂ (80.2 €/2019/ton_{CO₂}) [78], [80].

The resulting high-purity CO₂ of the MEA process can be compressed and transported by trucks or pipeline [78]. As far as the pipeline transport is concerned, the captured CO₂ can be compressed up to 80 bar with triethylene glycol (TEG) dehydration and pumped to 110 bar [79].

According to latest developments in the MEA technology, it has been stated that a specific variation of this process can provide high purity captured CO₂ (up to 99.99 %) at a cost of 40 \$/ton_{CO₂} [78], [88]. With the average exchange rate of the time (1.1956 \$/€), the unit cost of captured CO₂ can be expressed as 33.46 €/ton_{CO₂}. Such a project is under implementation by Dalmia Cement in India, using Carbon Clean's CDRMax® technology, which combines the use of a proprietary solvent (amine promoted buffer salts, APBS) with novel heat integration [78], [89].

For the purpose of this study, it is assumed that the flue gases of a cement plant will be used, using the MEA CCU Carbon Clean's CDRMax® technology technology (see Table 3.3). Also, it is assumed that the captured CO₂ will be supplied by TITAN cement plant, at a pressure of 69.7 bar and a temperature of 225°C, so that it can be fed directly to the methanol reactor (see the reactor's specifications in Table 3.10).

Although the captured CO₂ from the flue gases of natural gas power plants is cheaper, this option is excluded, because the impurities of SO₂ and NO_x in their flue gases reduce the Faradaic efficiency of the CO₂ electrolysis process. Despite the fact that the capture cost of CO₂ from the flue gases of coal power plants is almost the same as in the case of cement plants, this option is also excluded, because the impurities concentration of SO₂ and NO_x in the flue gases of coal power plants is 3-4 times higher than in the flue gases of natural gas power plants [84].

Table 3.3: Specifications for carbon capture

Specification	Value
Carbon source	Cement plant
CCU Technology	MEA with Carbon Clean's CDRMax®
CO ₂ purity	99.99% wt [78], [88]
Pressure	69.7 bar (according to the specifications of the methanol reactor in Table 3.10)
Temperature	225°C (according to the specifications of the methanol reactor in Table 3.10)
Capture Cost	33.46 €/ton _{CO₂} [78], [88]

3.3. PLANT LOCATION

THE plant location is assumed to be in Greece, with coordinates 38.108977° and 23.525769° (see Figure A.1 in Appendix A). This location has been selected, because there is a big cement plant very close to the selected area. This cement plant is owned by TITAN Cement Group and is located in Kamari, Greece. The annual production capacity of the cement plant is 2.6 million tonnes of cement and its CO_2 emissions are equal to $697.9 \text{ kg/ton}_{\text{cement}}$ [90], [91]. The annual CO_2 emissions of this cement plant are adequate for the CO_2 feed requirements of this thesis system. Also, the short distance between the two plants (roughly 2km) means that the transportation and storage cost of captured CO_2 can be neglected.

Another reason for selecting the aforementioned location is its solar resource potential. According to Global Solar Atlas v2.4, the average Global tilted irradiation at optimum angle is $1929 \text{ kWh/m}^2/\text{year}$ and $5.284 \text{ kWh/m}^2/\text{day}$ [92]. Taking into account that the long-term average of global horizontal irradiation (GHI) varies from 2 to $8 \text{ kWh/m}^2/\text{day}$ [93], the theoretical power potential of the selected location is good. In Figure 3.1, the sun path, the horizon profile and the active area can be seen for the selected location. Information on the seasonal variation of the solar irradiation (for the selected location) are given in section 3.5.

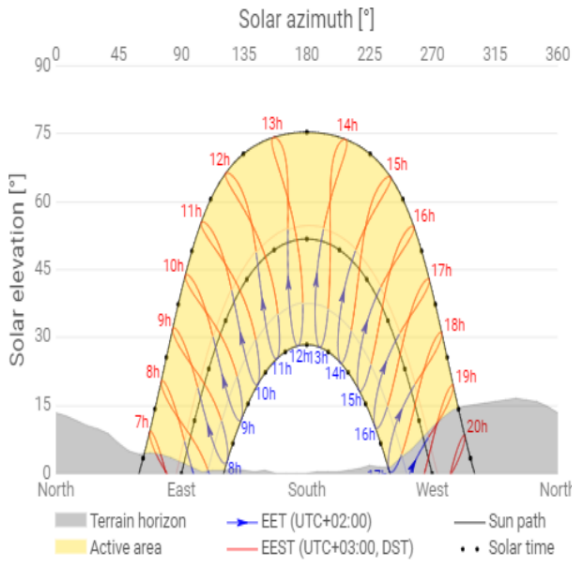


Figure 3.1: Horizon and sun path in the selected plant location, according to Global Solar Atlas v2.4 [92]

3.4. SYSTEM OVERVIEW

THIS section gives an overview of the system configuration, as it is presented in Figure 3.2. As it can be seen, the system feedstocks are water and captured CO_2 , while the

system product is methanol. The CO_2 is captured from the flue gases of a cement plant and supplied by TITAN cement plant at the given specifications of Table 3.3.

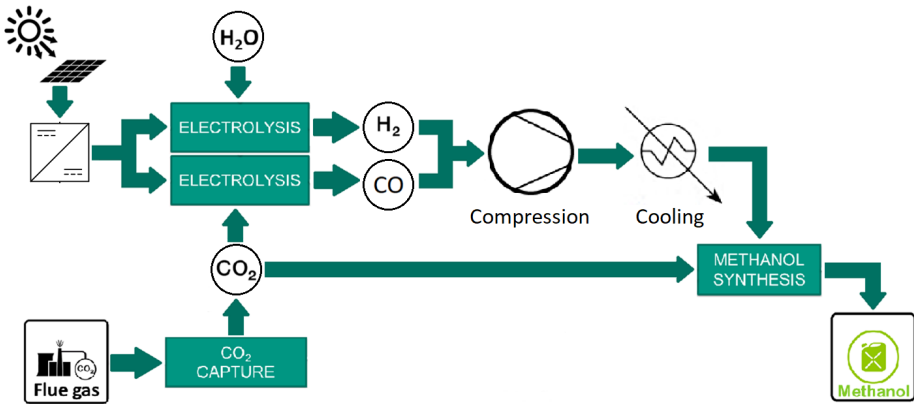


Figure 3.2: Graphic design of the main system

According to the selected methanol synthesis process (see Table 3.9), a mixture of CO_2 , CO and H_2 (i.e. the so-called syngas) needs to be supplied to a methanol reactor. The CO is provided by the CO_2 electrolyzers, while H_2 is provided by the H_2O electrolyzers. As it was mentioned in section 3.2, the CO_2 will be supplied at the required specifications of the methanol reactor (see Table 3.10). Therefore, CO_2 is not further processed by the system (i.e. it is fed only to the CO_2 electrolyzers and methanol reactor).

The energy source of the system is solar energy and PV panels are exploited for converting the sunlight into electricity. The CO_2 and H_2O electrolyzers are directly connected to the PV panels, without the use of batteries. Power electronics are used for regulating the current and voltage to the operating level of the system equipment. More specifically, DC-DC converters are exploited and connected between the PVs and the electrolyzers. DC-DC converters have been selected, because the PVs produce DC voltage and the rest of the system (i.e. electrolyzers etc.) runs on DC voltage.

Both types of electrolyzers consist of many stacks, which are connected in parallel, so that the electrolyzers can operate dynamically. Since the PVs power output is not constant, the electrolyzers will be able to follow this intermittent power output by switching on and off their stacks. The required number of stacks in operation depends on the PVs power output and the defined efficiency range of the electrolyzer. More information about that is given in section 3.6, where the system's control logic is presented.

According to the syngas specifications (see Table 3.10), H_2 and CO (produced via electrolysis) need to be compressed and cooled, before they are fed into the methanol reactor. As far as electrolysis is concerned, the outlet pressure of both gases is lower than the preferred one. Due to compression, both gases need to be cooled, because their tem-

perature is higher than the preferred one. The electricity for the compressors and cooling units is also supplied by the PVs. The required electrical power for this auxiliary equipment is subtracted from the power output of the DC-DC converters and subsequently the difference of this subtraction is fed into the electrolyzers. In the subsection 3.9.5, more information about the power supply of the whole system is given.

Contrary to the electrolyzers, the methanol reactor operates continuously and is independent from the intermittent PVs power output. This can be achieved by the exploitation of buffer tanks, which are installed between the syngas production and methanol reactor. Therefore, the compressed and cooled CO and H₂ are stored in buffer tanks, before they are fed into the methanol reactor. In the following sections of this chapter, the design of the system's equipment and processes is presented. Finally, the MATLAB code written for this system is included in Appendix C.

3.5. SOLAR ENERGY

SOLAR energy has been chosen as the renewable energy source of this thesis system (i.e. supplying electrical energy to electrolyzers, auxiliary equipment etc.). The platform Photovoltaic Geographical Information System (PVGIS) 5.1 of the EU Science Hub has been used for the relevant data acquisition [94]. More specifically, the solar radiation and the performance of the potential PV system were estimated by PVGIS 5.1 for the selected plant location. In Figure A.2 of Appendix A, a screenshot of this platform (including the chosen parameters for the data download) can be seen.

The most recent records in PVGIS were relevant to the year 2016, which was a leap year with 8784 hours. All the acquired data was estimated for the year 2016 and consists of one value for every hour over the year. Based on the PVGIS user's manual, the data-set PVGIS-SARAH is suitable for the selected plant location, because this is the only data-set that covers Europe [95]. *PVGIS uses the global in-plane irradiance for the estimation of all the PV power outputs* [95]. The calculations of PVGIS are explained in Appendix B.

In Table 3.4, all the chosen parameters for the data download can be seen. Based on the PVGIS manual, the estimated overall system losses are equal to 14% by default and they contain losses in cables, power inverters, dirt on the modules etc [95]. However, all the acquired data was estimated without system losses (i.e. 0%), because it is assumed that the PV plant and methanol plant will be very close to each other, in order to neglect the losses in cables. Also, the efficiency curve of a power inverter will be taken into account in the design of this thesis system (see section 3.9.4).

In Figure 3.3, the global horizontal irradiation (GHI), direct normal irradiation (DNI) and global irradiation at the optimal inclination angle can be seen for the selected plant location in 2016. All these values represent the monthly sum of the solar radiation energy that hits one square meter, measured in kWh/m². GHI refers to the solar radiation that hits an horizontal plane (i.e. to the ground) and includes DNI and the diffuse horizontal irradiation (DHI) [95]. DNI refers to the solar radiation that hits a plane, which always faces the sun [95]. The global irradiation at the optimal inclination angle refers to solar

Table 3.4: Parameters for the download of hourly radiation data from PVGIS 5.1

Parameter	Value
Platform	PVGIS 5.1
Solar radiation database	PVGIS-SARAH
Year	2016
Latitude	38.108977°
Longitude	23.525769°
Mounting type	Fixed plane
Slope and Azimuth of PV modules	Optimized by the platform at 32° and -2° (respectively)
PV technology	Crystalline silicon (c-Si)
System loss	0%
Outputs	PV power and Radiation components (i.e. direct, diffuse and ground-reflected solar radiation)

radiation that hits a plane, which faces in the direction of the equator at the optimal inclination angle (with the highest annual irradiation) [95].

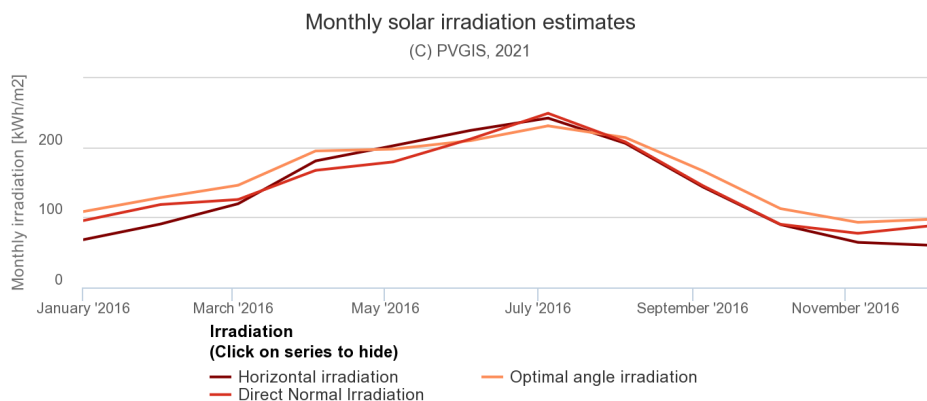


Figure 3.3: Monthly solar irradiation for the selected plant location in 2016, from PVGIS [94]

In Figure 3.4, the average daily solar radiation per month can be seen for the selected plant location in 2016. This Figure shows the seasonal variation of the daily solar radiation, in terms of GHI, DNI and DHI. The data of this Figure was generated for a fixed plane with slope of 32° and azimuth of -2° (see Table 3.4).

3.6. CONTROL LOGIC

SYSTEM'S control logic is a deterministic method that operates on a set of rules. Control logic affects the system operation and is the key part of this system. The main scope of this control logic is the control of the electrolyzers' dynamic operation (inside

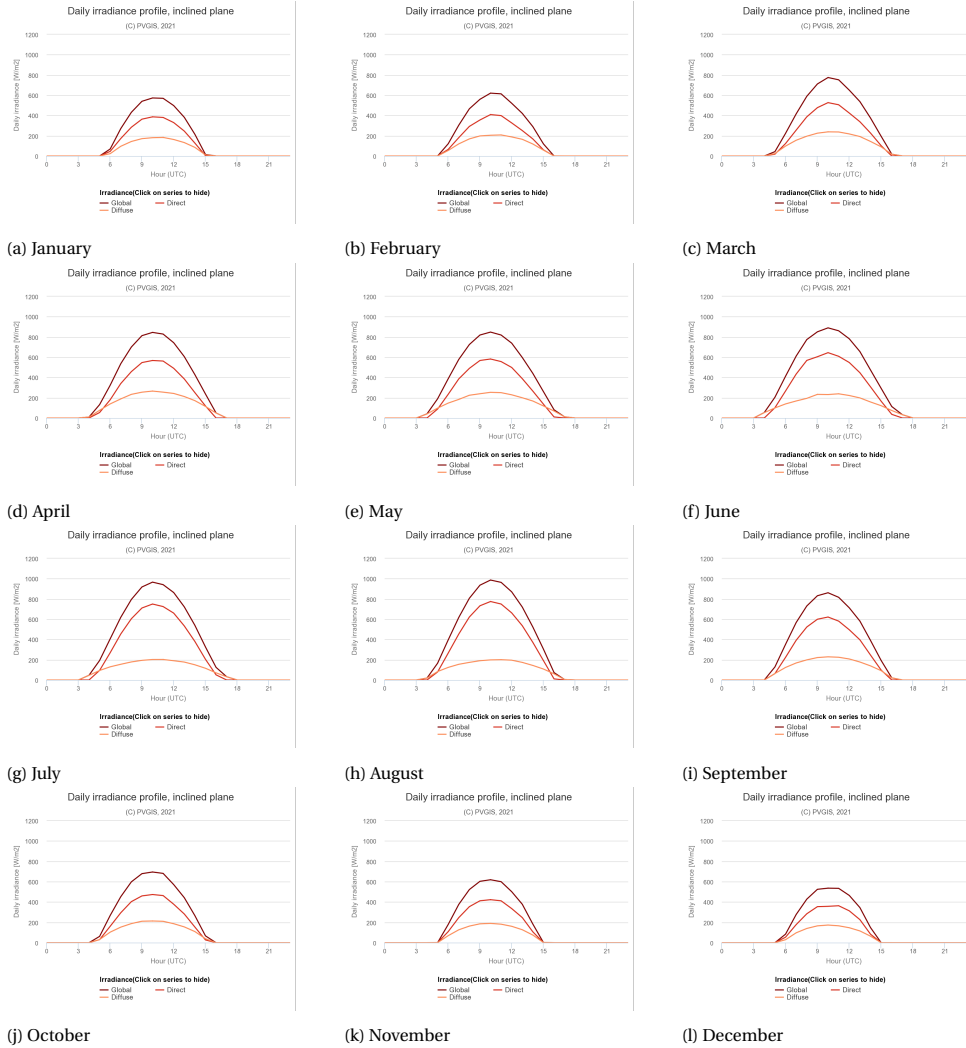


Figure 3.4: Average daily irradiance per month for the selected plant location in 2016, from PVGIS [94]

their efficiency range) and the decision on whether or not PVs power output should be dumped. The flowchart of the system's control logic is illustrated in Figure 3.5 and explained below.

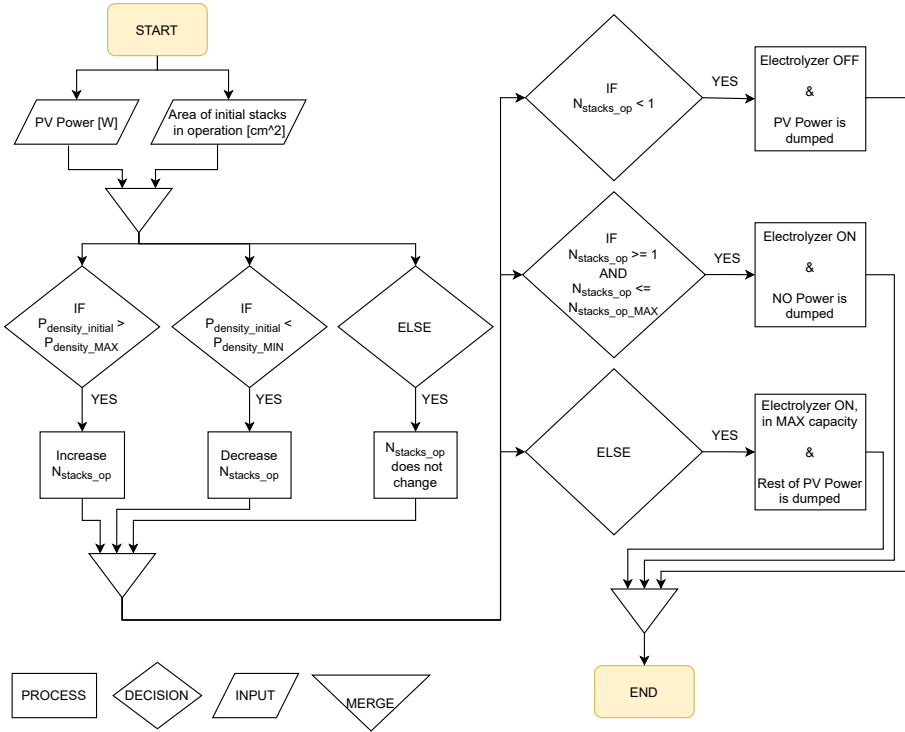


Figure 3.5: Control logic of the system

As far as the implementation of the control logic in Simulink is concerned, the Figure D.7 of Appendix D presents an overview of the relevant block. As it was previously mentioned in section 3.4, the required electrical power for the auxiliary equipment is subtracted from the power output of the DC-DC converters and subsequently the difference of this subtraction is fed and split into the electrolyzers. In the aforementioned Figure, the subtraction and the power split can be seen. More information about the power split is given in sections 4.5 and 4.6.

As soon as it has been estimated how much power will flow to the electrolyzers, the control logic of Figure 3.5 defines how many stacks in each electrolyzer should be in operation (i.e. $N_{\text{stacks,op}}$) and whether or not this input power should be dumped. Everything starts with taking into account the PVs power output and the initial reaction area of each electrolyzer. The initial reaction area is based on the initial $N_{\text{stacks,op}}$, which is equal to 40 stacks for each electrolyzer. Then, the initial power density of each electrolyzer ($P_{\text{density,initial}}$) is estimated.

The next step of the control logic is to define how many stacks should be in operation for each electrolyzer. In Appendix D, the Simulink models for the control logic of CO₂ and H₂O electrolyzers can be seen in Figures D.8 and D.9, respectively. For this estimation, two parameters should be taken into account for each electrolyzer: (i) the $P_{\text{density,initial}}$ and (ii) the acceptable range of P_{density} . In Tables 3.5 and 3.6, the selected range of P_{density} for the CO₂ and H₂O electrolyzers can be seen, respectively. In this step, there are 3 cases, as follows:

1. If the $P_{\text{density,initial}}$ is greater than the maximum P_{density} , then the $N_{\text{stacks,op}}$ should be increased, until the $P_{\text{density,initial}}$ is in the acceptable range. Increasing the $N_{\text{stacks,op}}$ means that the total reaction area of the electrolyzer increases as well and therefore the P_{density} decreases.
2. If the $P_{\text{density,initial}}$ is lower than the minimum P_{density} , then the $N_{\text{stacks,op}}$ should be decreased, until the $P_{\text{density,initial}}$ is in the acceptable range. Decreasing the $N_{\text{stacks,op}}$ means that the total reaction area of the electrolyzer decreases as well and therefore the P_{density} increases.
3. Otherwise, if the $P_{\text{density,initial}}$ is in the acceptable range, then the $N_{\text{stacks,op}}$ remains unchanged.

The above estimation step may result in decimal values for the $N_{\text{stacks,op}}$. But, this is not acceptable, since it is not possible for an electrolyzer to operate a fraction of a single stack. Therefore, the $N_{\text{stacks,op}}$ must always be an integer. This can be achieved by rounding up or down the $N_{\text{stacks,op}}$, when it should be increased or decreased, respectively. For example, if the $N_{\text{stacks,op}}$ should be increased and equals to 1.2, then it is rounded up to 2.

The final step of the control logic is to check whether or not the $N_{\text{stacks,op}}$ is in its acceptable range and whether or not the input power of the electrolyzers should be dumped. For these controls, two parameters have to be taken into account: (i) the $N_{\text{stacks,op}}$, as it was estimated above and (ii) the acceptable range of $N_{\text{stacks,op}}$. It has been decided that the maximum $N_{\text{stacks,op}}$ for the CO₂ and H₂O electrolyzers is 40 and 100 stacks, respectively (more information in sections 4.5 and 4.6). In this step, there are 3 cases, as follows:

1. If the $N_{\text{stacks,op}}$ is lower than 1, then the electrolyzer should be OFF. An electrolyzer cannot operate a fraction of a single stack. In this case, the input power of the electrolyzer should be dumped, because it cannot be exploited.
2. If the $N_{\text{stacks,op}}$ is greater than or equal to 1 and lower than or equal to its maximum value, then the electrolyzer is ON and all its input power is exploited. So, no power is dumped.
3. If the $N_{\text{stacks,op}}$ is greater than its maximum value, then the electrolyzer operates at its full capacity. The rest of the input power, which cannot be exploited, should be dumped.

As soon as the $N_{\text{stacks,op}}$ is estimated for each electrolyzer, the control logic ends and the PVs power output is either fed into the electrolyzers or dumped. This control logic

guarantees that the electrolyzers will either operate inside their selected efficiency range or not operate at all. The selected efficiency ranges for the CO₂ and H₂O electrolyzers can be seen in Tables 3.5 and 3.6, respectively. Moreover, the resulted efficiencies for the CO₂ and H₂O electrolyzers can be seen in Tables 4.4 and 4.5, respectively. Finally, the outcome of this control logic is the dynamic operation of the electrolyzers (see Figures 4.1 and 4.2 for the CO₂ electrolyzer and Figure 4.3 for the H₂O electrolyzer).

3.7. CO₂ ELECTROLYZER

POLYMER electrolyte membrane (PEM) electrolysis with gas diffusion electrodes (GDE) is chosen for the CO₂ reduction in this thesis system. In such low-temperature electrolysis systems, there is no liquid electrolyte and the electrodes are separated by a PEM membrane (i.e. solid state electrolyte). Also, GDEs are installed in both electrodes, so that the CO₂ mass transport between the electrocatalysts and the reactants (at the electrodes surface) is more efficient.

Based on the information gathered in section 2.4, the PEM electrolyzers offer good stability and have high ionic conductivity. The high ionic conductivity means that the cell resistance is low, because the PEM membrane is very thin. Since the PEM electrolyzer is combined with GDEs in both electrodes, the conversion rate of CO₂ is higher, because higher current densities and a higher Faradaic efficiency can be achieved. A major disadvantage of this technology is that if the PEM membrane dries, then the ion transport will negatively be affected. Therefore, it is assumed that the PEM membrane will not be allowed to get dried in this thesis system.

The rest of CO₂ electrolysis technologies were not chosen for this project due to the following reasons:

- Although, SOEC electrolyzers are very attractive, because they can exploit the waste heat of industrial processes and have high CO₂ conversion efficiencies, they are excluded from this project. This technology is not mature, not widely commercialized and can be difficult adapted to the intermittent nature of renewables.
- MCEC electrolyzers are also excluded from this project, because they are still on laboratory scale and under development.
- H-cell reactors is a mature technology, but they were not chosen for this project, because they are not suitable for industrial applications (i.e. low CO₂ conversion efficiency). Such electrolyzers have high cell resistance, operate at low current densities and the CO₂ mass transport is limited in aqueous solutions.

The market size of CO₂ electrolyzers is relatively small and therefore limited information about the performance of this machinery can be extracted. That's why; it has been chosen to design a PEM CO₂ electrolyzer for this project, which will be able to follow and exploit (as much as possible) the intermittent power output of the PV panels. The electrolyzer design is based on commercial electrolyzers and manufacturing practices. For the purpose of this study, an alkaline polymer electrolyte (APE) electrolyzer has

been chosen. Such electrolyzers belong in the group of PEM electrolyzers. The specifications of the APE electrolyzer can be seen in Table 3.5. In the following subsections, the electrolyzer design, specifications and performance parameters are presented.

Table 3.5: Specifications of the APE CO₂ electrolyzer

Specification	Value
Type	Polymer electrolyte membrane (PEM) electrolysis
Electrolyte	Alkaline polymer electrolyte membrane (APEM) [96]
Membrane Thickness	30 μm [96]
Electrodes	Gas diffusion electrodes (GDE) [96]
Cathode	Cobalt phthalocyanine (CoPc) [96]
Anode	Iridium oxide (IrO ₂) [96]
Feed to the Cathode	Dry CO ₂ at 31.25 sccm/cm ² [96]
Feed to the Anode	Pure water [96]
Operating Temperature	60°C [96]
Operating Pressure	10 bar [97]
Connection of Stacks	In parallel
Connection of cells	In series
Cells per stack	199 [98]
Area of each cell, A_{cell}	1000 cm ² [99]
CO purity	99.9%
H ₂ purity	99.9%
Cell Voltage Range, V_{cell}	1.95 - 2.85 V
Current Density Range, J	13.95 - 203.1 mA/cm ²
Power Density Range, P_{density}	27.25 - 578.84 mW/cm ²
Energy Efficiency Range	45 - 55%

3.7.1. DESIGN

The APE electrolyzer for this project is designed by scaling up a cell of an APE CO₂ electrolyzer, whose performance parameters are included in the study of Yin et al. [96]. In the APE cell, gas diffusion electrodes are employed and the APE membrane (between the electrodes) is 30 μm wide [96]. The APE membrane encourages the long-term operation of the cell and facilitates its maintenance, because there is no KOH or KHCO₃ solution as an electrolyte (i.e. no risk of cell's failure due to solution's leakage on the cathode) [96]. Also, in this study, two kinds of cathode catalysts have been tested: i) gold (Au) and ii) cobalt phthalocyanine (CoPc) [96]. The anode catalyst is made of iridium oxide (IrO₂) [96]. The structure of the APE cell for CO₂ electrolysis can be seen in Figure 3.6 [96]. As it can be seen, dry CO₂ is fed to the cathode and pure water is fed to the anode [96].

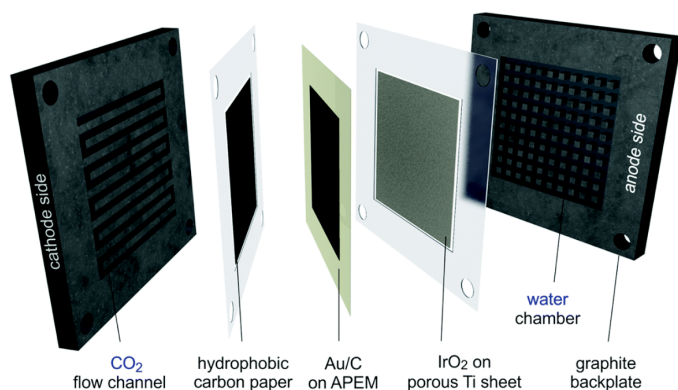


Figure 3.6: Structure of the APE cell for CO₂ electrolysis [96]

It is assumed that the APE electrolyzer of this thesis has the same aforementioned design specifications, structure and performance parameters as the APE cell that was studied by Yin et al. [96]. Moreover, it is assumed that the cathode of the APE electrolyzer for this project is made of CoPc and not Au, because CoPc is a non-precious and more commercial metal compared to Au. The model of this thesis APE electrolyzer was built in MATLAB/Simulink.

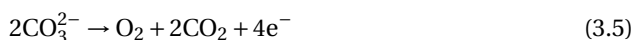
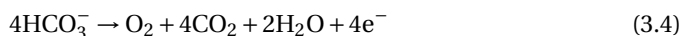
3.7.2. REACTIONS

The electrolysis reactions in the chosen APE cell are described in the following equations [96]. The initial charge carrier in the APE cell is hydroxide (OH⁻) [96]. When the APE cell is set to operation, then the cell will be carbonated (because CO₂ will be fed to it) and the OH⁻ will be partially replaced by CO₃²⁻ and HCO₃⁻ [96]. The APE membrane allows the anions transport from cathode to anode, encouraging the CO₂ reduction. Another role of the APE membrane is that it keeps the cell's environment alkaline (compared to a KHCO₃ solution) and this is beneficial for the CO₂ reduction reaction over the H₂ evolution reaction (HER) [96]. For the purpose of this thesis, it is assumed that the following reactions occur in the APE CO₂ electrolyzer.

Cathodic reactions:



Anodic reactions:



Overall cell reactions:



3.7.3. OPERATING CONDITIONS

According to the study of Yin et al., the optimal operating temperature for the APE cell is 50-60°C, whereby the Faradaic efficiency of CO production (FE_{CO}) is around 90% and the cell voltage is around 2.85V [96]. Also, the performance parameters of this cell were tested at 60°C in the aforementioned study. Therefore, the operating temperature of the APE electrolyzer for this project is assumed to be equal to 60°C. A water heat exchanger is assumed to be installed in the system, for keeping the electrolyzer temperature constant at 60°C.

The tested APE cell has an area of 3.2 cm² and the CO₂ is fed to the cathode at 100 sccm (standard cubic centimeters per minute) [96]. Therefore, it is assumed that the specific CO₂ feed rate for this thesis electrolyzer is equal to 31.25 sccm/cm². Finally, the operating pressure of this thesis CO₂ electrolyzer is assumed to be equal to 10 bar, because the commercial water electrolyzer HySTAT[®]-60-10 (manufactured by Hydrogenics) operates at the same pressure [97].

3.7.4. PERFORMANCE PARAMETERS

In Figure 3.7, the J- V_{cell} curve of the APE cell (with CoPc cathode) can be seen, when the cell operates at 60°C [96]. This curve correlates the current density J (mA/cm²) and cell voltage V_{cell} (V). As shown in this Figure, V_{cell} increases continuously with J , reaching its maximum value of 2.85V at 200 mA/cm².

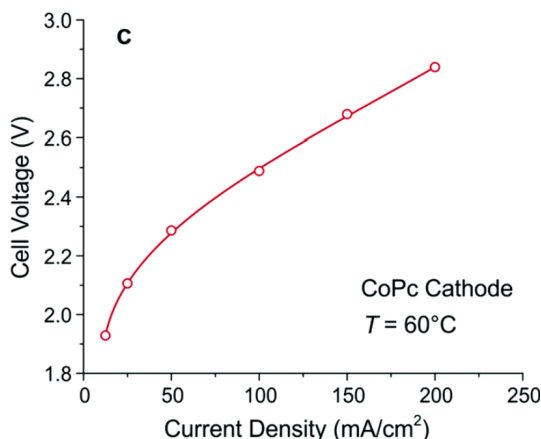


Figure 3.7: Experimental J-V curve, related to the cell performance of the APE CO₂ electrolyzer, at an operating temperature of 60°C [96]

In Figure 3.8, the energy efficiency (EE) and Faradaic efficiencies of CO and H₂ pro-

duction (FE_{CO} and FE_{H_2} , respectively) can be seen, regarding the APE cell (with CoPc cathode) being operated at 60 °C [96]. As shown in this Figure, the FE_{CO} reaches its maximum value of 90% at 2.85V. Also, it seems that the optimal energy efficiency region appears at 2.1–2.3 V, whereby EE is around 55%.

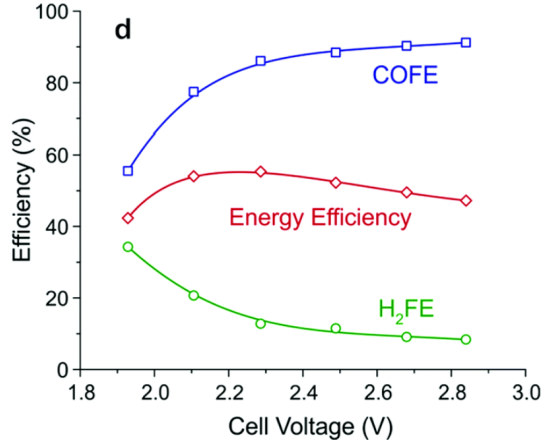


Figure 3.8: Experimental energy efficiency (EE) and Faradaic efficiencies of CO and H₂ production (FE_{CO} and FE_{H_2} , respectively), related to the cell performance of the APE CO₂ electrolyzer, at an operating temperature of 60°C [96]

By exploiting the data of Figure 3.7, we can estimate the power density ($P_{density}$), using the equation 3.8. Therefore, there is a unique value of $P_{density}$ for every point on the J- V_{cell} curve.

$$P_{density} = J \times V_{cell}, \quad [mW/cm^2] \quad (3.8)$$

Figures 3.7 and 3.8 were inputted into Simulink as Lookup tables. Based on Simulink and Figure 3.8, the V_{cell} must range from 1.95V to 2.85V, so that the EE is at least 45% (reaching its maximum value of 55%). Subsequently, the J must range from 13.95 mA/cm² to 203.1 mA/cm², based on Figure 3.7. Therefore, the operational range of $P_{density}$ is 27.25-578.84 mW/cm² for the aforementioned EE range.

Finally, it is assumed that the APE CO₂ electrolyzer for this project produces high purity CO and H₂ (i.e. 99.9%) and follows the performance curves of Figures 3.7 and 3.8. Also, the aforementioned ranges of V_{cell} , J, $P_{density}$ and EE are assumed to be used by this thesis CO₂ electrolyzer.

3.7.5. STRUCTURE DESIGN

It is assumed that the APE electrolyzer of this project will consist of stacks, which will be connected in parallel. Each stack will consist of 199 cells, which will be connected in series, according to manufacturing practices for commercial electrolyzers of scale in MW

[98]. The area of each cell is assumed to be 1000 cm², based on the commercial electrolyzer HySTAT[®]-60-10 [99]. Therefore, each cell of the APE electrolyzer of this project follows the J-V_{cell} curve of Figure 3.7 and the V_{cell}-EE, V_{cell}-FE_{CO} and V_{cell}-FE_{H2} curves of Figure 3.8.

3.7.6. MODEL IMPLEMENTATION

As it was previously mentioned in the subsection 3.7.1, the model of the APE CO₂ electrolyzer of this thesis was implemented in MATLAB/Simulink (see Figure D.1 in Appendix D). The implementation steps are as follows:

1. Based on equation 3.8 and Figures 3.7 and 3.8, five Lookup tables were created in Simulink: i) P_{density} - V_{cell}, ii) V_{cell} - J, iii) V_{cell} - EE, iv) V_{cell} - FE_{CO} and v) V_{cell} - FE_{H2}.
2. P_{density} is calculated according to the delivered power (that flows from the PVs to the electrolyzer) and the active area of the CO₂ electrolyzer. The active area of the electrolyzer depends on the number of stacks that are in operation.
3. V_{cell} is estimated based on the calculated P_{density} and the relevant Lookup table.
4. Subsequently, the values of J, EE, FE_{CO} and FE_{H2} are estimated based on V_{cell} and the relevant Lookup tables.
5. For the purpose of the results verification, the energy efficiency of the overall cell reaction (see equation 3.6), η , can be estimated using the following equation [96]:

$$\eta = \frac{\Delta H}{n_e \times F \times V_{cell}}, \quad [\%] \quad (3.9)$$

where ΔH stands for the enthalpy change of the overall cell reaction (see equation 3.6) and is equal to 283 kJ/mol [96]. Also, n_e is the number of electrons transferred (i.e. 2) and F is the Faraday constant (i.e. 96485 C/mol).

6. Next, the production rate of CO per cell ($N_{CO,cell}$) can be estimated using the following equation [96]:

$$N_{CO,cell} = \frac{I_{cell} \times FE_{CO}}{n_e \times F} = \frac{J \times A_{cell} \times FE_{CO}}{n_e \times F}, \quad [\text{mol/h}] \quad (3.10)$$

where I_{cell} is the cell current and depends on J.

7. The production rate of H₂ per cell ($N_{H2,cell}$) can be estimated using the above equation and FE_{H2}:

$$N_{H2,cell} = \frac{I_{cell} \times FE_{H2}}{n_e \times F} = \frac{J \times A_{cell} \times FE_{H2}}{n_e \times F}, \quad [\text{mol/h}] \quad (3.11)$$

8. Finally, the total production rates of CO ($N_{CO,total}$) and H₂ ($N_{H2,total}$) can be estimated based on the number of cells (n_{cells}) that are in operation (see the following equations):

$$N_{CO,total} = N_{CO,cell} \times n_{cells}, \quad [\text{mol/h}] \quad (3.12)$$

$$N_{H2,total} = N_{H2,cell} \times n_{cells}, \quad [\text{mol/h}] \quad (3.13)$$

3.8. H₂O ELECTROLYZER

ALKALINE electrolysis (AEL) is chosen for the water splitting in this thesis system. Based on the information gathered in Table 2.2, the AEL technology is mature, reliable and widely used in many large scale applications. The main advantages of AEL technology over the PEM and SOEC technologies are its durability (up to 90,000 hours), low capital expenditures and low maintenance costs. The main disadvantage of AEL electrolyzers is that they have a limited dynamic operation and slow loading response (affecting negatively their efficiency and the gas purity). However, this disadvantage can be tackled, if the system components of an AEL electrolyzer are properly engineered to operate with an intermittent power supply [48].

The rest of water electrolysis technologies were not chosen for this project due to the following reasons:

- Although, SOEC technology is the most efficient electrolysis technology among all the others, it is excluded from this project, because it is on laboratory scale, very expensive, not mature and not currently suitable for large scale projects (with long-term operation).
- Despite the fact that PEM technology can be theoretically better adapted to the intermittent power output of renewable sources (compared to AEL and SOEC), this technology was also excluded from this project, because PEM is more expensive and has shorter lifetime, compared to AEL.

Taking into account the limited information on the performance of commercialized H₂O electrolyzers in dynamic operation, it has been chosen to design an AEL electrolyzer for this project. The electrolyzer is designed, in order to be able to follow the intermittent power output of the PV panels. The dynamic operation of the AEL electrolyzer gives the possibility for a better exploitation of PVs power output. The electrolyzer design is based on commercial electrolyzers and manufacturing practices. The specifications of the AEL electrolyzer can be seen in Table 3.6. In the following subsections, the electrolyzer design, specifications and performance parameters are presented.

3.8.1. DESIGN

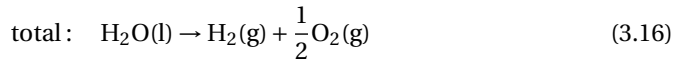
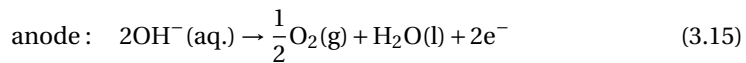
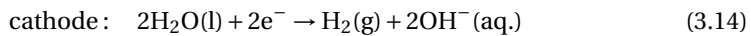
The AEL electrolyzer for this project is designed by scaling up the AEL water electrolyzer H₂ IGen 300/1/25, manufactured by Vandenberg Hydrogen Systems (now named Hydrogenics). The model of the AEL electrolyzer of this thesis was built in MATLAB/Simulink. In the study of Ursua et al. [100], experiments with the AEL electrolyzer H₂ IGen 300/1/25 were performed, regarding its electrical performance (based on its I-V curves, the hydrogen flow rate generated by the electrolyzer, the purity of H₂ & O₂ gases produced and its efficiency). Therefore, it is assumed that the AEL electrolyzer of this project has the same performance characteristics as the AEL electrolyzer H₂ IGen 300/1/25 that was studied by Ursua et al. [100]. It is also assumed that the half-reactions of the AEL electrolyzer H₂ IGen 300/1/25 occur in the AEL electrolyzer of this project.

Table 3.6: Specifications of the AEL water electrolyzer

Specification	Value
Type	Alkaline electrolysis
Electrolyte	KOH at 30 wt.% (7.64 mol/kg) [100]
Operating Temperature	65°C [100]
Operating Pressure	10 bar [97]
Connection of Stacks	In parallel
Connection of cells	In series
Cells per stack	199 [98]
Area of each cell, A _{cell}	1000 cm ² [99]
H ₂ purity	99.9% [97]
O ₂ purity	99.9% [97]
Cell Voltage Range, V _{cell}	1.387 - 1.703 V
Current Density Range, J	21.62 - 399.9 mA/cm ²
Power Density Range, P _{density}	30 - 681 mW/cm ²
Energy Efficiency Range	75.83 - 81.90%

3.8.2. REACTIONS

The overall electrolysis reaction in the chosen AEL electrolyzer is described in equation 3.16 [100]. The electrodes are immersed in an aqueous solution of KOH at 30 wt.% (7.64 mol/kg) as an electrolyte [100]. A typical set-up of an AEL electrolyzer can be seen in Figure 2.5. At the cathode, the reduction half-reaction takes place, where the water is reduced to hydroxide ions (OH⁻) and H₂ (see equation 3.14) [100]. The H₂ gas leaves the cathode and OH⁻ migrates to the anode through the diaphragm [100]. At the anode, the oxidation half-reaction takes place, where OH⁻ is oxidised to O₂ and water (see equation 3.15) [100]. So, the O₂ gas leaves the anode and the water returns to the KOH solution [100].



3.8.3. OPERATING CONDITIONS

The operating temperature of the AEL electrolyzer is assumed to be equal to the rated operating temperature of the AEL electrolyzer H₂ IGen 300/1/25 (i.e. 65°C), in order to maximize the ionic conductivity [100]. Also, it is assumed that a water heat exchanger keeps the operating temperature constant at 65°C. The experimental I-V curve of the AEL electrolyzer H₂ IGen 300/1/25 can be seen in Figure 3.9 [100]. As it can be seen in

this Figure, the effect of pressure is almost negligible on the I-V curve. That's why; it is assumed that the AEL electrolyzer of this project operates at a pressure of 10 bar. Another reason for assuming that the operating pressure is equal to 10 bar is that the commercial AEL electrolyzer HySTAT[®]-60-10 (manufactured by Hydrogenics) operates at the same pressure [97].

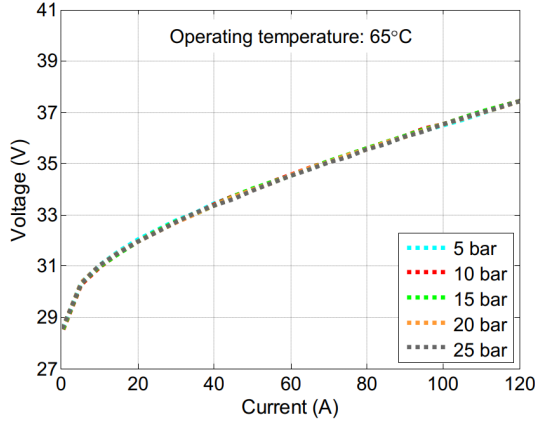


Figure 3.9: Experimental I-V curve for the AEL water electrolyzer H₂ IGen 300/1/25, in relation to pressure and for an operating temperature of 65°C [100]

3.8.4. PERFORMANCE PARAMETERS

The electrolyzer H₂ IGen 300/1/25 is formed by only 22 round cells, which are connected in series (forming 1 stack) and each cell has an area of 300 cm² [100]. This data was used for converting the I-V curve of Figure 3.9 to J-V_{cell} curve, where J stands for current density (mA/cm²) and V_{cell} stands for cell voltage (V). It is assumed that the AEL electrolyzer of this project has the same J-V_{cell} curve (at 10 bar and 65°C) as the electrolyzer H₂ IGen 300/1/25 (see Figure 3.10). This is an important step for the scale up of the electrolyzer H₂ IGen 300/1/25.

The specific energy consumption (Wh/Nm³) and the energy efficiency (EE) of the electrolyzer H₂ IGen 300/1/25 can be seen in Figure 3.11 (left and right, respectively) [100]. It is assumed that the AEL electrolyzer of this project has the same EE curve (at 10 bar and 65°C) as the electrolyzer H₂ IGen 300/1/25 has, but the current density (J) was taken into account and not the current (I). In Figure 3.12, the curve that correlates EE and J can be seen, regarding the electrolyzer of this project.

By combining Figures 3.10 and 3.12, we can estimate the operational range of power density (P_{density}), so that the energy efficiency (EE) ranges from 75.83% to 81.90%. Both Figures were inputted into Simulink as Lookup tables. Based on Simulink and Figure 3.12, J ranges from 21.62 mA/cm² to 399.9 mA/cm² for the aforementioned EE range. Also, based on Figure 3.10, V_{cell} ranges from 1.387 V to 1.703 V for the aforementioned

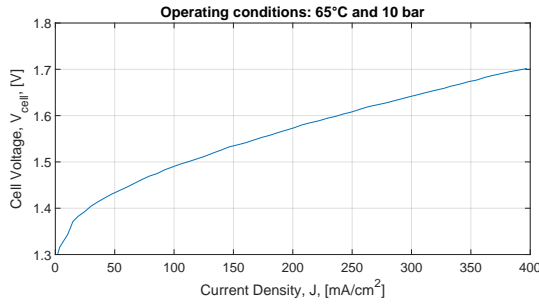


Figure 3.10: Experimental J - V_{cell} curve for the AEL water electrolyzer of this project, for the operating conditions of 65°C and 10 bar

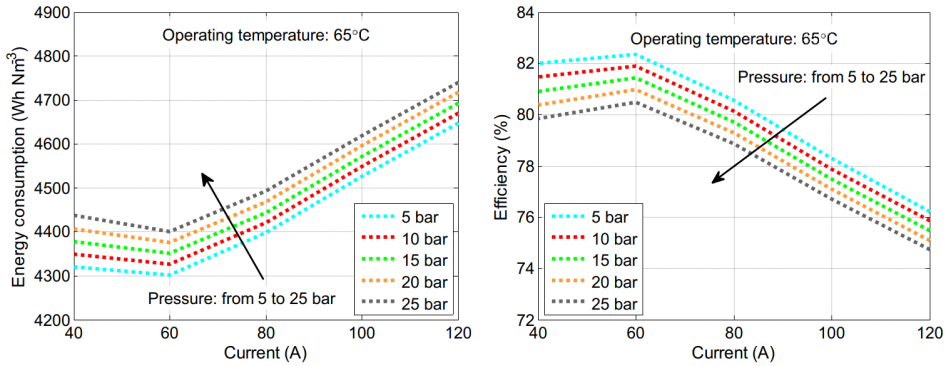


Figure 3.11: Specific energy consumption (left) and energy efficiency (right) for the AEL water electrolyzer, in relation to pressure and for an operating temperature of 65°C [100]

J range. The range of V_{cell} is acceptable, since the theoretical thermodynamic voltage for water electrolysis is 1.23 V [68]. Also, we can estimate the P_{density} for every point on the J - V_{cell} curve of Figure 3.10, by using the equation 3.8. Therefore, by combining both Figures, P_{density} must range from 30 mW/cm² to 681 mW/cm² for the aforementioned EE range.

Finally, it is assumed that the electrolyzer of this project will produce high purity H₂ (i.e. 99.9%), since the impurities of O₂ in the generated H₂ is less than 1 ppm [97]. Also, it is assumed that the O₂ generated by this electrolyzer will be 99.9% pure [97]. Such impurities exist, because there is a slight amount of H₂ and O₂ escaping through the diaphragm and electrolyte pathways [100].

3.8.5. STRUCTURE DESIGN

It is assumed that the AEL electrolyzer of this project will consist of stacks, which will be connected in parallel. Each stack will consist of 199 cells, which will be connected in series, according to manufacturing practices for AEL electrolyzers of scale in MW [98]. The area of each cell is assumed to be 1000 cm², based on the electrolyzer HySTAT[®]-60-

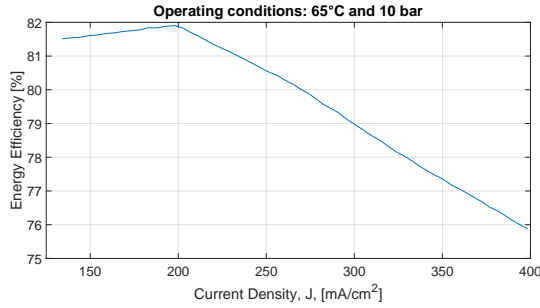


Figure 3.12: Experimental J-EE curve for the AEL water electrolyzer of this project, for the operating conditions of 65°C and 10 bar

10 [99]. Therefore, each cell of the AEL electrolyzer of this project follows the J- V_{cell} curve of Figure 3.10 and the J-EE curve of Figure 3.12.

3.8.6. MODEL IMPLEMENTATION

As it was previously mentioned in the subsection 3.8.1, the model of the AEL electrolyzer of this thesis was implemented in MATLAB/Simulink (see Figure D.2 in Appendix D). The implementation steps are as follows:

1. Based on equation 3.8 and Figures 3.10 and 3.12, three Lookup tables were created in Simulink: i) $P_{\text{density}} - J$, ii) $P_{\text{density}} - V_{\text{cell}}$ and iii) $J - EE$.
2. As in the case of the CO_2 electrolyzer (see subsection 3.7.6), P_{density} is calculated according to the delivered power (that flows from the PVs to the electrolyzer) and the active area of the H_2O electrolyzer.
3. Using the Lookup tables and the calculated P_{density} , J and V_{cell} are estimated.
4. Subsequently, the EE is estimated based on J and the relevant Lookup table.
5. The energy efficiency of the overall cell reaction (see equation 3.16), η , can be estimated using the equation 3.9. For the reaction 3.16, ΔH is equal to 285.8 kJ/mol [12]. As in the case of the reaction 3.6, n_e is equal to 2 for the reaction 3.16 as well.
6. Next, the Faradaic Efficiency of H_2 production per cell (FE_{H_2}) can be estimated using the following equation [96]:

$$FE_{\text{H}_2} = \frac{EE}{\eta}, \quad [\%] \quad (3.17)$$

7. As in the case of CO_2 electrolyzer, here the production rate of H_2 per cell ($N_{\text{H}_2, \text{cell}}$) can be estimated using the equation 3.11.
8. The production rate of O_2 per cell ($N_{\text{O}_2, \text{cell}}$) can be estimated as half of $N_{\text{H}_2, \text{cell}}$, according to the specifications of the electrolyzer HySTAT[®]-60-10 [99].

$$N_{\text{O}_2, \text{cell}} = \frac{N_{\text{H}_2, \text{cell}}}{2}, \quad [\text{mol/h}] \quad (3.18)$$

9. Finally, the total production rates of H₂ ($N_{\text{H}_2,\text{total}}$) and O₂ ($N_{\text{O}_2,\text{total}}$) depend on the number of cells (n_{cells}) that are in operation. As in the case of CO₂ electrolyzer, $N_{\text{H}_2,\text{total}}$ can be estimated using the equation 3.13. However, $N_{\text{O}_2,\text{total}}$ can be estimated using the following equation:

$$N_{\text{O}_2,\text{total}} = N_{\text{O}_2,\text{cell}} \times n_{\text{cells}}, \quad [\text{mol/h}] \quad (3.19)$$

3.9. AUXILIARY EQUIPMENT

AUXILIARY equipment plays an important role in processing systems, since it supports the inline production process and aims to maximize the overall processing efficiency and productivity [101]. For the system of this thesis, it is assumed that the auxiliary equipment is supplied power by the same PVs of the whole system and consists only of compressor, cooling units, buffer tanks and DC-DC converter. In the following subsections, the role and design of the auxiliary equipment is presented.

3.9.1. COMPRESSOR

The products of all the electrolyzers need to be compressed, before they are fed to the methanol converter. According to the specifications of this converter, the syngas inlet pressure must be equal to 69.7 bar (see Table 3.10). As it was previously mentioned in section 3.2, it is assumed that the CO₂ gas will be supplied to this thesis system at a pressure of 69.7 bar (see Table 3.3). As far as CO and H₂ gases are concerned, they are produced at 10 bar by both types of electrolyzers (see Tables 3.5 and 3.6). Therefore, CO and H₂ need to be compressed up to 69.7 bar. For simplicity, it is assumed that an adiabatic centrifugal compressor is employed, which is a single stage mechanical compressor. In Figure D.3 of Appendix D, the Simulink model of the compressor can be seen.

The following equations have been implemented in Simulink for estimating the required electrical power for the compression of CO and H₂ ($P_{\text{comp,CO}}$ and $P_{\text{comp,H}_2}$ respectively):

$$P_{\text{comp,CO}} = E_{\text{comp,CO}} \times N_{\text{CO,total}}, \quad [\text{W}] \quad (3.20)$$

$$P_{\text{comp,H}_2} = E_{\text{comp,H}_2} \times N_{\text{H}_2,\text{total}}, \quad [\text{W}] \quad (3.21)$$

where $E_{\text{comp,CO}}$ stands for the specific energy for the compression of CO in J/mol and $E_{\text{comp,H}_2}$ stands for the specific energy for the compression of H₂.

The specific energy for compression is estimated by MATLAB, using the following equations [102]:

$$E_{\text{comp,CO}} = \frac{R \times T_{1,\text{CO}} \times k_{\text{CO}} \times z_{\text{CO}}}{(k_{\text{CO}} - 1) \times \eta_a \times \eta_m} \times \left[\left(\frac{P_{2,\text{CO}}}{P_{1,\text{CO}}} \right)^{\frac{k_{\text{CO}}-1}{k_{\text{CO}}}} - 1 \right], \quad [\text{J/mol}] \quad (3.22)$$

$$E_{\text{comp,H}_2} = \frac{R \times T_{1,\text{H}_2} \times k_{\text{H}_2} \times z_{\text{H}_2}}{(k_{\text{H}_2} - 1) \times \eta_a \times \eta_m} \times \left[\left(\frac{P_{2,\text{H}_2}}{P_{1,\text{H}_2}} \right)^{\frac{k_{\text{H}_2}-1}{k_{\text{H}_2}}} - 1 \right], \quad [\text{J/mol}] \quad (3.23)$$

In Table 3.7, the parameters values and descriptions of the equations 3.22 and 3.23 are presented.

Table 3.7: Parameters values and descriptions for equations 3.22 and 3.23

Parameter	Value
Adiabatic compressor efficiency, η_a	$\eta_a = 80\%$ [103]
Mechanical driver efficiency of the compressor, η_m	$\eta_m = 98\%$ [103]
Universal gas constant, R	$R = 8.3145 \frac{\text{J}}{\text{K}\cdot\text{mol}}$
Adiabatic coefficient or specific heat ratio, k [104]	$k_{\text{CO}} = 1.4013$ $k_{\text{H}_2} = 1.4054$
Average compressibility factor, z [105]	$z_{\text{CO}} = 0.99964$ $z_{\text{H}_2} = 1.0006$
Temperature of CO and H ₂ before compression, T_1	$T_{1,\text{CO}} = 60^\circ\text{C}$, (see Table 3.5) $T_{1,\text{H}_2} = 65^\circ\text{C}$, (see Table 3.6)
Pressure of CO and H ₂ before compression, P_1	$P_{1,\text{CO}} = 10 \text{ bar}$, (see Table 3.5) $P_{1,\text{H}_2} = 10 \text{ bar}$, (see Table 3.6)
Pressure of CO and H ₂ after compression, P_2	$P_{2,\text{CO}} = 69.7 \text{ bar}$ $P_{2,\text{H}_2} = 69.7 \text{ bar}$

As far as the volumetric flow rates of the gases CO and H₂ are concerned, the relevant rates before compression (V_1) can be estimated in m³/h, using the ideal gas law (see the following equations) [106]. P_1 and T_1 are constants, but the molar flow rates of

these gases (n) are not, since n is based on the production of the electrolyzers (which is intermittent). Therefore, V_1 is variable.

$$P_{1,\text{CO}} \times V_{1,\text{CO}} = n_{\text{CO}} \times R \times T_{1,\text{CO}} \quad (3.24)$$

$$P_{1,\text{H}_2} \times V_{1,\text{H}_2} = n_{\text{H}_2} \times R \times T_{1,\text{H}_2} \quad (3.25)$$

Moreover, the volumetric flow rates of CO and H₂ after compression (V_2) can be estimated in m³/h, using the adiabatic condition (since an adiabatic compressor has been employed in this system) [107]. The adiabatic condition is presented in Equation 3.26. So, V_2 of CO and H₂ can be estimated using the equations 3.27 and 3.28. Since V_1 is variable and P_1 and P_2 are constants, V_2 is variable as well.

$$P \times V^k = \text{constant} \quad (3.26)$$

$$P_{1,\text{CO}} \times V_{1,\text{CO}}^{k_{\text{CO}}} = P_{2,\text{CO}} \times V_{2,\text{CO}}^{k_{\text{CO}}} \quad (3.27)$$

$$P_{1,\text{H}_2} \times V_{1,\text{H}_2}^{k_{\text{H}_2}} = P_{2,\text{H}_2} \times V_{2,\text{H}_2}^{k_{\text{H}_2}} \quad (3.28)$$

The volumetric flow rates of CO and H₂ need to be estimated at all steps of this thesis system, because they will be used for the modelling of the buffer tanks.

3.9.2. COOLING UNITS

As it was mentioned in the above section, the CO and H₂ gases need to be compressed through an adiabatic process. This means there is no heat or mass transfer between the system and its surroundings, during compression. Therefore, the temperature of CO and H₂ increases during compression. That's why; it is important to cool these gases down, before they are fed to the methanol converter. According to the specifications of the methanol converter, the syngas inlet temperature must be equal to 225°C (see Table 3.10). For simplicity, it is assumed that air-cooled chillers will be employed as cooling units in this project, based on the plant location and its air temperatures. In Figure D.4 of Appendix D, the Simulink model of the cooling units can be seen.

The temperature of CO and H₂ after compression (T_2) needs to be estimated in K, so that the cooling load can be estimated as well. Using the ideal gas law and taking into account that the molar flow rate of CO and H₂ do not change through compression (i.e. n_{CO} and n_{H_2}), V_2 can be estimated using the following equations [106]:

$$\frac{P_{1,\text{CO}} \times V_{1,\text{CO}}}{T_{1,\text{CO}}} = \frac{P_{2,\text{CO}} \times V_{2,\text{CO}}}{T_{2,\text{CO}}} \quad (3.29)$$

$$\frac{P_{1,\text{H}_2} \times V_{1,\text{H}_2}}{T_{1,\text{H}_2}} = \frac{P_{2,\text{H}_2} \times V_{2,\text{H}_2}}{T_{2,\text{H}_2}} \quad (3.30)$$

Moreover, the cooling load (Q_c) for the CO and H₂ compression can be estimated in J/h or W, using the following equation [108]:

$$Q_{c,CO} = n_{CO} \times C_{p,CO} \times (T_{3,CO} - T_{2,CO}), \quad \text{[J/h]} \quad (3.31)$$

$$Q_{c,H_2} = n_{H_2} \times C_{p,H_2} \times (T_{3,H_2} - T_{2,H_2}), \quad \text{[J/h]} \quad (3.32)$$

where the molar capacity of CO ($C_{p,CO}$) is equal to 30.47 J/mol*K at 600 K [109] and the molar capacity of H₂ (C_{p,H_2}) is equal to 29.32 J/mol*K at 600 K [110]. The temperature of CO and H₂ after cooling (T_3) is equal to the syngas inlet temperature (i.e. 225°C).

Finally, the applied electrical power for cooling (P_{cool}) depends on Q_c . The ratio of Q_c to P_{cool} is defined as the energy efficiency ratio (EER) and presented in the following equation [111]. A typical value of EER for air-cooled units is equal to 3 for cooling, according to Carrier [112]. The same EER value is assumed for this project.

$$EER = \frac{Q_c}{P_{cool}} \quad (3.33)$$

3.9.3. BUFFER TANKS

The syngas production is intermittent, because the electrolyzers operation follows the PVs power output. However, the downstream production of methanol is assumed to be a continuous process. That's why; the use of buffer tanks is required, so that the intermittent syngas production can be connected to the methanol reactor. Therefore, the operation of the methanol converter will be independent from the intermittent PVs power output. The specifications of the buffer tanks for this project can be seen in Table 3.8 and are explained in the following paragraphs.

It has been chosen that there will be one buffer tank for the storage of H₂ (produced by both types of electrolyzers) and one buffer tank for the storage of CO. The first buffer tanks has to be made out of a low alloy (Cr-Mo) steel, so that the hydrogen embrittlement is avoided. The latter buffer tank can be made out of carbon steel [113].

Both buffer tanks will store the gases at a pressure of 69.7 bar and a temperature of 225°C (according to the feeding specifications of the methanol reactor in Table 3.10). These feeding requirements are met due to the operation of the compressors and the cooling units (i.e. in previous steps of processing). At 225°C, CO and H₂ can be stored as gases, because the critical temperature of CO is -140.3°C and the critical temperature of H₂ is -240°C [114]. Also, H₂ can be stored in high-pressure gas cylinders with a maximum pressure of 200 bar [115].

So, the stored CO and H₂ will be ready to be fed into the methanol reactor, without further processing. But, in order to guarantee the continuous operation of the methanol reactor, the following conditions must be met:

- The buffer tanks must be of a floating-roof cone type, because the stored amount of CO and H₂ will vary, according to the operation of the methanol converter and the electrolyzers.

- CO and H₂ will be fed into the reactor at a constant rate
- There must always be enough stored CO and H₂ in the buffer tanks for the continuous operation of the methanol reactor

The syngas feeding rate will be estimated according to the syngas composition and the required hourly production of methanol. It is assumed that the methanol reactor will not operate during the whole year, but only for a fraction of it. This is necessary for the buffer tanks, so that they can store some necessary quantity of CO and H₂, before the start-up of the methanol reactor.

The following approach has been implemented, regarding the operation of the buffer tanks:

- If the syngas production is higher than the required feeding rate for the methanol reactor, then the surplus of syngas will be stored.
- If the syngas production is lower than the required feeding rate for the methanol reactor, which is in operation, then the deficit of syngas will be covered by its stored quantity in the buffer tanks.

Table 3.8: Specifications of the buffer tanks

Specification	Value
Type	floating-roof cone
Tank's material for storing CO	carbon steel
Tank's material for storing H ₂	low alloy (Cr-Mo) steel [113]
Operating pressure	69.7 bar
Operating temperature	225°C

3.9.4. DC-DC CONVERTER

The voltage level of the PVs power output needs to be converted, so that it can be fed into the rest of the system equipment (i.e. electrolyzers, compressors etc.). Therefore, a DC-DC converter is necessary for the power conversion, because the PVs produce DC voltage and the rest of the system equipment runs on DC voltage. As it was mentioned in section 3.5, the efficiency curve of a DC-DC converter is taken into account in the design of this thesis system. It is assumed that the DC-DC converter for this project will be based on the switching technology of Infineon CoolMOS IPW60R045CP MOSFET [116]. The efficiency curve of this switching technology is represented by the red line of Figure 3.13 and estimated for a maximum power input of 1 MW [116]. In case that, more than one DC-DC converter is required for this thesis project, then it is assumed, that all DC-DC converters are uniformly loaded and their operating efficiency is the same.

The model of the DC-DC converter was implemented in MATLAB/Simulink (see Figure D.5 in Appendix D). The implementation steps are as follows:

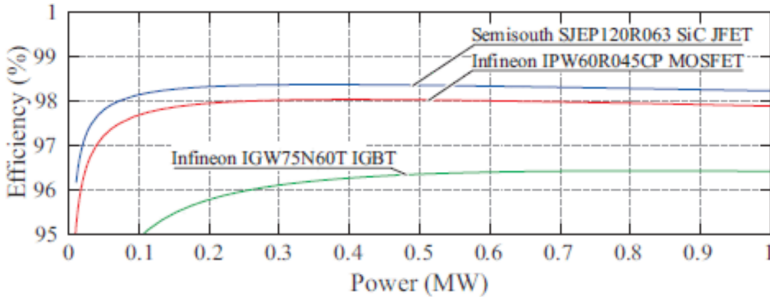


Figure 3.13: Energy efficiency of the DC-DC converter with the switching technology of Infineon CoolMOS IPW60R045CP MOSFET in relation to input power, using a DAB topology with triangular modulation[116]

1. The peak power output of the PVs is rounded up by MATLAB. For example, if the peak power output of the PVs is equal to 5.2 MW, then it is rounded up to 6 MW.
2. Since the efficiency curve of the DC-DC converter is estimated for a maximum power input of 1 MW, the required number of DC-DC converters, n_{DC} , can be estimated by the following equation:

$$n_{DC} = \frac{P_{PV,peak,rounded_up}}{P_{in,max}}, \quad [\text{pieces}] \quad (3.34)$$

In the aforementioned example, 6 DC-DC converters would be required. If the peak power output of the PVs was not rounded up, then 5.2 DC-DC converters would be required. But, a decimal value for the required number of DC-DC converters would not be possible. Also, the rounding-up gives some spare capacity to the system for power conversion.

3. Then, the hourly power output of the PVs is divided by n_{DC} , so that the power input of each DC-DC converter is estimated.

$$P_{in} = \frac{P_{PV,hourly}}{n_{DC}}, \quad [\text{MW}] \quad (3.35)$$

4. Using the Lookup table and the calculated P_{in} , the operating efficiency of each DC-DC converter is estimated.
5. Finally, the hourly power output of all PVs is multiplied with the operating efficiency of the DC-DC converters, so that the power output of the converters is estimated and fed into the rest of the system equipment.

3.9.5. POWER SUPPLY

For the purpose of this study, it has been decided that the PVs supply electrical energy not only to the electrolyzers, but also to the auxiliary equipment. The sum of the required electrical power for the auxiliary equipment is based on P_{cool} , $P_{comp,CO}$ and $P_{comp,H2}$, as they have been estimated by the equations 3.33, 3.20 and 3.21, respectively.

In Simulink, the total required electrical power for the auxiliary equipment is subtracted from the power output of the DC-DC converters. Subsequently, the difference of this subtraction is fed into the electrolyzers (see Figure D.7 in Appendix D). Using a "Unit Delay" block in Simulink, the signal of the total required electrical power for the auxiliary equipment is held and delayed by a sample time of 0.01, before the subtraction takes place (see Figures D.6 in Appendix D). The Simulink model of the whole system contains an algebraic loop and this loop needs to be broken, so that the aforementioned subtraction can take place. The break of this algebraic loop is possible, using a "Unit Delay" block with a discrete sample time.

3.10. METHANOL SYNTHESIS PROCESS

THE conversion of syngas to methanol is done through the CO₂ hydrogenation process (as it was described in section 2.2.2), which is assumed to be a continuous process for this project. As it was mentioned in section 3.9.3, the downstream production of methanol is assumed to be a continuous process, because buffer tanks are used for the connection between the syngas production and methanol reactor, which will be independent from the intermittent PVs power output. This downstream production process is based on the reaction of CO₂ hydrogenation (see equation 2.4) and the water-gas shift (WGS) reaction (see equation 2.5). Based on reaction 2.4, the water is a by-product, since a third of the fed H₂ is converted to water. That's why; CO needs to be fed into the methanol reactor for reacting with H₂O (see equation 2.5).

This process has been selected for this thesis system, because it has been decided that the syngas (i.e a mixture of CO, CO₂ and H₂) is fed into a commercial catalyst, which is made of copper-zinc oxide with aluminium oxide (CuO/ZnO/Al₂O₃). The use of CuO/ZnO/Al₂O₃ catalysts improves the catalytic activity (for operating temperatures higher than 250°C) [40] and enables the high selectivity of methanol (i.e. >99% with recycle) [117]. This methanol synthesis process (including the use of CuO/ZnO/Al₂O₃ catalysts) is followed for industrial scale projects [118].

In commercial units, the conversion of carbon to methanol ranges from 20% to 67% per-pass, depending on the syngas composition and the reactor type [119]. The remaining syngas that has not been converted can be recycled [117], [119], [120]. If the recycle ratio of the unconverted gas is between 2 and 5, then carbon can be almost completely converted to methanol (i.e. 93-99%) [117], [119]. Therefore, it is assumed that the non-converted syngas is recycled for this thesis system, so that the relevant conversion rate and methanol selectivity are equal to 99%.

As far as the syngas composition for CuO/ZnO/Al₂O₃ catalysts is concerned, a typical mixture is 65-90% H₂, 5-25% CO and 4-14% CO₂ and H₂:CO > 2:1 [119]. As it has been mentioned in section 2.2, the stoichiometric number (SN) of syngas needs to be greater than 2 for commercial applications, so that a surplus of hydrogen is fed into the methanol reactor. In Figure 3.14, some typical molar ratios of CO/H₂ and CO₂/H₂ for industrial applications can be seen [121]. It can be seen that the SN of these typical feeds is greater than 2 and their corresponding points lie below the stoichiometric line (whereby

the SN is equal to 2) [121]. It is assumed that the syngas produced by the electrolyzers of this thesis system meets the aforementioned requirements.

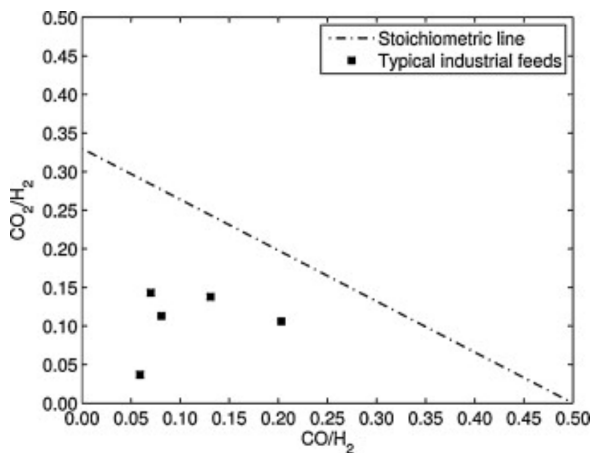


Figure 3.14: Typical syngas compositions for industrial applications along with the stoichiometric line [121]

For the purpose of this study, it is assumed that the methanol synthesis process of this thesis is based on the steady-state kinetic model of Bussche and Froment [122], which uses a CuO/ZnO/Al₂O₃ catalyst and is based on the aforementioned reactions [122]. The main features of the methanol synthesis process for this project can be seen in Table 3.9. Finally, a single-stage Lurgi quasi-isothermal reactor has been chosen for the catalytic conversion of syngas to methanol, because such reactors can operate in the temperature and pressure ranges of Table 3.9 and reach high conversion and recycle rates (for more information, see section 3.11).

3.11. METHANOL REACTOR

THE methanol reactor of this thesis system operates continuously and follows the steady-state kinetic model of Bussche and Froment [122], according to the simulation proposed by Chen et al. [123], because CuO/ZnO/Al₂O₃ catalysts and similar syngas compositions have been employed. As it will be presented below, the reactor's model of Chen et al. [123] meets the requirements of Table 3.9 for this project.

In the study of Chen et al. [123], a single-stage Lurgi quasi-isothermal reactor was simulated in Aspen Plus version v7.1 (see Figure 3.15). The reactor simulation was based on the following assumptions: i) unidimensional model, ii) negligible axial dispersion and heat conduction, iii) constant catalyst effectiveness and iv) energy losses to the surrounding are neglected [123].

This simulation was carried out for producing methanol of about 90 kT/year and the

Table 3.9: Main features of the methanol synthesis process

Specification	Value
Process type	CO ₂ hydrogenation based on the model of Bussche and Froment [122]
Catalyst	CuO/ZnO/Al ₂ O ₃
Range of process temperature	250-300°C [16], [40], [42]
Range of process pressure	50-100 bar [16], [40], [42]
Syngas composition	65-90% H ₂ , 5-25% CO and 4-14% CO ₂ and H ₂ :CO > 2:1 [119]
Stoichiometric number (SN) of syngas	>2
Methanol selectivity	>99% with recycle [117]
Conversion rate of syngas to methanol	93-99% with recycle (20-67% per-pass) [117], [119]
Recycle ratio	2-5 [119]
Reactor type	single-stage Lurgi quasi-isothermal

simulation data was compared with industrial data (with good agreement) [123]. Therefore, it has been decided that the reactor's model of Chen et al. [123] will be scaled down, so that the reactor of this project is able to fulfill the production capacity of 4 kT/year (see Table 3.1). The specifications of the methanol reactor for this project can be seen in Table 3.10 and are explained in the following paragraphs.

In the simulation study of Chen et al. [123], the reactor's length was 7m and its diameter was 0.04m, filled with particles of CuO/ZnO/Al₂O₃ catalyst. The catalyst cylindrical particles had a diameter of 5.4mm and a density of 1190kg/m³ [123]. Using this data, the estimated catalyst mass per tube is equal to 10.468 kg_{cat}/tube.

Iyer et al. [121] mentioned that a molar ratio of CO/H₂ 0.081, a molar ratio of CO₂/H₂ 0.113 and a SN of 4.6 have been used as feed specifications by the model of Chen et al. [123]. Similar molar ratios were reported by the study of Walid et al. [118] (i.e. H₂/CO₂ = 9 and H₂/CO = 12) for the simulation model of Chen et al. [123]. Since both studies present similar syngas composition for the model of Chen et al., it is assumed that the composition of the syngas produced by this thesis system is based on the aforementioned feed specifications (i.e. H₂ : CO₂ : CO = 83.8% : 9.5% : 6.7%).

Also, Dieterich et al. [119] have mentioned that the per-pass conversion of carbon to methanol was equal to 36% in the model of Chen et al. [123]. So, it is assumed that the methanol reactor of this project has the aforementioned conversion per-pass and an overall conversion of 99% with a recycle ratio of 2.75 (fulfilling the conversion requirements of Table 3.9).

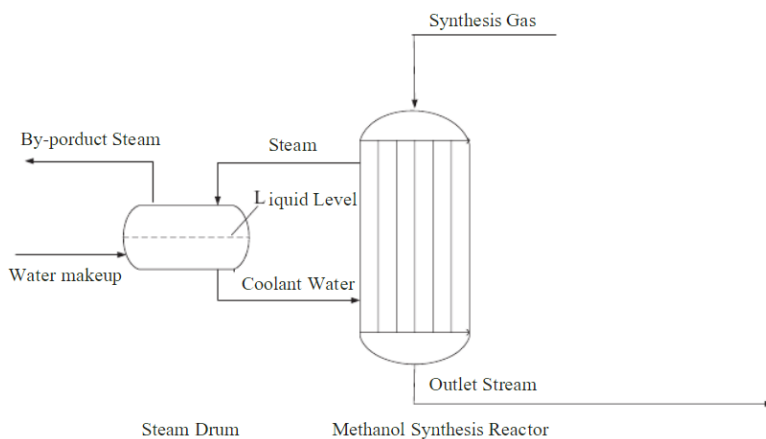


Figure 3.15: Flow diagram of a single-stage Lurgi quasi-isothermal reactor [123]

The simulation study of Chen et al. [123] showed that the required hourly methanol production was equal to 10526.4 kg/h, for reaching the capacity of 90 kT/year. Taking into account, that the reactor of this study consisted of 1620 tubes [123], the estimated methanol production per tube is equal to 6.498 kg/h/tube. Also, using the catalyst mass per tube, the estimated methanol production per catalyst particle is equal to 0.621 kg/kg_{cat}/h. Subsequently, using the molar mass of methanol (i.e. 32.04 g/mol), the estimated methanol molar production per catalyst particle is equal to 0.01939 mol/g_{cat}/h.

The scaling down of the reactor of Chen et al. [123] will be done, according to the specifications: i) catalyst mass per tube, ii) methanol production per tube, iii) methanol production per catalyst particle and iv) methanol molar production per catalyst particle. These specifications are important for defining the size of the methanol reactor and the required catalyst quantity. The reaction kinetics that take place in the reactor of Chen et al. [123] are presented in Appendix E.

Table 3.10: Specifications of the methanol reactor

Specification	Value
Reactor type	single-stage Lurgi quasi-isothermal
Reactor tube diameter	0.04 m [123]
Reactor length	7 m [123]
Catalyst	CuO/ZnO/Al ₂ O ₃
Catalyst particle shape	cylinder [123]
Catalyst diameter	5.4 mm [123]
Catalyst particle density	1190 kg/m ³ [123]
Catalyst mass per tube	10.468 kg _{cat} /tube
Steam drum pressure	29 bar [123]
Cooling water volumetric flow rate	13.8 m ³ /h [123]
Syngas composition	H ₂ : CO ₂ : CO = 83.8% : 9.5% : 6.7% [118], [121]
Syngas SN	4.6 [121]
Syngas inlet temperature	225°C [123]
Syngas inlet pressure	69.7 bar [123]
Conversion rate of syngas to methanol	99% (36% per-pass) [119]
Recycle ratio	2.75
Methanol selectivity	>99% [117]
Methanol outlet temperature	255°C [123]
Methanol outlet pressure	66.7 bar [123]
Methanol production per tube	6.498 kg/h/tube
Methanol production per catalyst particle	0.621 kg/kg _{cat} /h
Methanol molar production per catalyst particle	0.01939 mol/g _{cat} /h

4

SYSTEM SIZING AND PRODUCTION RESULTS

This chapter presents the sizing approach and production results of the proposed thesis system. The sizing approach was done through empirical analysis of the various system parameters and is presented in section 4.1. The estimated energy requirements and production output of the whole system are included in section 4.2. As soon as the system's energy requirements were estimated, the PV panels were sized (see section 4.3). The next sizing step was related to the size of the DC-DC converters (see section 4.4). The size and production results of the CO₂ and H₂O electrolyzers were based on the production output of the electrolyzers and are included in sections 4.5 and 4.6, respectively. In section 4.7, the size and production results of the methanol converter and the buffer tanks are presented. Moreover, the size and production results of the compressors and cooling units are presented in sections 4.8 and 4.9, respectively. In section 4.10, the amount of system's dumped energy is presented. Finally, the summary of this chapter is included in section 4.11.

4.1. SIZING APPROACH

THE system of this thesis project was sized by doing an empirical analysis of the various system parameters and not by using an optimisation tool. The system parameters were empirically analysed, so that a system equilibrium could be reached. The system equilibrium is defined as a relation between the system size and system efficiency. In other words, the target of the sizing approach is the minimization of the system size and the increase of the system efficiency.

The system sizing was done by following a backward approach (i.e. starting at the end of the system and going to the start). In this approach, it is assumed that some parameters are held as constants and the rest of the parameters are considered as variables. In Table 4.1, the constant and variable parameters of this approach can be seen. As soon

as the constant parameters were estimated, they were held as constants during the sizing approach. However, the variable parameters were not held constant, because they were changing until the system equilibrium was reached.

Table 4.1: Parameters of the system sizing approach

Ref. Number	Parameters	Constant	Variable
1	Installed peak PV power	x	
2	Number of stacks in H ₂ O electrolyzer	x	
3	Number of stacks in CO ₂ electrolyzer	x	
4	Power split between H ₂ O and CO ₂ electrolyzer		x
5	Tubes of methanol reactor		x
6	Buffer tanks capacity of H ₂ and CO		x
7	Feeding rates of f H ₂ and CO		x
8	Activation step of methanol reactor		x

Following the backward sizing approach, the system components were sized according to the following order:

1. PV panels
2. DC-DC Converters
3. CO₂ electrolyzer
4. Power split between H₂O and CO₂ electrolyzer
5. H₂O electrolyzer
6. Methanol Reactor
7. Buffer Tanks
8. Compressors and Cooling Units

4.2. ESTIMATIONS OF ENERGY REQUIREMENTS AND PRODUCTION OUTPUT

THE sizing backward approach aims to roughly estimate the energy requirements and production output in the whole system. It needs to be estimated how much electrical energy is necessary, so that the system can produce 4kT of methanol per year (see Table 4.2). The approach steps are as follows:

1. The mass of methanol needs to be converted to moles, using the molar mass of methanol (i.e. 32.04 g/mol).

$$N_{\text{CH}_3\text{OH}} = \frac{4 \text{ kT}_{\text{CH}_3\text{OH}}}{32.04 \text{ g/mol}_{\text{CH}_3\text{OH}}} = 124,836,153 \text{ mol}_{\text{CH}_3\text{OH}}$$

2. Since, one mole of methanol (CH_3OH) contains two moles of hydrogen (H_2), the required production of H_2 can be estimated. This estimation must take into account the conversion rate of the methanol reactor, which is equal to 99% (see Table 3.10). Therefore, the required amount of H_2 can be estimated, as follows:

$$N_{\text{H}_2} = \frac{124,836,153 \text{ mol}_{\text{CH}_3\text{OH}} \times 2}{99\%} = 252,194,248 \text{ mol}_{\text{H}_2}$$

Using the required amount of H_2 , we can estimate the required supply of water, which will be fed to the electrolyzer. One mole of H_2O is required for the production of one mole of H_2 via electrolysis. Therefore, the required supply of H_2O can be estimated as follows:

$$N_{\text{H}_2\text{O}} = N_{\text{H}_2} = 252,194,248 \text{ mol}_{\text{H}_2\text{O}}$$

3. According to the methanol reactor specifications, the syngas composition must be $\text{H}_2 : \text{CO}_2 : \text{CO} = 83.8\% : 9.5\% : 6.7\%$ (see Table 3.10). Using these ratios, the required amount of CO and CO_2 can be estimated, as follows:

$$N_{\text{CO}} = 252,194,248 \text{ mol}_{\text{H}_2} \times \frac{6.7\%}{83.8\%} = 20,163,502 \text{ mol}_{\text{CO}}$$

$$N_{\text{CO}_2} = 252,194,248 \text{ mol}_{\text{H}_2} \times \frac{9.5\%}{83.8\%} = 28,590,040 \text{ mol}_{\text{CO}_2}$$

As it has been mentioned in section 3.2, the required amount of CO_2 will be supplied by TITAN cement plant, fulfilling the required CO_2 specifications of Table 3.3.

Using the required amount of CO , we can estimate the required supply of CO_2 that has to be fed to the electrolyzer. One mole of CO_2 is required for the production of one mole of CO via electrolysis. Therefore, the required supply of CO_2 to the electrolyzer can be estimated as follows:

$$N_{\text{CO}_2,\text{electr}} = N_{\text{CO}} = 20,163,502 \text{ mol}_{\text{CO}_2}$$

4. The total energy required for the CO_2 electrolyzer can be estimated, using the energy required for CO_2 electrolysis, which is equal to 283 kJ/mol [96] and the required production of CO (see the following calculation). This estimation must take into account the energy efficiency of the CO_2 electrolyzer. According to Table 3.5 and Figure 3.8, the energy efficiency of the CO_2 electrolyzer ranges from 45-55%. Therefore, the energy efficiency of 50% is assumed for this estimation.

$$\frac{20,163,502 \text{ mol}_{\text{CO}} \times 283 \text{ kJ/mol}}{50\%} = 3.17 \times 10^9 \text{ Wh}$$

5. The total energy required for the H_2O electrolyzer is estimated like the total energy required for the CO_2 electrolyzer. The energy required for H_2O electrolysis is equal to 285.8 kJ/mol [12]. According to Table 3.6 and Figure 3.12, the energy efficiency

of the H₂O electrolyzer ranges from 75.83-81.90%. Therefore, the energy efficiency of 77% is assumed for this estimation.

As it was stated in the subsection 3.7.3, the Faradaic efficiency of CO production (FE_{CO}) is around 90% in the CO₂ electrolyzer [96]. Assuming that the production of 20,163,502 mol_{CO} is 90% of the total production output, then 2,240,389 mol_{H₂} will be produced in the CO₂ electrolyzer, due to HER. This amount of H₂ should be subtracted from the total required amount of H₂. The result of this subtraction must be produced by the H₂O electrolyzer. Therefore, the total energy required for the H₂O electrolyzer can be estimated, as follows:

$$\frac{(252,194,248 - 2,240,389) \text{ mol}_{\text{H}_2} \times 285.8 \text{ kJ/mol}}{77\%} = 2.58 \times 10^{10} \text{ Wh}$$

6. Next, the required energy for compression of CO and H₂ should be estimated, using the relevant specific energies for compression and the production amounts. According to Table 3.7 and the equation 3.22, the specific energy for the compression of CO is equal to 9.1725 kJ/mol_{CO}. Moreover, according to the same Table and the equation 3.23, the specific energy for the compression of H₂ is equal to 9.2016 kJ/mol_{H₂} and 9.3397 kJ/mol_{H₂}, when the H₂ is produced by the CO₂ and H₂O electrolyzers respectively.

Therefore, the required energy for the compression of CO is equal to:

$$20,163,502 \text{ mol}_{\text{CO}} \times 9.1725 \text{ kJ/mol} = 5.14 \times 10^7 \text{ Wh}$$

The required energy for the compression of H₂, produced by the CO₂ electrolyzer, is equal to:

$$2,240,389 \text{ mol}_{\text{H}_2} \times 9.2016 \text{ kJ/mol} = 5.73 \times 10^6 \text{ Wh}$$

The required energy for the compression of H₂, produced by the H₂O electrolyzer, is equal to:

$$(252,194,248 - 2,240,389) \text{ mol}_{\text{H}_2} \times 9.3397 \text{ kJ/mol} = 6.48 \times 10^8 \text{ Wh}$$

7. Next, the required energy for cooling of CO and H₂ should be estimated. This estimation is done according to the following steps:

- (a) In terms of simplicity, it is assumed that the total amount of CO and H₂ pro-

duced is fed uniformly (across the year) to the methanol converter.

$$\begin{aligned} \frac{20,163,502 \text{ mol}_{\text{CO}}}{8784 \text{ hours/year}} &= 2,295 \text{ mol}_{\text{CO}}/\text{hour} \\ \frac{2,240,389 \text{ mol}_{\text{H}_2}}{8784 \text{ hours/year}} &= 255 \text{ mol}_{\text{H}_2}/\text{hour} \text{ (produced by CO}_2 \\ &\text{electrolyzer)} \\ \frac{(252,194,248 - 2,240,389) \text{ mol}_{\text{H}_2}}{8784 \text{ hours/year}} &= 28,456 \text{ mol}_{\text{H}_2}/\text{hour} \text{ (produced} \\ &\text{by H}_2\text{O electrolyzer)} \end{aligned}$$

- (b) As far as the CO production rate (n_{CO}) is concerned, its volumetric flow rate before compression ($V_{1,\text{CO}}$) needs to be calculated, using the equation 3.24. The values of R , $P_{1,\text{CO}}$ and $T_{1,\text{CO}}$ from Table 3.7 will be used.

$$\begin{aligned} V_{1,\text{CO}} &= \frac{2,295 \text{ mol}_{\text{CO}}/\text{hour} \times 8.3145 \text{ m}^3 \cdot \text{Pa}/\text{K} \cdot \text{mol} \times 333.15 \text{ K}}{10^5 \text{ Pa}} \\ &= 6.358 \text{ m}^3/\text{hour} \end{aligned}$$

- (c) The volumetric flow rate of CO after compression ($V_{2,\text{CO}}$) needs to be estimated, using the equation 3.27. The values of $P_{2,\text{CO}}$ and k_{CO} from Table 3.7 will be used.

$$V_{2,\text{CO}} = \left(\frac{10 \text{ bar}}{69.7 \text{ bar}} \right)^{\left(\frac{1}{1.4013} \right)} \times 6.358 \text{ m}^3/\text{hour} = 1.591 \text{ m}^3/\text{hour}$$

- (d) The temperature of CO after compression ($T_{2,\text{CO}}$) needs to be estimated, using the equation 3.29. The values of $P_{1,\text{CO}}$, $P_{2,\text{CO}}$ and $T_{1,\text{CO}}$ from Table 3.7 will be used.

$$T_{2,\text{CO}} = \frac{69.7 \text{ bar} \times 1.591 \text{ m}^3/\text{hour} \times 333.15 \text{ K}}{10 \text{ bar} \times 6.358 \text{ m}^3/\text{hour}} = 580.9 \text{ K}$$

- (e) The total required energy for cooling of CO can be estimated, using the equations 3.31 and 3.33 in combination. The temperature of CO after cooling ($T_{3,\text{CO}}$) is equal to the syngas inlet temperature (i.e. 498.15 K) and the molar capacity of CO ($C_{p,\text{CO}}$) is equal to 30.47 J/mol*K at 600 K [109].

$$\begin{aligned} \frac{30.47 \text{ J/mol} \cdot \text{K} \times (580.9 - 498.15) \text{ K} \times 20,163,502 \text{ mol}_{\text{CO}}}{3600 \times 3} \\ = 4.71 \times 10^6 \text{ Wh} \end{aligned}$$

- (f) Following the same estimations steps as above, the total required energy for cooling of H₂ (produced by the CO₂ electrolyzer) is equal to 5.18 × 10⁵ Wh. Also, the total required energy for cooling of H₂ (produced by the H₂O electrolyzer) is equal to 6.37 × 10⁷ Wh. These estimations were done using the equations 3.25, 3.28, 3.30, 3.32 and 3.33 and the relevant values of H₂ from Table 3.7.

8. Adding all the aforementioned energy requirements and assuming that the efficiency of the DC-DC converters is equal to 98%, **the total energy requirement of the whole system is equal to 3.03×10^{10} Wh**. The following Table 4.2 represents all the estimated energy requirements and production output data for this thesis system.

Table 4.2: Estimated energy requirements and production output data for the whole system

Parameter	Estimated Value
CH ₃ OH required production	124,836,153 mol _{CH₃OH}
H ₂ required production	252,194,248 mol _{H₂}
H ₂ O required supply to electrolyzer	252,194,248 mol _{H₂O}
CO required production	20,163,502 mol _{CO}
CO ₂ required supply to electrolyzer	20,163,502 mol _{CO₂}
CO ₂ required supply to methanol converter	28,590,040 mol _{CO₂}
Energy required for CO ₂ electrolyzer	3.17×10^9 Wh
Energy required for H ₂ O electrolyzer	2.58×10^{10} Wh
Energy required for the compression of CO	5.14×10^7 Wh
Energy required for the compression of H ₂ (produced by CO ₂ electrolyzer)	5.73×10^6 Wh
Energy required for the compression of H ₂ (produced by H ₂ O electrolyzer)	6.48×10^8 Wh
Energy required for the cooling of CO	4.71×10^6 Wh
Energy required for the cooling of H ₂ (produced by CO ₂ electrolyzer)	5.18×10^5 Wh
Energy required for the cooling of H ₂ (produced by H ₂ O electrolyzer)	6.37×10^7 Wh
Total required energy (without DC-DC converters)	2.97×10^{10} Wh
Total required energy (with DC-DC converters)	3.03×10^{10} Wh

4.3. PV PANELS

THE installed peak PV power for this thesis system was estimated by using: i) the total required energy (with DC-DC converters) for the whole system (as it can be seen in Table 4.2) and ii) the energy yield of 1 MWp PV system in the selected plant location. According to the platform PVGIS 5.1 of the EU Science Hub [94], a PV system of 1 MWp generates 1.70×10^9 Wh/year. Therefore, an installed peak PV power of 17.84 MWp is required for generating 3.03×10^{10} Wh/year.

For simplicity, it has been decided that **the installed peak PV power for this thesis system is equal to 18 MWp**. According to PVGIS 5.1, such a PV system can reach a maxi-

maximum power output of 21.10 MW and generate 3.054×10^{10} Wh/year. These values are also presented in Table 4.3.

Table 4.3: Sizing data and production results of the PVs

Parameter	Value
Installed peak PV power	18 MWp
Maximum PV power	21.10 MW
Energy Yield	3.054×10^{10} Wh

4.4. DC-DC CONVERTERS

THE maximum power output of the PV panels was rounded up to 22 MW and therefore **22 DC-DC converters are required for this thesis system** (see equation 3.34). As it was mentioned in section 3.9.4, the maximum power input per converter is equal to 1 MW and the rounding-up gives some spare capacity to the system for power conversion.

4.5. CO₂ ELECTROLYZER

THE power capacity of the CO₂ electrolyzer is defined in this section, by estimating the required number of its stacks. As it has been previously mentioned in section 3.9.5, the required electrical power for the auxiliary equipment is subtracted from the power output of the PVs and the rest of this power is fed to the electrolyzers. According to Table 4.2, the required electrical energy for the auxiliary equipment is 2.6% of the total required energy. Therefore, for simplicity, it is assumed that the required electrical power for the auxiliary equipment will not be taken into account in the estimations of this section.

The power output of the PV panels need to be split between CO₂ and H₂O electrolyzers. The approach of the power split is based on the syngas composition, as it is presented in Table 3.10. Since the syngas consists of H₂ by 83.8% and CO by 6.7%, the power input of the CO₂ electrolyzer is equal to 7.5% of the PVs power output (the rest is fed to the H₂O electrolyzer). The maximum PVs power output will be used (according to the data of PVGIS 5.1), so that the capacity of the CO₂ electrolyzer is estimated.

Moreover, it is assumed that the operating V_{cell} of the CO₂ electrolyzer is equal to 2.4V, since it ranges from 1.95V to 2.85V. According to the electrolyzer's model in Simulink, the V_{cell} of 2.4 V corresponds to J of 82.9 mA/cm² and P_{density} of 198.96 mW/cm². These assumed operating parameters are in accordance with the electrolyzer's specifications in Table 3.5. As soon as the required number of stacks is estimated, then the power capacity of the electrolyzer is estimated using its maximum power density (see Table 3.5), as follows.

$$P_{PV,max} = 21.10 \text{ MW}$$

$$N_{CO_2,stacks} = \frac{21.10 \times 10^9 \text{ mW} \times 7.5\%}{198.96 \text{ mW/cm}^2 \times 199,000 \text{ cm}^2/\text{stack}} = 39.96 \text{ stacks}$$

$$\approx 40 \text{ stacks}$$

$$P_{CO_2,capacity} = 40 \text{ stacks} \times 199,000 \text{ cm}^2/\text{stack} \times 578.84 \text{ mW/cm}^2$$

$$= 4.61 \text{ MW}$$

4

Therefore, the CO₂ electrolyzer of this thesis system consists of **40 stacks** and has a **power capacity of 4.61 MW**. Unfortunately, such a CO₂ electrolyzer could produce $1.490 \times 10^7 \text{ mol}_{CO}$ and $2.986 \times 10^6 \text{ mol}_{H_2}$, according to Simulink. This CO production was much lower than the required CO production (i.e. $20,163,502 \text{ mol}_{CO}$), as it was estimated in section 4.2. That's why; **the power split rate was increased from 7.5% to 10.2%, but the power capacity of the CO₂ electrolyzer remained unchanged** (the new power split rate can be seen in Figure D.7 of Appendix D). With this configuration, the CO₂ electrolyzer could produce $2.019 \times 10^7 \text{ mol}_{CO}$ and $3.526 \times 10^6 \text{ mol}_{H_2}$, according to Simulink. Table 4.4 presents the sizing data and production results of the CO₂ electrolyzer.

Table 4.4: Sizing data and production results of the CO₂ electrolyzer

Parameter	Value
Number of stacks	40
Power capacity	4.61 MW
CO production	$2.019 \times 10^7 \text{ mol}_{CO}$
CO ₂ required supply	$2.019 \times 10^7 \text{ mol}_{CO_2}$
H ₂ production	$3.526 \times 10^6 \text{ mol}_{H_2}$
Power input	10.2% of PV power output
Energy input	$2.973 \times 10^9 \text{ Wh}$
Energy efficiency [min - mean - max]	45.07% - 50.86% - 55.32%

Finally, the following Figure 4.1 presents the dynamic operation of the CO₂ electrolyzer's stacks. Also, the complementary Figure 4.2 presents more clearly the dynamic operation of the CO₂ electrolyzer's stacks in the interval 2000-2300. As far as the verification of the aforementioned results is concerned, the overall efficiency of the CO₂ electrolyzer's model is equal to 53.38%, which is very close to the simulation results of Table 4.4. The overall efficiency can be estimated as follows (using the energy required for CO₂ electrolysis, which is equal to 283 kJ/mol [96]):

$$N_{CO} = 2.019 \times 10^7 \text{ mol}_{CO}$$

$$E_{out} = 2.019 \times 10^7 \text{ mol}_{CO} \times 283 \text{ kJ/mol}_{CO} = 1.5871 \times 10^9 \text{ Wh}$$

$$\eta_{overall} = \frac{1.5871 \times 10^9 \text{ Wh}}{2.973 \times 10^9 \text{ Wh}} = 53.38\%$$

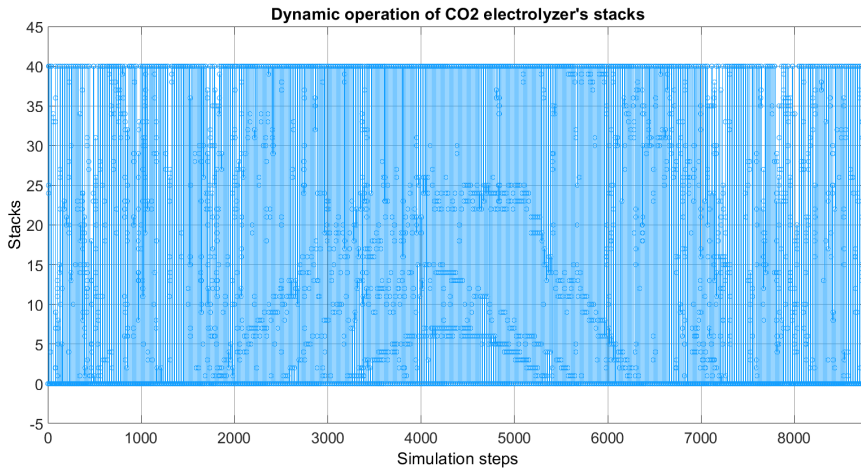


Figure 4.1: Dynamic operation of the CO₂ electrolyzer's stacks

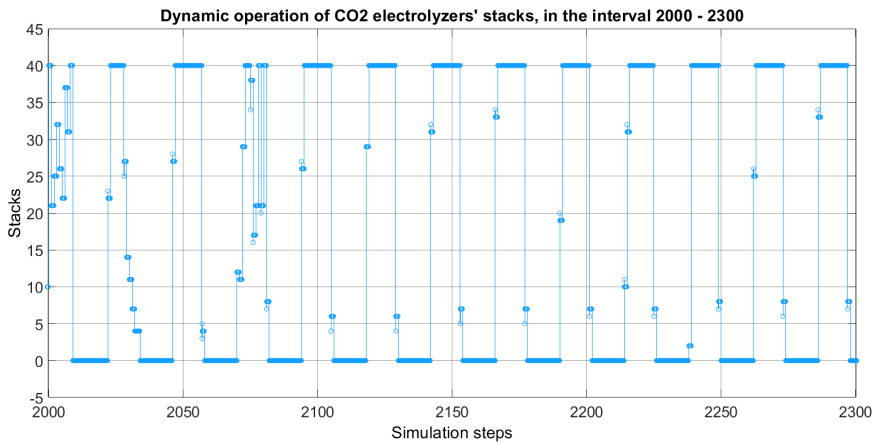


Figure 4.2: Dynamic operation of the CO₂ electrolyzer's stacks, in the interval 2000 - 2300

4.6. H₂O ELECTROLYZER

THE sizing approach of the H₂O electrolyzer is similar to the sizing approach of the CO₂ electrolyzer. As in the case of the CO₂ electrolyzer, the required electrical power for the auxiliary equipment will not be taken into account in the estimations of this section.

Since 10.2% of the PV power output is fed to the CO₂ electrolyzer, then **89.8% of the PV power output is fed to the H₂O electrolyzer** (the latter power split rate can be seen in Figure D.7 of Appendix D). Taking into account the maximum power density of the H₂O electrolyzer (see Table 3.6), 140 stacks are required for the operation of the electrolyzer (see the following calculation).

4

$$\begin{aligned}
 P_{PV,max} &= 21.10 \text{ MW} \\
 N_{H_2O,stacks} &= \frac{21.10 \times 10^9 \text{ mW} \times 89.8\%}{681 \text{ mW/cm}^2 \times 199,000 \text{ cm}^2/\text{stack}} = 139.8 \text{ stacks} \\
 &\approx 140 \text{ stacks}
 \end{aligned}$$

However, this amount of stacks is oversized, because the H₂O electrolyzer produces $2.503 \times 10^8 \text{ mol}_{H_2}$. Taking into account the H₂ production of the CO₂ electrolyzer (see Table 4.4), this gives us a total H₂ production of $2.54 \times 10^8 \text{ mol}_{H_2}$, which is more than the total required amount of H₂ (i.e. 252,194,248 mol_{H₂}). That's why; it has been decided to decrease the amount of stacks of the H₂O electrolyzer from 140 to 100. This decision is supported by the Figure 4.3, which shows that more than 100 stacks are barely required for the electrolyzer's operation. Also this Figure presents the dynamic operation of the H₂O electrolyzer's stacks.

Taking into account **the limit of 100 stacks in the electrolyzer's operation**, the H₂O electrolyzer could produce $2.492 \times 10^8 \text{ mol}_{H_2}$ and $1.246 \times 10^8 \text{ mol}_{O_2}$, according to Simulink. Adding this H₂ production and the H₂ production of the CO₂ electrolyzer (see Table 4.4), the total required amount of H₂ (i.e. 252,194,248 mol_{H₂}) is fulfilled. Also, **the power capacity of the H₂O electrolyzer is estimated as 13.55 MW** (see the following calculation). Table 4.5 presents the sizing data and production results of the H₂O electrolyzer.

$$\begin{aligned}
 P_{H_2O,capacity} &= 100 \text{ stacks} \times 199,000 \text{ cm}^2/\text{stack} \times 681 \text{ mW/cm}^2 \\
 &= 13.55 \text{ MW}
 \end{aligned}$$

As far as the verification of the aforementioned results is concerned, the overall efficiency of the H₂O electrolyzer's model is equal to 75.95%, which is very close to the simulated results. The overall efficiency can be estimated as follows (using the energy required for H₂O electrolysis, which is equal to 285.8 kJ/mol [12]):

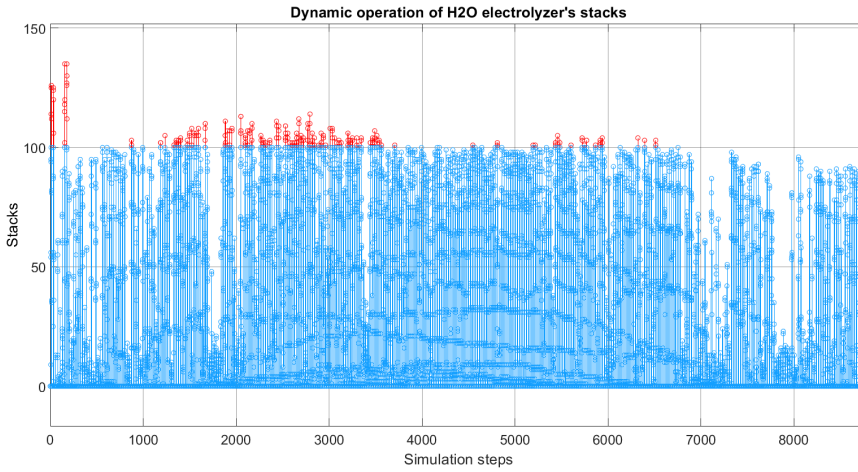


Figure 4.3: Dynamic operation of the H₂O electrolyzer's stacks (no limit in the amount of stacks with red and limit of 100 stacks with blue)

Table 4.5: Sizing data and production results of the H₂O electrolyzer

Parameter	Value
Number of stacks	100
Power capacity	13.55 MW
H ₂ production	$2.492 \times 10^8 \text{ mol}_{\text{H}_2}$
H ₂ O required supply	$2.492 \times 10^8 \text{ mol}_{\text{H}_2\text{O}}$
O ₂ production	$1.246 \times 10^8 \text{ mol}_{\text{O}_2}$
Power input	89.8% of PV power output
Energy input	$2.605 \times 10^{10} \text{ Wh}$
Energy efficiency [min - mean - max]	75.83% - 76.52% - 81.71%

$$\begin{aligned}
 N_{\text{H}_2} &= 2.492 \times 10^8 \text{ mol}_{\text{H}_2} \\
 E_{\text{out}} &= 2.492 \times 10^8 \text{ mol}_{\text{H}_2} \times 285.8 \text{ kJ/mol}_{\text{H}_2} = 1.9784 \times 10^{10} \text{ Wh} \\
 \eta_{\text{overall}} &= \frac{1.9784 \times 10^{10} \text{ Wh}}{2.605 \times 10^{10} \text{ Wh}} = 75.95\%
 \end{aligned}$$

4.7. METHANOL REACTOR AND BUFFER TANKS

THE components and parameters of the methanol synthesis process are estimated in this section. Taking into account the estimation results of the above sections, the parameters 5-8 of the Table 4.1 will be estimated and optimized together, because they all affect the methanol synthesis process. The target of this optimization is the minimiza-

tion of the methanol converter and the buffer tanks of H₂ and CO.

The estimation steps are as follows:

1. As it has been mentioned in sections 3.9.3 and 3.10, the methanol synthesis process is assumed to be a continuous process, which will be independent from the intermittent PVs power output. This means that the methanol reactor needs to be switched off for some time, so that some amount of H₂ and CO can be stored in the buffer tanks. As soon as the stored amount is sufficient, then the methanol reactor starts operating. Therefore, it was found that **the methanol reactor needs to be out of operation for 500 hours and in operation for 8284 hours.**
2. Taking into account the required amounts of H₂ and CO (see section 4.2), the molar feeding rates of H₂ and CO can be estimated as follows:

$$NR_{CO} = \frac{20,163,502 \text{ mol}_{CO}}{8284 \text{ hours}} = 2,434 \text{ mol}_{CO}/\text{hour}$$

$$NR_{H_2} = \frac{252,194,248 \text{ mol}_{H_2}}{8284 \text{ hours}} = 30,444 \text{ mol}_{H_2}/\text{hour}$$

3. At this point, the molar feeding rates of H₂ and CO need to be converted to volumetric rates (VR_{H₂} and VR_{CO} respectively), because the last ones are necessary for the estimation and monitoring of their buffer tanks capacity. Using the value of R from Table 3.7 and the syngas inlet temperature and pressure from Table 3.10 in the equations 3.24 and 3.25, the volumetric feeding rates of H₂ and CO can be estimated as follows:

$$VR_{CO} = \frac{2,434 \text{ mol}_{CO}/\text{hour} \times 8.3145 \text{ m}^3 \cdot \text{Pa}/\text{K} \cdot \text{mol} \times 498.15 \text{ K}}{69.7 \times 10^5 \text{ Pa}}$$

$$= 1.446 \text{ m}^3/\text{hour}$$

$$VR_{H_2} = \frac{30,444 \text{ mol}_{H_2}/\text{hour} \times 8.3145 \text{ m}^3 \cdot \text{Pa}/\text{K} \cdot \text{mol} \times 498.15 \text{ K}}{69.7 \times 10^5 \text{ Pa}}$$

$$= 18.090 \text{ m}^3/\text{hour}$$

4. As far as the molar feeding rate of CO₂ is concerned, this is constant and estimated as 3,451 mol_{CO₂}/hour (using the same approach as in the above point 2).
5. Given the aforementioned VR_{CO} and VR_{H₂}, the required buffer tanks capacities are equal to 1,310 m³ and 16,245 m³, respectively. These capacity values guarantee that there is always enough amount of H₂ and CO for the smooth operation of the methanol reactor. Figure 4.4 presents the percentage change of the buffer tanks capacities (given the above volumetric capacities).
6. Taking into account the aforementioned VR_{CO} and VR_{H₂} and the conversion rate of the methanol reactor (i.e. 99%), the system could produce **1.248 × 10⁸ mol_{CH₃OH} or 3.999 kT**. This production result is very close to the production target of 4 kT/year and the required molar production of CH₃OH in Table 4.2 (i.e. 124,836,153 mol_{CH₃OH}).

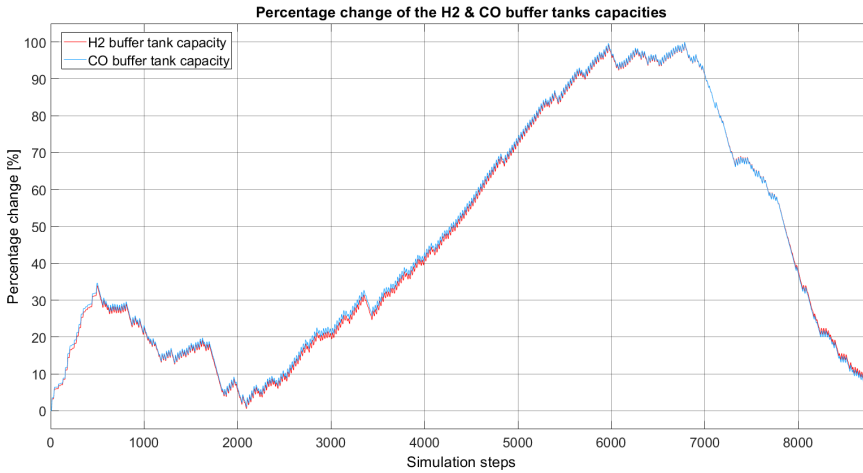


Figure 4.4: Percentage change of the H₂ and CO buffer tanks capacities

This production output requires a methanol converter, which consists of **75 tubes and has a catalyst mass of 786.69 kg_{cat}**. The size of the methanol converter was estimated as follows, using the values of catalyst mass per tube (i.e. 10,468 g_{cat}/tube) and methanol molar production per catalyst particle (i.e. 0.01939 mol/g_{cat}/h) of Table 3.10:

$$\begin{aligned}
 N_{\text{tubes}} &= \frac{1.248 \times 10^8 \text{ mol}_{\text{CH}_3\text{OH}}}{8284 \text{ hours}} \\
 &= \frac{99\% \times 10,468 \text{ g}_{\text{cat}}/\text{tube} \times 0.01939 \text{ mol}_{\text{CH}_3\text{OH}}/\text{g}_{\text{cat}}/\text{hour}}{10,468 \text{ g}_{\text{cat}}/\text{tube} \times 0.01939 \text{ mol}_{\text{CH}_3\text{OH}}/\text{g}_{\text{cat}}/\text{hour}} \\
 &= 75 \text{ tubes} \\
 M_{\text{catalyst}} &= 75 \text{ tubes} \times 10,468 \text{ g}_{\text{cat}}/\text{tube} = 786.69 \text{ kg}_{\text{cat}}
 \end{aligned}$$

All the above sizing data and production results of the methanol converter and the buffer tanks are summarized in Table 4.6.

4.7.1. ACTIVATION STEP OF THE METHANOL CONVERTER

In the previous section, it was estimated that the activation step of 501 is the optimum for the operation of the methanol converter, taking into account the parameters of Table 4.6. In this subsection, the effect of changing the activation step will be presented.

Decrease of activation step

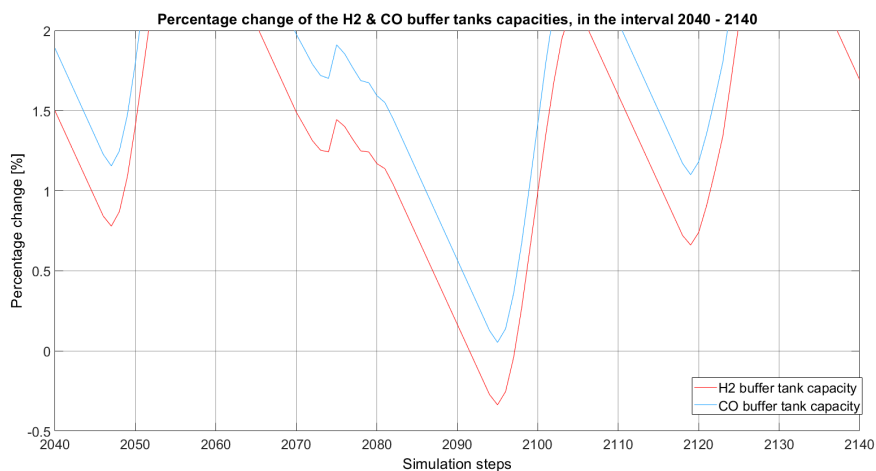
If the activation step is decreased, then the buffer tanks capacities, the tubes of the methanol converter and the feeding rates of H₂ and CO will be decreased. In such a case, less storage of CO and H₂ and a smaller methanol converter are required, because the converter will operate for more time throughout the year. However, the converter's operation will not be smooth and continuous, because a deficit of H₂ and/or CO will be present. The production rates of H₂ and CO are not sufficient, because they remain unchanged (i.e. no change in the electrolyzers and PVs size). For example, Figure 4.5 shows

Table 4.6: Sizing data and production results of the methanol converter and the buffer tanks

Parameter	Value
CH ₃ OH production	1.248×10^8 mol _{CH₃OH} or 3.999 kT
H ₂ volumetric feeding rate	18.090 m ³ /hour
H ₂ molar feeding rate	30,444 mol _{H₂} /hour
CO volumetric feeding rate	1.446 m ³ /hour
CO molar feeding rate	2,434 mol _{CO} /hour
CO ₂ molar feeding rate	3,451 mol _{CO₂} /hour
H ₂ buffer tank capacity	16,245 m ³
CO buffer tank capacity	1,310 m ³
Activation step of methanol converter	501
Tubes of methanol converter	75 tubes
Catalyst mass of methanol converter	786.69 kg _{cat}

4

the deficit of H₂ in the interval 2090-2098, when the activation step decreases from 501 to 491.

Figure 4.5: Percentage change of the H₂ and CO buffer tanks capacities, in the interval 2040-2140

Increase of activation step

If the activation step is increased, then the buffer tanks capacities, the tubes of the methanol converter and the feeding rates of H₂ and CO will be increased. In such a case, more storage of CO and H₂ and a larger methanol converter are required, because the converter will operate for less time throughout the year. This would cause an increase of the capital expenditures regarding the methanol synthesis process.

4.8. COMPRESSORS

As far as the CO and H₂ gases compression is concerned, 3 types of compressors are required, because there are 3 different streams (i.e. CO stream, H₂ stream produced by the CO₂ electrolyzer and H₂ stream produced by the H₂O electrolyzer). Since the molar flow rate of each stream is different, the specific energy for the compression of each gas is also different (see section 3.9.1). The maximum molar flow rates of each stream will be taken into account for the estimation of the power capacity of each compressor.

Therefore, the estimation steps for the sizing of the compressors are as follows:

1. According to Simulink, the maximum molar production rate of CO is equal to $1.3677 \times 10^4 \text{ mol}_{\text{CO}}/\text{hour}$. According to Table 3.7 and the equation 3.22, the specific energy for the compression of CO is equal to 9.1725 kJ/mol_{CO}. Therefore, the power capacity of the compressor for the CO stream can be estimated as follows:

$$\begin{aligned} NR_{\text{CO,produced,max}} &= 1.3677 \times 10^4 \text{ mol}_{\text{CO}}/\text{hour} \\ P_{\text{CO,comp,capacity}} &= 1.3677 \times 10^4 \text{ mol}_{\text{CO}}/\text{hour} \times 9.1725 \text{ kJ/mol} = \\ &= 34.85 \text{ kW} \approx 35 \text{ kW} \end{aligned}$$

2. According to Simulink, the maximum molar production rate of H₂ (produced by the CO₂ electrolyzer) is equal to 1,651 mol_{H₂}/hour. According to Table 3.7 and the equation 3.23, the specific energy for the compression of this H₂ stream is equal to 9.2016 kJ/mol_{H₂}. Therefore, the power capacity of the compressor for this H₂ stream can be estimated as follows:

$$\begin{aligned} NR_{\text{H}_2 \text{ (from CO}_2 \text{ el),produced,max}} &= 1,651 \text{ mol}_{\text{H}_2}/\text{hour} \\ P_{\text{H}_2 \text{ (from CO}_2 \text{ el),comp,capacity}} &= 1,651 \text{ mol}_{\text{H}_2}/\text{hour} \times 9.2016 \text{ kJ/mol} = \\ &= 4.22 \text{ kW} \approx 5 \text{ kW} \end{aligned}$$

3. According to Simulink, the maximum molar production rate of H₂ (produced by the H₂O electrolyzer) is equal to $1.2945 \times 10^5 \text{ mol}_{\text{H}_2}/\text{hour}$. According to Table 3.7 and the equation 3.23, the specific energy for the compression of this H₂ stream is equal to 9.3397 kJ/mol_{H₂}. Therefore, the power capacity of the compressor for this H₂ stream can be estimated as follows:

$$\begin{aligned} NR_{\text{H}_2 \text{ (from H}_2\text{O el),produced,max}} &= 1.2945 \times 10^5 \text{ mol}_{\text{H}_2}/\text{hour} \\ P_{\text{H}_2 \text{ (from H}_2\text{O el),comp,capacity}} &= 1.2945 \times 10^5 \text{ mol}_{\text{H}_2}/\text{hour} \times 9.3397 \text{ kJ/mol} = \\ &= 335.84 \text{ kW} \approx 336 \text{ kW} \end{aligned}$$

The following Table 4.7 presents the sizing data and production results for all the compressors. As it can be seen, the total energy input of the compressors is equal to $7.070 \times 10^8 \text{ Wh}$. Adding the estimated energy requirements for compression of Table 4.2, this gives us an estimated total energy requirement of $7.056 \times 10^8 \text{ Wh}$. It can be understood that both values are very close to each other.

Table 4.7: Sizing data and production results of the compressors

Parameter	Value
Power capacity of the compressor (for the CO stream)	35 kW
Power capacity of the compressor (for the H ₂ stream produced by the CO ₂ electrolyzer)	5 kW
Power capacity of the compressor (for the H ₂ stream produced by the H ₂ O electrolyzer)	336 kW
Total energy input for compression	7.070×10^8 Wh

4.9. COOLING UNITS

SIMILARLY to the approach for the sizing of the compressors, the three types of cooling units are sized based on the maximum molar flow rates of each stream (i.e. CO stream, H₂ stream produced by the CO₂ electrolyzer and H₂ stream produced by the H₂O electrolyzer). The cooling units are sized in terms of their cooling capacity and input power. The sizing approach of this section is categorized as follows:

1. As far as the sizing of the cooling unit for the CO stream, the estimation steps are as follows:

- (a) According to Simulink, the maximum molar production rate of CO is equal to 1.3677×10^4 mol_{CO}/hour

$$NR_{CO,produced,max} = 1.3677 \times 10^4 \text{ mol}_{CO}/\text{hour}$$

- (b) The ratio of $V_{2,CO}$ to $V_{1,CO}$ (i.e. volumetric flow rates of CO after and before compression, respectively) is a constant number and equal to 0.2502, because the pressures $P_{1,CO}$ and $P_{2,CO}$ are also constants (see Table 3.7). This ratio is calculated as follows, using the equation 3.27:

$$\frac{V_{2,CO}}{V_{1,CO}} = \left(\frac{10 \text{ bar}}{69.7 \text{ bar}} \right)^{\left(\frac{1}{1.4013} \right)} = 0.2502$$

- (c) The temperature of CO after compression ($T_{2,CO}$) needs to be estimated, using the equation 3.29. The values of $P_{1,CO}$, $P_{2,CO}$ and $T_{1,CO}$ from Table 3.7 will be used.

$$T_{2,CO} = \frac{69.7 \text{ bar}}{10 \text{ bar}} \times 333.15 \text{ K} \times 0.2502 = 580.9 \text{ K}$$

- (d) The cooling capacity of the cooling unit for the CO stream can be estimated using the equation 3.31 and $NR_{CO,produced,max}$ (see the following calculation). The temperature of CO after cooling ($T_{3,CO}$) is equal to the syngas inlet temperature (i.e. 498.15 K) and the molar capacity of CO ($C_{p,CO}$) is equal to 30.47

J/mol*K at 600 K [109].

$$\begin{aligned}
 Q_{c,CO,capacity} &= \\
 &= \frac{30.47 \text{ J/mol} * \text{K} \times (580.9 - 498.15) \text{ K} \times 1.3677 \times 10^4 \text{ mol}_{CO}/\text{hour}}{3600 \text{ seconds/hour}} = \\
 &= 9,579.2 \text{ W} \approx 9.6 \text{ kW}
 \end{aligned}$$

- (e) The relevant input power for such a cooling unit is estimated, using the equation 3.33 and an EER value of 3 (see the following calculation):

$$P_{cool,CO,capacity} = \frac{9.6 \text{ kW}}{3} = 3.2 \text{ kW}$$

2. As far as the sizing of the cooling unit for the H₂ stream (produced by the CO₂ electrolyzer) is concerned, the estimation steps are similar to those of the above point 1. The estimation for the current stream is done, based on the maximum molar production rate of H₂ (produced by the CO₂ electrolyzer), which is equal to 1,651 mol_{H₂}/hour. Also, the equations 3.25, 3.28, 3.30, 3.32 and 3.33 and the relevant values of H₂ from Table 3.7 were used in this estimation.

Therefore, the cooling capacity of the cooling unit for the H₂ stream (produced by the CO₂ electrolyzer) is estimated as 1.2 kW and the relevant input power is estimated as 0.4 kW. These values were calculated as follows:

$$\begin{aligned}
 Q_{c,H2 \text{ (from CO}_2 \text{ el),capacity} &= \\
 &= \frac{29.32 \text{ J/mol} * \text{K} \times (583.28 - 498.15) \text{ K} \times 1,651 \text{ mol}_{H_2}/\text{hour}}{3600 \text{ seconds/hour}} = \\
 &= 1,144.7 \text{ W} \approx 1.2 \text{ kW} \\
 P_{cool,H2 \text{ (from CO}_2 \text{ el),capacity} &= \frac{1.2 \text{ kW}}{3} = 0.4 \text{ kW}
 \end{aligned}$$

3. The sizing of the cooling unit for the H₂ stream (produced by the H₂O electrolyzer) is estimated exactly as the other H₂ stream of the above point 2. Therefore, the cooling capacity of the cooling unit for the H₂ stream (produced by the H₂O electrolyzer) is estimated as 1.2 kW and the relevant input power is estimated as 0.4 kW. These values were calculated as follows:

$$\begin{aligned}
 Q_{c,H2 \text{ (from } H_2 \text{O el),capacity} &= \\
 &= \frac{29.32 \text{ J/mol} * \text{K} \times (592 - 498.15) \text{ K} \times 1.2945 \times 10^5 \text{ mol}_{H_2}/\text{hour}}{3600 \text{ seconds/hour}} = \\
 &= 98,945.6 \times 10^4 \text{ W} \approx 99 \text{ kW} \\
 P_{cool,H2 \text{ (from } H_2 \text{O el),capacity} &= \frac{99 \text{ kW}}{3} = 33 \text{ kW}
 \end{aligned}$$

The following Table 4.8 presents the sizing data and production results for all the cooling units. As it can be seen, the total energy input of cooling units is equal to 6.905×10^7 Wh. Adding the estimated energy requirements for cooling of Table 4.2, this gives us an estimated total energy requirement of 6.893×10^7 Wh. It can be understood that both values are very close to each other.

Table 4.8: Sizing data and production results of the cooling units

Parameter	Value
Cooling capacity of the cooling unit (for the CO stream)	9.6 kW
Input power for the cooling unit (for the CO stream)	3.2 kW
Cooling capacity of the cooling unit (for the H ₂ stream produced by the CO ₂ electrolyzer)	1.2 kW
Input power for the cooling unit (for the H ₂ stream produced by the CO ₂ electrolyzer)	0.4 kW
Cooling capacity of the cooling unit (for the H ₂ stream produced by the H ₂ O electrolyzer)	99 kW
Input power for the cooling unit (for the H ₂ stream produced by the H ₂ O electrolyzer)	33 kW
Total energy input for cooling	6.905×10^7 Wh

4.10. DUMP ENERGY

THE supplied energy by the PV panels to the system is equal to 30.54 GWh/year (see Table 4.3). Unfortunately, this energy yield cannot be fully exploited by the system. This happens, because there are cases, where the supplied energy by the PVs is so little that the electrolyzers cannot operate even 1 stack of them and are switched off. So, this energy cannot be exploited by the electrolyzers and needs to be dumped, because there are no batteries implemented in the system and thus this energy cannot be stored. According to Simulink, **the dump energy is equal to 1.212×10^8 Wh/year or 0.12 GWh/year**. So, **the dump energy accounts for 0.40% of the total input energy**.

4.11. SUMMARY

IN this chapter the sizing approach and production results of the proposed thesis system were presented. The system was sized by doing an empirical analysis of the various system parameters and not by using an optimization tool. Moreover, the system was sized by following a backward approach, so that the system size was minimised and its efficiency was increased.

Initially, it was estimated that the total energy requirement of the system was equal to 30.3 GWh, so that the system could reach the production target of 4 kT of methanol. Based on this energy requirement, it was found that the installed peak PV power for this system is equal to 18 MWp and its maximum power output is equal to 21.10 MW. That's why; the required amount of DC-DC converters for this system is equal to 22 units.

Also, the required electrical power for the auxiliary equipment is subtracted from the PVs power output and the rest of this power is fed to the CO₂ electrolyzer by 10.2% and to the H₂O electrolyzer by 89.8% (based on the syngas composition).

According to the energy and production requirements, it was found that the power capacity of the CO₂ electrolyzer is equal to 4.61 MW (consisting of 40 stacks) and its efficiency ranges from 45.07% to 55.32% (due to its dynamic operation). Also, it was found that the power capacity of the H₂O electrolyzer is equal to 13.55 MW (consisting of 100 stacks) and its efficiency ranges from 75.83% to 81.71% (due to its dynamic operation). It has to be mentioned that the number of stacks of the H₂O electrolyzer is limited from 140 pieces to 100, because the produced H₂ was more than the necessary quantity and more than 100 stacks were barely required for the electrolyzer's operation.

As far as the methanol synthesis process is concerned, it was found that the methanol reactor needs to be out of operation for 500 hours, so that some amount of CO and H₂ can be stored in the buffer tanks. At the 501th simulation step, the methanol converter starts operating and keeps running continuously until the simulation end. The converter needs to consist of 75 tubes, which contain 786.69 kg of catalysts. Under these operating conditions, the methanol converter is able to produce 3.999 kT of methanol. If the methanol converter was out of operation for more than 500 hours, then it would operate for less hours, leading to an increase in its size and the size of the buffer tanks. However, if the methanol converter was out of operation for less than 500 hours, then there would be a deficit of H₂ and/or CO, leading to a non-smooth and non-continuous operation of the converter.

Regarding the auxiliary equipment, it was found that 3 different types of compressors and cooling units are required, because there are 3 different streams (i.e. CO stream, H₂ stream produced by the CO₂ electrolyzer and H₂ stream produced by the H₂O electrolyzer). The power capacity of the compressor for the first stream is equal to 35 kW and the cooling capacity of the cooling unit for this stream is equal to 9.6 kW. For the second stream, the values are equal to 5 kW and 1.2 kW, respectively. For the last stream, the values are equal to 336 kW and 99 kW, respectively.

Finally, it can be seen that the proposed system can produce almost 4 kT of methanol, when the electrolyzers are in dynamic operation and the methanol converter operates continuously with the use of buffer tanks. Also, the system is able to exploit 99.6% of the PVs energy yield (i.e. dumping the rest of it).

5

ECONOMIC ANALYSIS

This chapter presents the economic potential of the proposed thesis system. The first step of the system's economic analysis is the estimation of the equipment prices (including purchasing prices, operating costs and lifetime) and is presented in section 5.1. The next analysis step is the estimation of the market prices of methanol, feedstocks and dumped energy (see section 5.2). Taking into account the aforementioned prices, the system's capital and operational expenditures can be estimated (see sections 5.3 and 5.4, respectively). Based on these expenditures, a cash flow analysis has been carried out and the end-of-life net present value of the system has also been estimated (see section 5.5). Moreover, the levelized cost of methanol has been estimated in section 5.6. Finally, the environmental benefit of this system is mentioned in section 5.7 and the whole chapter is summarized in section 5.8.

5.1. EQUIPMENT PRICES ESTIMATION

THIS section describes the cost areas and the required assumptions for the economic analysis of this thesis system. The information of this section covers the purchasing prices, operating costs and lifetime of the required machinery and equipment. The following subsections presents the cost data of each equipment.

5.1.1. PV PANELS

In December 2020, the purchasing price for mainstream c-Si PV modules was equal to 0.22 €/Wp [124]. Another cost that has to be taken into account in the estimation of the PVs capital cost is related to the Balance of System (BoS) components. The BoS includes, eg, mounting structures, cabling, other electrical components, infrastructure, installation work, planning, documentation, and other work. A typical cost factor for the BoS components is equal to 0.20 €/Wp for Europe in 2019 and without any grid connection [125].

As far as the operation and maintenance (O&M) cost of the PVs is concerned, this cost

factor was equal to 5 €/kWp/year for Europe in 2019 [125]. This O&M price is suitable for the PV system of this thesis (i.e. 18 MWp), because this price is related to PV systems, whose size ranges from 10 to 50 MWp [125]. Finally, the lifetime of the PVs is equal to 25 years [125]. All the aforementioned data has been chosen for this study and is presented in Table 5.1.

Table 5.1: Cost data for the PVs

Cost factor	Value
Purchasing price of c-Si PV modules	0.22 €/Wp [124]
BoS cost	0.20 €/Wp [125]
O&M cost	5 €/kWp/year [125]
Lifetime	25 years [125]

5

5.1.2. DC-DC CONVERTERS

For the DC-DC converters, it is assumed that the converters cost depends on the power rating and their cost is the same as the cost of DC-AC inverters. In 2019, the price of DC/AC inverters was equal to 0.025 €/Wp for utility-scale projects [125]. Also, the inverters lifetime is assumed to be half of the PVs lifetime (i.e. 12.5 years) [125]. The aforementioned data has been chosen for the DC/DC converters of this study and is presented in Table 5.2.

Table 5.2: Cost data for the DC-DC converters

Cost factor	Value
Purchasing price	0.025 €/Wp [125]
Lifetime	12.5 years [125]

5.1.3. CO₂ ELECTROLYZER

The estimation of the CO₂ electrolyzer costs is based on the publication by Shin et al. [126], which is related to a techno-economic assessment of a PEM CO₂ electrolyzer. As it can be seen in Table 3.5, the CO₂ electrolyzer of this thesis system is also of PEM type. According to this publication, the capital cost of a PEM CO₂ electrolyzer is equal to 550 \$/kW and its BoS components cost accounts for 61% of its total cost [126]. The exchange rate used to convert the price in EUR has been extracted by the European Central Bank (ECB) database. According to ECB, the yearly average exchange rate EUR to USD is equal to 1.1956 \$/€ [127].

As far as the maintenance of the CO₂ electrolyzer is concerned, its annual O&M cost is equal to 2.5% of its capital cost [126]. Apart from that, the membrane electrode assembly (MEA) needs to be replaced every year and this job considers the cost of membrane and catalysts for the anode and cathode [126]. The MEA replacement costs 1,180 \$/m²

[126]. However, the cell compartment needs to be replaced every 7 years at a cost of 15% of the electrolyzer's capital cost [126]. Finally, the lifetime of the CO₂ electrolyzer is equal to 20 years [126]. All the aforementioned data has been chosen for the CO₂ electrolyzer of this study and is presented in Table 5.3.

Table 5.3: Cost data for the CO₂ electrolyzer

Cost factor	Value
Electrolyzer cost	460.02 €/kW [126]
BoS cost	61% of its electrolyzer cost [126]
O&M cost	2.5% per year of its capital cost [126]
MEA replacement cost	986.95 €/m ² /year [126]
Cell compartment replacement cost (every 7 years)	15% of its capital cost [126]
Lifetime	20 years [126]

5.1.4. H₂O ELECTROLYZER

The estimation of the H₂O electrolyzer capital costs is mainly based on the report of Dikschas et al. issued by Fraunhofer Institute [128]. According to this report, the cost of an AEL H₂O electrolyzer was equal to 750 €/kW in 2017 [128]. As in the case of the CO₂ electrolyzer, it is assumed that the BoS components cost of the H₂O electrolyzer accounts for 61% of its total cost [126].

Bertuccioli et al. have estimated the O&M cost for AEL H₂O electrolyzers, which is equal to 2.2% per year of the initial capital cost for a 10 MW electrolyzer and 1.85% per year of the initial capital cost for a 20 MW electrolyzer [129]. Therefore, the O&M cost of the AEL H₂O electrolyzer of this thesis system is assumed to be 2.08% of the initial capital cost, since its power capacity is equal to 13.55 MW. As far as the electrolyzers stacks replacement is concerned, this costs 50% of investment cost and needs to be done between 60,000 and 90,000 operating hours [130]. The lifetime of AEL H₂O electrolyzers ranges from 20 to 30 years [130]. Due to the dynamic operation of H₂O electrolyzer in this thesis system, it has been decided that the stacks will be replaced every 60,000 operating hours or 7 years (i.e. each year consists of 8,760 operating hours) and the electrolyzer's lifetime will be equal to 20 years. All the aforementioned data has been chosen for the H₂O electrolyzer of this study and is presented in Table 5.4.

5.1.5. METHANOL REACTOR AND BUFFER TANKS

The capital cost of the methanol reactor depends mainly on its catalyst type, which is made of copper-zinc oxide with aluminium oxide (CuO/ZnO/Al₂O₃), as it can be seen in Table 3.9. That's why; the capital cost estimation is based on the publication by Zhang et al., which mentions some cost data for a methanol reactor with CuO/ZnO/Al₂O₃ catalyst [131]. According to this report, the catalyst costs 21.36 \$/kg and needs to be replaced every 4 years [131]. As in the case of the CO₂ electrolyzer, it is assumed that the BoS compo-

Table 5.4: Cost data for the H₂O electrolyzer

Cost factor	Value
Electrolyzer cost	750 €/kW [128]
BoS cost	61% of its electrolyzer cost [126]
O&M cost	2.08% per year of the initial capital cost [129]
Stack replacement cost (every 60,000 operating hours or 7 years)	50% of investment cost [130]
Lifetime	20 years [130]

nents cost of the methanol reactor accounts for 61% of its total cost [126]. The annual maintenance cost of the methanol reactor is equal to 3% of its initial capital cost and is based on general plant maintenance standards [132]. All the aforementioned data is presented in Table 5.5.

5

Table 5.5: Cost data for the methanol reactor

Cost factor	Value
Catalyst cost	17.87 €/kg [131]
BoS cost	61% of its electrolyzer cost [126]
Maintenance cost	3% per year of the initial capital cost [132]
Catalyst lifetime	4 years [131]

The capital cost of the H₂ and CO buffer tanks is estimated, using the following equation, which is for storage tanks of floating-roof type [133] :

$$C_p = 475 \times V^{0.51}, \quad [\$] \quad (5.1)$$

where V is the volume of the storage tank in gallons and the cost, C_p , is calculated in USD.

5.1.6. COMPRESSORS

The capital cost of the compressors is estimated, using the following equation [134]:

$$C = \log(P_{\text{comp}}) + \left[a \times (P_{\text{comp}})^2 \right] + [b \times P_{\text{comp}}] + c, \quad [\$] \quad (5.2)$$

where P_{comp} is the compressor power capacity (kW) and its cost, C , is calculated in USD. For a centrifugal compressor (like the compressors type of this thesis system), the coefficient a is equal to 0.03867, the coefficient b is equal to 446.7 and the coefficient c is equal to 1.378×10^5 [134].

Finally, the annual maintenance cost of the compressors is equal to 3% of their initial capital cost and is based on general plant maintenance standards [132]. The compressors lifetime is equal to 40 years [135].

5.1.7. COOLING UNITS

The capital cost of the cooling units, which are air-cooled chillers, is estimated according to a technical primer issued by the Florida Power & Light Company (FPL) [136]. According to the FPL document, the cost of an air-cooled chiller, whose cooling capacity is lower than 150 tons, ranges from \$400 to \$1,000 [136]. One ton of cooling is equal to 3.516 kW of cooling [136]. This cost range is suitable for the cooling units of this thesis system, because their cooling capacity does not exceed 99 kW or 28.2 tons (see Table 4.8). Therefore, the price of 700 \$/ton is chosen for the air-cooled chillers of this system.

Finally, the annual maintenance cost of the cooling units is equal to 3% of their initial capital cost and is based on general plant maintenance standards [132]. Since, this machinery has a simple design and operation, it is assumed that its lifetime is equal to 40 years.

5.2. SALES, DUMP ENERGY AND FEEDSTOCK PRICES ESTIMATION

REVENUES, energy loss and feedstock expenses have been estimated based on their market prices. Table 5.6 presents the prices for the revenues, energy loss and feedstock expenses that have been used for the economic assessment of this thesis system. Methanex (the world's largest producer and supplier of methanol) sells methanol at the price of 410 €/ton in Europe (according to its latest price sheet on June 22, 2021) [137].

The price of oxygen has been increased by 51% from Q1 2015 to Q1 2021 [138]. In the 1st quarter of 2021, the price of oxygen has reached 379.9 \$/ton [138].

According to the latest developments on the carbon capture technology, the captured CO₂ can be supplied at 40 \$/ton at a very high purity (up to 99.99%) [78]. For more information on that, please have a look at Table 3.3.

The required supply of H₂O to the water electrolyzer, which is equal to 2.492×10^8 mol_{H₂O} (see Table 4.5), needs to be converted in m³. Taking into account the water molar mass (i.e. 18.015 g/mol) and its density (i.e. 997 kg/m³), the water required supply is equal to 4,503 m³/year or 375.25 m³/month. According to Athens Water Supply and Sewerage Company (EYDAP S.A.), the tariff for such a monthly water consumption is equal to 0.83 €/m³ for industrial clients [139].

As it was mentioned in section 4.10, the dump energy of this thesis system is equal to 0.12 GWh/year. The cost of this energy loss can be estimated, using the PV tender tariff in Greece. According to the PV Status Report 2019 issued by the European Union, the PV tender tariff in Greece was equal to 0.06278 €/kWh in July 2019 [140].

Table 5.6: Prices for revenues, dump energy and feedstock expenses

Item	Price
Methanol	410 €/ton [137]
Oxygen	317.58 €/ton [138]
Captured CO ₂	33.46 €/ton [78]
Water	0.83 €/m ³ [139]
Dump energy	0.06278 €/kWh [140]

5.3. CAPITAL EXPENDITURES ESTIMATION

THE estimation of the capital investment has been done using the method "Percentage of Delivered-Equipment Cost", which is mentioned in the book of Peters et al [141]. This method is commonly used for study and preliminary estimates [141]. In this method, all the items of the total capital investment (TCI) are estimated as percentages of the total delivered-equipment cost (TDEC). Therefore, the TDEC estimation is required. However, it must be stated that the cost for land is usually not included in TCI, because, by law, the land cannot be depreciated [141]. That's why; **the cost of land has not been taken into account in the economic assessment of this project.**

TDEC can be estimated by adding the total purchased-equipment cost (TPEC) and its delivery cost. Usually, the delivery cost is extra and not included in TPEC, because the equipment is quoted as f.o.b. (i.e. free on board, because the client pays the equipment transport) [141]. Therefore, a delivery cost of 10% of the TPEC can be assumed for predesign estimates [141]. The TPEC can be estimated using the equipment cost data of section 5.1 and the sizing results of chapter 4. The following Table 5.7 presents the TPEC, delivery cost and TDEC for the whole system of this project.

Figure 5.1 shows the cost centers' shares of TPEC per equipment type, according to the data of Table 5.7. As it can be seen, the most expensive equipment is the AEL H₂O electrolyzer. Also, c-Si PV modules account for 25% of TPEC and PEM CO₂ electrolyzer accounts for almost 12% of TPEC. Those three types of equipment account for more than 90% of TPEC. This is reasonable, since this equipment is the core of this thesis system.

TCI is the sum of the fixed capital investment (FCI) and working capital (WC) [141]. FCI refers to the capital that is necessary for the equipment manufacture and plant construction [141]. However, WC refers to the capital that is necessary for the start-up and operation of the plant (e.g. raw materials, supplies, cash liquidity etc.) [141]. According to the aforementioned TCI estimation method, it can be assumed that WC is equal to 15% of the TCI [141].

As far as FCI is concerned, this cost is divided into direct and indirect costs [141]. These cost factors can be determined as percentages of TDEC. Table 5.8 presents the items of direct and indirect costs as well as their values, according to the aforementioned

Table 5.7: Worksheet for the total equipment cost of the project

Equipment	Installed Capacity	Unit Cost	Total Cost
c-Si PV modules (including BoS)	18 MWp	0.42 €/Wp	€ 7,560,000
DC-DC converters	22 MW	0.025 €/Wp	€ 550,000
AEL H ₂ O electrolyzer	13.55 MW	750 €/kW	€ 10,163,925
BoS cost for the AEL H ₂ O electrolyzer	-	61% of the total electrolyzer cost	€ 6,498,247
PEM CO ₂ electrolyzer	4.61 MW	460.02 €/kW	€ 2,119,573
BoS cost for the PEM CO ₂ electrolyzer	-	61% of the total electrolyzer cost	€ 1,355,137
Methanol converter	786.69 kg _{cat}	17.87 €/kg _{cat}	€ 14,055
BoS cost for the methanol converter	-	61% of the total converter cost	€ 8,986
H ₂ storage tank	16,245 m ³	-	€ 958,820
CO storage tank	1,310 m ³	-	€ 265,508
Centrifugal compressor for CO stream	35 kW	-	€ 128,374
Centrifugal compressor for H ₂ stream (from CO ₂ electrolyzer)	5 kW	-	€ 117,125
Centrifugal compressor for H ₂ stream (from H ₂ O electrolyzer)	336 kW	-	€ 244,446
Air-cooled chiller for CO stream	9.6 kW	-	€ 1,599
Air-cooled chiller for H ₂ stream (from CO ₂ electrolyzer)	1.2 kW	-	€ 200
Air-cooled chiller for H ₂ stream (from H ₂ O electrolyzer)	99 kW	-	€ 16,485
Total purchased-equipment cost (TPEC)	-	-	€ 30,002,479
Delivery cost	-	10% of TPEC	€ 3,000,248
Total delivered-equipment cost (TDEC)	-	-	€ 33,002,727

TCI estimation method. The values of these cost factors are relevant to a fluid processing plant, since the system of this thesis handles liquids and gases.

Finally, TCI can be estimated using WC, the cost factors of Table 5.8 and TDEC. Table 5.9 presents the worksheet for the TCI estimation of this project. As it can be seen, the TDEC of this project is equal to 33 M€, FCI is equal to 166.3 M€ and **TCI is equal to 195.7 M€**. So, TCI is 5.93 times higher than TDEC. According to another TCI estimation

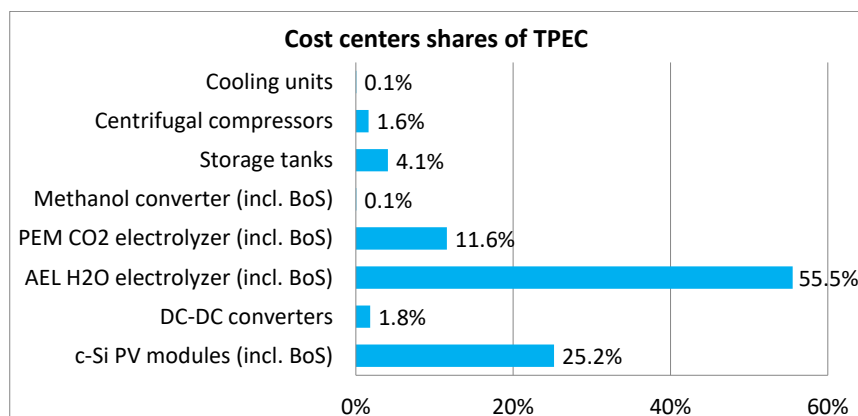


Figure 5.1: Cost centers shares of TPEC per equipment type

Table 5.8: List of direct and indirect costs for the estimation of fixed capital investment [141]

Cost Type	Cost Item	% of TDEC
Direct	Delivered equipment	100
Direct	Delivered equipment installation	47
Direct	Instrumentation and controls (installed)	36
Direct	Piping (installed)	68
Direct	Electrical systems (installed)	11
Direct	Buildings	18
Direct	Yard improvements	10
Direct	Service facilities (installed), like fire protection, waste disposal etc.	70
Indirect	Engineering and supervision	33
Indirect	Construction expenses	41
Indirect	Legal expenses	4
Indirect	Contractor's fee	22
Indirect	Contingency	44

method, which is called "Lang Factors for Approximation of Capital Investment", TCI is 6 times higher than TDEC for fluid processing plants [141]. We see that the proposed TCI estimation method has a good accuracy, since the factor of TCI/TDEC is very close to the relevant Lang factor.

5.4. OPERATIONAL EXPENDITURES ESTIMATION

THE operational expenditures is the sum of the revenues, equipment maintenance cost and feedstock expenses per year. The estimation of these expenditures has been

Table 5.9: Worksheet for the total capital investment of the project

Cost Item	Unit Cost in % of TDEC	Total Cost
Total delivered-equipment cost (TDEC)	100	€ 33,002,727
Delivered equipment installation	47	€ 15,511,282
Instrumentation and controls (installed)	36	€ 11,880,982
Piping (installed)	68	€ 22,441,854
Electrical systems (installed)	11	€ 3,630,300
Buildings	18	€ 5,940,491
Yard improvements	10	€ 3,300,273
Service facilities (installed)	70	€ 23,101,909
Total direct costs (TDC)	-	€ 118,809,818
Engineering and supervision	33	€ 10,890,900
Construction expenses	41	€ 13,531,118
Legal expenses	4	€ 1,320,109
Contractor's fee	22	€ 7,260,600
Contingency	44	€ 14,521,200
Total indirect costs (TIC)	-	€ 47,523,927
Fixed capital investment (FCI = TDC + TIC)	-	€ 166,333,745
Working Capital (WC, 15% of TCI)	-	€ 29,372,427
Total capital investment (TCI = WC + FCI)	-	€ 195,706,172

done using the purchased-equipment cost (PEC) of Table 5.7, the equipment cost data of section 5.1 and the sizing results of chapter 4. Table 5.10 presents the worksheet for the estimation of the operational expenditures of this project.

As it can be seen in Table 5.10, **the system generates a gross profit of € 855,535 per year**. However, it has to be noted that the annual maintenance of the system requires almost 2 M€ per year, while the revenues are almost 2.9 M€ per year. Looking at the maintenance costs of Table 5.10 in detail, we see that the most expensive maintenance jobs are the MEA replacement of the CO₂ electrolyzer and the stacks replacement of the H₂O electrolyzer. This is also supported by Figure 5.2, which presents the cost centers' shares of TAMC per equipment type (based on the data of Table 5.10). The MEA replacement of the CO₂ electrolyzer accounts for almost 40% of TAMC and the stacks replacements of the H₂O electrolyzer accounts for almost 37% of TAMC.

5.5. NPV RESULTS

FOR the estimation of the economic potential of this thesis system, a cash flow analysis was performed, in order to determine the end-of-life net present value (NPV). This

Table 5.10: Worksheet for the operational expenditures of the project

Annual Maintenance	Unit Cost	Total Cost
c-Si PV modules	5 €/kWp	€ 90,000
DC-DC converters replacement (every 12.5 years)	0.025 €/Wp	€ 44,000
AEL H ₂ O electrolyzer	2.08% of PEC	€ 211,410
AEL H ₂ O electrolyzer stacks replacement cost (every 60,000 hours or 7 years)	50% of PEC	€ 725,995
PEM CO ₂ electrolyzer	2.5% of PEC	€ 52,989
Cell compartment replacement cost for CO ₂ electrolyzer (every 7 years)	15% of PEC	€ 45,419
MEA replacement cost for CO ₂ electrolyzer (every year)	986.95 €/m ²	€ 785,614
Methanol converter	3% of PEC	€ 422
Methanol converter stacks replacement cost (every 4 years)	17.87 €/kg _{cat}	€ 3,514
Centrifugal compressors (all of them)	3% of PEC	€ 14,698
Air-cooled chillers (all of them)	3% of PEC	€ 549
Total annual maintenance cost (TAMC)	-	€ 1,974,609

Annual Feedstock Supply	Unit Cost	Total Cost
Water supply to the H ₂ O electrolyzer	0.83 €/m ³	€ 3,737
CO ₂ captured (fed to the methanol converter and CO ₂ electrolyzer)	33.46 €/ton	€ 71,824
Total annual feedstock cost (TAFC)	-	€ 75,561

Sales	Unit Price	Total Price
Methanol	410 €/ton	€ 1,639,525
Oxygen	317.58 €/ton	€ 1,266,180
Gross Revenues (GR)	-	€ 2,905,705

Gross earnings (GE=GR-TAMC-TAFC)	-	€ 855,535
---	---	------------------

analysis requires the discount of future cash flows in present values. The sum of all the discounted future cash flows, in a given time period, is the NPV [142]. Therefore, the NPV method is useful for evaluating the capital of a project, by determining whether the investment will generate a net profit or not [142]. NPV can be estimated by the following equation [142]:

$$NPV = \sum_{t=1}^n \frac{R_t}{(1+i)^t} \quad (5.3)$$

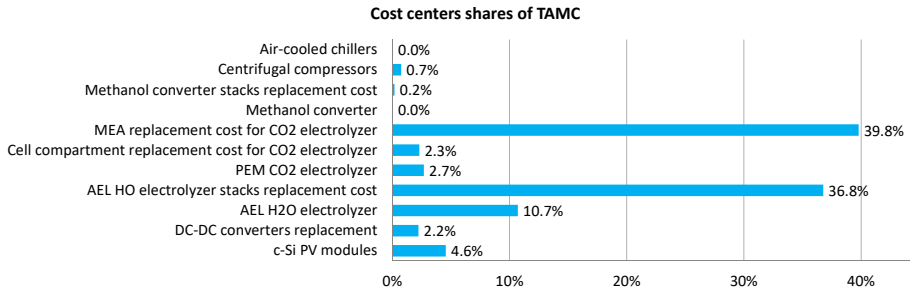


Figure 5.2: Cost centers shares of TAMC per equipment type

where R_t is the undiscounted cash flow at a given time period, i is the discount rate and t is the time period (i.e. up to 20 years).

Taking into account the equipment lifetime (see section 5.1), it is assumed that the operation life of the system will be 20 years (i.e. $n=20$ years). Also, it is assumed that the discount rate is equal to 10% (i.e. $i=10\%$) [143]. The project's depreciation is determined by the MACRS depreciation scheme over 10 years (see Table E1 in Appendix F) [143]. Moreover, in the depreciation schedule, a salvage value of 20% will be taken into account [143]. The salvage value is the estimated book value of all the assets after depreciation at the end of project's lifetime [144]. In other words, the salvage value of an asset determines how much money the business expects to make, if this asset is sold at the end of its useful life. In terms of taxes, the corporate tax in Greece is equal to 22% [145]. All the aforementioned parameters, which have been taken into account in the cash flow analysis, are presented in Table 5.11.

Table 5.11: Parameters for cash flow analysis

Parameter	Value
Project lifetime (n)	20 years
Discount rate (i)	10% [143]
Depreciation scheme	MACRS depreciation scheme over 10 years [143]
Salvage value	20% [143]
Tax on corporate income	22% [145]

As it can be seen in Table 5.10, the project will have GR of € 2,905,705 and GE of € 855,535 per year. At this part of the cash flow analysis, the earnings before tax (EBT) are estimated by subtracting the annual depreciation from GE [146]. Therefore, taking into account the MACRS depreciation scheme, EBT will be negative for the first 11 years of the project's lifetime. During this time period, the annual depreciation is higher than GE, since FCI (i.e. € 166,333,745, in Table 5.9) is going to be depreciated in 11 years. For the rest of the project's lifetime, EBT will be positive, since there will be no depreciation

for these years.

Furthermore, the net income is estimated according to EBT. If EBT is negative, then there will be no taxable income (i.e. no taxes are applied) and the project will have a net loss. On the other hand, if EBT is positive, then taxes will be applied at a rate of 22% and the project will have a net profit. The undiscounted cash flow, R_t , can be estimated by adding the net income and depreciation, because depreciation is an accountable measure and not an outlay of cash [147]. It should be mentioned that R_t is equal to TCI (i.e. € 195,706,172, in Table 5.9) in year 0 and equal to the sum of net income and salvage value in year 20. As it was previously stated, salvage value is an expected cash flow at the end of an asset's useful life. Finally, NPV can be estimated using the R_t of every year and the equation 5.3.

Based on what mentioned above, Table E.2 in Appendix F presents the cash flow analysis for this project. Figure 5.3 presents an overview of the cumulative NPV over the project lifetime (20 years). According to the aforementioned Table and Figure, the cumulative present value is equal to TCI (i.e. -195.7 M€) in year 0 and increased by 8.3% (reaching -179.5 M€) at the end of the project lifetime. The cumulative present value keeps increasing (see Figure 5.3), because the annual cash flows are positive (see Table E.2) and the project has a gross profit every year. In the 20th year of operation, the cumulative present value is dramatically increased, because the project's salvage value (i.e. 20%) has been included in this year's cash flow. Although, the cumulative present value of this project increases over its lifetime, **the project's NPV is negative and equal to -179.5 M€**. The NPV negativity shows that this investment would result in a **net loss and be economically unfeasible**.

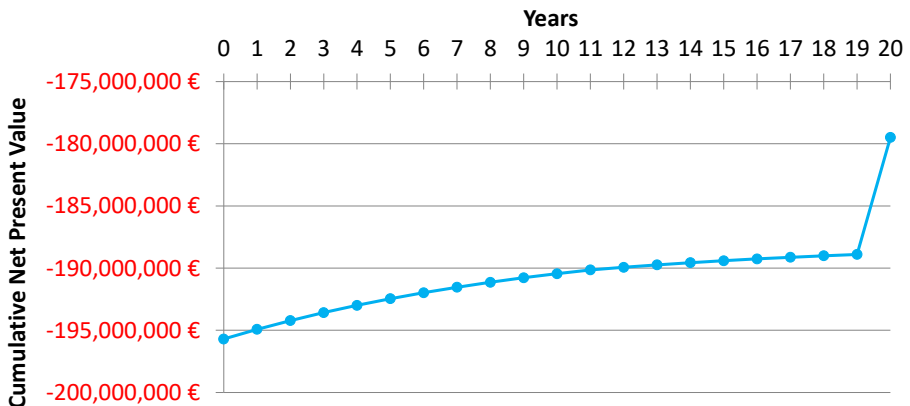


Figure 5.3: Cumulative NPV over the project lifetime (20 years)

5.6. LCOM RESULTS

ANOTHER way for the economic assessment of this project would be the estimation of the levelized cost of methanol (LCOM). As in the case of the levelized cost of energy (LCOE), LCOM could show the minimum required selling price of methanol, so that the investment could break even (i.e. revenues equal costs) over its lifetime [148]. The estimation of the LCOM can be done identically to the estimation of the LCOE. So, LCOM can be estimated using the following equation [149]:

$$LCOM = \frac{I_0 + \sum_{t=1}^n \frac{OM_t}{(1+r)^t}}{\sum_{t=1}^n \frac{M_t}{(1+r)^t}} \quad (5.4)$$

where I_0 is the total capital cost, OM_t is the undiscounted operation and maintenance cost at a given time period, r is the discount rate, M_t is the undiscounted production of methanol at a given time period and t is the time period.

As it was mentioned in the above section 5.5, the project's lifetime is equal to 20 years (i.e. $n=20$ years). It can be assumed that the discount rate is equal to 6% [149]. Also, I_0 is equal to TCI (i.e. € 195,706,172), OM_t is equal to the sum of TAFC and TAMC (i.e. € 2,050,170) and M_t is equal to 3.999 kT of methanol.

According to the aforementioned cost data and the equation 5.4, **LCOM is equal to 4.44 €/kg**. Taking into account the selling price of methanol (i.e. 410 €/ton, see section 5.2), the LCOM value is almost 10 times higher than the methanol's selling price and this would yield a lower return on capital. Therefore, it is clear that such an investment results in a **loss and is economically unfeasible**.

5.7. ENVIRONMENTAL BENEFIT

THE environmental benefit of the proposed system is the recycling of CO₂ emissions. Since the CO₂ comes from the flue gases of a cement plant, this amount of CO₂ is recycled and not emitted into the atmosphere. As it has been mentioned in previous sections, 28,590,040 mol_{CO₂} need to be fed into the methanol reactor and 20,190,000 mol_{CO₂} need to be fed into the CO₂ electrolyzer (see Tables 4.2 and 4.4, respectively). Therefore, **the total amount of recycled CO₂ is equal to 2,147 tons per year** (using the CO₂ molar mass, 44.01 g/mol).

Based on World Bank data, the CO₂ emissions per capita in the European Union was equal to 6.424 tons in 2018 [150]. Also, a typical passenger vehicle emits 4.6 tons of CO₂ per year, according to the Environmental Protection Agency of USA [151]. Therefore, the total amount of recycled CO₂ by the proposed system could correspond to the annual CO₂ emissions of 467 passenger vehicles or 334 European citizens.

5.8. SUMMARY

THE economic potential of this thesis system was estimated and analyzed in this chapter. The first step towards this analysis was the estimation of the system's equip-

ment prices, including purchasing prices, operating costs and lifetime. Then, the market prices of methanol, feedstocks and dumped energy were estimated. The cost of dumped energy was based on the PV tender tariff in Greece.

The aforementioned prices were used in the estimation of the system's total capital investment, i.e. TCI. The TCI estimation was based on the method "Percentage of Delivered-Equipment Cost", which is mentioned in the book of Peters et al [141]. It is worth mentioning that the cost of land was excluded by the TCI estimation, since the land cannot be depreciated by law [141].

According to the equipment prices and the method followed, **the system's TPEC is equal to 30 M€ and its TDEC equals to 33 M€** (including 10% of TPEC as delivery cost). The most expensive equipment is the H₂O electrolyzer, PV modules and CO₂ electrolyzer (accounting for 55.5%, 25.2% and 11.6% of TPEC, respectively).

Moreover, the system's FCI was estimated, according to the factors for direct and indirect costs of Table 5.8 (following the aforementioned method). It was found that FCI is equal to 166.3 M€. Taking into account the working capital (i.e. 15% of TCI), **the system's TCI is equal to 195.7 M€**.

As far as the **system's operational expenditures** are concerned, it was found that they are equal to **almost 2 M€ per year**, from which 1.97 M€ are spent for maintenance and the rest for feedstocks supply. The most expensive maintenance jobs are the MEA replacement of the CO₂ electrolyzer (i.e. 40% of TAMC) and the stacks replacement of the H₂O electrolyzer (i.e. 37% of TAMC). On the other hand, the system's revenues are equal to almost 2.91 M€ per year. Therefore, the system has an **annual gross profit of € 855,535**.

A cash flow analysis was carried out, using TCI and the parameters of Table 5.11. According to this analysis, it was found that the cumulative present value of this project increases over its lifetime (i.e. 20 years). However, **the project's NPV is negative and equal to -179.5 M€** in the 20th year of operation. Although, the cumulative present value is increased by 8.3% at the end of the project lifetime, such **an investment would result in a net loss**.

The above conclusion is also supported by the fact that LCOM is almost 10 times higher than the methanol's market price. **LCOM is equal to 4.44 €/kg**, while the methanol's market price is equal to 410 €/ton. This high difference would result in a **lower return on capital**. Finally, **the environmental benefit of the proposed system is the recycling of 2,147 tons of CO₂ per year, although such a project would be economically unfeasible**.

6

CONCLUSIONS AND RECOMMENDATIONS

This chapter presents the conclusions that can be drawn by answering the research questions, based on this thesis findings. Also, this chapter provides recommendations for future research and development related to PtX schemes for producing methanol.

6.1. CONCLUSIONS

THE scope of this thesis was the evaluation of the techno-economic potential of a PtX scheme, which produces methanol, exploiting H₂O and CO₂ electrolyzers, captured CO₂, a methanol reactor and PV panels. In such a system, it was decided that the electrolyzers are in dynamic operation (i.e. under variable operating efficiency and following the intermittent PVs power output) and the methanol reactor was in constant operation (i.e. independent of the PVs power output). The findings of this thesis can be concluded and summarized by answering the research questions of section 1.3, as follows:

- *How can the whole process for methanol production be modelled and designed at industrial scale, when the system is connected to renewables?*

The system of this thesis has been designed according to the findings of the literature review and modelled in MATLAB/Simulink. An overview of the system configuration can be seen in Figure 3.2. In the following paragraphs, the way the system has been designed and modelled is presented.

To begin with, it has been decided that the production aim of the proposed system is equal to 4 kT/year. This production target is an example of industrial scale, because it is the same as the production capacity of the George Olah plant (the world's first CO₂-to-methanol plant powered by wind farms), located in Svartsengi,

Iceland.

Based on the available literature, it has been decided that the methanol is produced through the CO₂ hydrogenation process. This process has been selected, because the syngas can be fed into a commercial CuO/ZnO/Al₂O₃ catalyst, which enables the high selectivity of methanol (i.e. >99% with recycle). This synthesis process requires a methanol converter, which converts the syngas to methanol. According to Table 3.9, the syngas should consist of CO, CO₂ and H₂.

As far as the feedstocks supply is concerned, it has been decided that the supplied CO₂ will be captured from the flue gases of a cement plant. Since the captured CO₂ is fed to the methanol reactor and CO₂ electrolyzer, the capture of CO₂ from the flue gases of natural gas and coal power plants was not selected, due to the presence of SO₂ and NO_x impurities in their flue gases. Such impurities reduce the Faradaic efficiency of the CO₂ electrolysis process. It has been assumed that the captured CO₂ is supplied by a cement plant, meeting the specifications of Table 3.3. Also, the required amount of CO is produced via CO₂ electrolysis. The last component of syngas (i.e. H₂) is produced via H₂O electrolysis process, with O₂ being produced as a by-product of this process.

6

Solar energy has been selected as the renewable energy source of the proposed system. The PVs power output has been estimated by acquiring the relevant data from the PVGIS platform of the EU Science Hub. It has been decided that the PVs supply electrical energy to the electrolyzers and auxiliary equipment, as well. In Simulink, the total required electrical power for the auxiliary equipment is subtracted from the total PVs power output and the rest of this power is fed to the electrolyzers.

Power electronics are required for regulating the current and voltage of the PVs power output to the operating level of the system equipment. More specifically, DC-DC converters are exploited and connected between the PVs and the rest of the equipment. Such converters have been selected, because the PVs produce DC voltage and the rest of the system (i.e. electrolyzers etc) runs on DC voltage, as well. Therefore, it has been assumed that all the system's DC-DC converters are uniformly loaded and their operating efficiency is the same. The converters have been modelled, based on the efficiency curve of a DC-DC MOSFET converter (found in literature).

The system's H₂O electrolyzer has been designed by scaling up the alkaline water electrolyzer H₂ IGen 300/1/25, whose performance characteristics were found in literature. The scaling-up has been done based on the J-V_{cell} and J-Energy Efficiency curves of the electrolyzer H₂ IGen 300/1/25 (see subsections 3.8.4 and 3.8.6 for more information). It has also been assumed that the H₂O electrolyzer of this project has the same half-reactions and operating conditions as the electrolyzer

H₂ IGen 300/1/25 has. Moreover, it has been assumed that the H₂O electrolyzer of this project consists of stacks, which are connected in parallel. Finally, Table 3.6 presents all the specifications of the system's H₂O electrolyzer.

The CO₂ electrolyzer of the proposed system has been designed by scaling up the cell of an APEM CO₂ electrolyzer, whose performance characteristics were found in literature. The scaling-up has been done based on i) the J-V_{cell}, ii) V_{cell}-Energy Efficiency, iii) V_{cell}-Faradaic Efficiency of CO and iv) V_{cell}-Faradaic Efficiency of H₂ curves of the aforementioned cell (see subsections 3.7.4 and 3.7.6 for more information). It has also been assumed that the CO₂ electrolyzer of this project has the same half-reactions and operating conditions as the aforementioned cell. Moreover, it has been assumed that the CO₂ electrolyzer of this project consists of stacks, which are connected in parallel. Finally, all the specifications of the system's CO₂ electrolyzer can be seen in Table 3.5.

Based on the selected methanol synthesis process, it has been decided that a single-stage Lurgi quasi-isothermal reactor will convert the syngas to methanol (see Table 3.9). Such a reactor can operate in the desired temperature and pressure operating ranges of Table 3.9, reaching high conversion and recycle rates. The methanol reactor of the proposed system has been designed by scaling down the model of a single-stage Lurgi quasi-isothermal reactor, which was found in literature (its simulation results were related to a methanol production of 90 kT/year). The scaling-down has been done based on the following parameters of the Lurgi reactor found in literature: i) the catalyst mass per tube, ii) the methanol production per tube, iii) the methanol production per catalyst particle and iv) the methanol molar production per catalyst particle (see section 3.11 for more information). It has also been assumed that the methanol reactor of this project has the same syngas compositions, conversion rate and recycle ratio as the Lurgi reactor of the literature has. Finally, all the specifications of the system's methanol reactor are presented in Table 3.10.

Taking into account the feeding requirements of the system's methanol reactor (see Table 3.10), the electrolysis products (i.e. H₂ and CO) had to be further compressed and cooled down. Therefore, compressors and cooling units have been designed and modelled in Simulink, so that H₂ and CO can properly be fed in the methanol reactor.

Finally, the last part of the system design and modelling is related to the power split between the CO₂ and H₂O electrolyzers. As it has been mentioned above, the PVs firstly supply electrical energy to the auxiliary equipment and the rest of the PVs power output is fed to the electrolyzers. But, it has been decided that the power is split between the electrolyzers according to the required syngas composition (i.e. H₂ : CO₂ : CO = 83.8% : 9.5% : 6.7%, see Table 3.10). Therefore, more power should flow to the H₂O electrolyzer than to the CO₂ electrolyzer, because

more H_2 than CO is required for the methanol synthesis. More information about the power split is given in the sections 4.5 and 4.6.

- *How can the intermittent power output of PV panels be integrated in such a production process?*

The proposed system, as it has been described in the above research question, cannot follow completely the intermittent power output of the PV panels. This is not acceptable, because the electrolyzers do not operate in their desired efficiency range. For example, if the PVs power output is too low, the electrolyzers may not even exploit this power, because too many stacks will be in operation and the input current may not be sufficient for electrolysis. In such an example, the PVs energy output should have been stored in batteries or dumped.

That's why; a control logic that controls the electrolyzers' operation is required. Such a control logic is responsible for the electrolyzers' dynamic operation (inside their desired efficiency range) and subsequently for the system's operational flexibility. Another scope of this control logic is the decision on whether or not the PVs power output should be dumped. The flowchart of this control logic can be seen in Figure 3.5.

6

As it can be seen in the aforementioned Figure, if the PVs power output is too low, less stacks of the electrolyzers are required to be in operation for exploiting this power input. Such dynamic operation is possible, because the stacks of the electrolyzers are connected in parallel. However, if less than 1 stack of an electrolyzer is required to be in operation, then the electrolyzer is off and its energy input is dumped. It is not possible to operate only a fraction of a single stack. The number of stacks in operation is always an integer. On the other hand, if the PVs power output is too high, the electrolyzer can operate up to its maximum capacity and the rest of its energy input is dumped. Therefore, this control logic ensures that either the electrolyzers will operate in their desired efficiency range (following the intermittent PVs power output) or not.

Contrary to the electrolyzers, it has been decided that the methanol synthesis process is continuous, constant and independent from the intermittent power output of the PVs. The equipment that connects the methanol reactor to the rest of the system is the buffer tanks of CO and H_2 . These buffer tanks are required, because they store the electrolysis products (i.e. CO and H_2) and ensure that the supply of H_2 and CO to the methanol reactor is constant and continuous. Therefore, the operation of the methanol reactor and the methanol production rate are constant.

Due to the implementation of the aforementioned control logic and the buffer tanks, it is possible for the system to follow the intermittent power output of the

PVs. This is done due to the dynamic operation of the electrolyzers and the constant operation of the methanol reactor.

Finally, the system does not require any batteries, because there is no need for electrical energy storage. The excess of energy is stored chemically in the buffer tanks. Also, the cost of buffer tanks is lower than the cost of batteries, because buffer tanks are a simple and economical piece of equipment.

- *What is the techno-economic performance of the intermittent production process and how can it be compared to the existing market of methanol?*

As far as the production results are concerned, it has been found that the system can produce 3.999 kT of methanol per year, requiring an energy input of 30.3 GWh/year. This production result is very close to the production target (i.e. 4 kT/year). The installed peak PV power is equal to 18 MWp and their energy yield is equal to 30.54 GWh/year. Also, it has been found that the system exploits 99.60% of the PVs energy yield per year and the dumped energy is equal to 121.20 MWh/year.

The system is able to exploit such a high percentage of its energy input, because the electrolyzers can operate dynamically inside their desired efficiency range and subsequently can follow the intermittent PVs power output. The control logic, as it was described in the above research question, results in the efficiency ranges of 45.07-55.32% for the CO₂ electrolyzer and 75.83-81.71% for the H₂O electrolyzer. Therefore, a battery bank would not have such an important impact on the system's performance, because the system almost reaches its production target.

The consumed amount of captured CO₂ is equal to 2,147 tons per year and is fed into the electrolyzer and methanol converter. This amount of CO₂ is recycled by the system and not emitted into the atmosphere. This feature of the system explains its environmental benefit.

In terms of economic analysis, the system's TPEC is equal to 30 M€ and its TDEC equals to 33 M€ (including 10% of TPEC as delivery cost). Such high equipment prices result in a total capital investment of 195.7 M€ (including 15% of TCI as working capital). Also, the system's operational expenditures are equal to almost 2 M€ per year. Both types of electrolyzers affect the most the total capital and operational expenditures of the system.

According to the cash flow analysis of section 5.5, the system has an annual gross profit of € 855,535 per year. However, this gross profit is not enough for making this project attractive. The system's NPV is negative and equal to -179.5 M€ at the end of its lifetime (i.e. 20 years). That's why; such an investment would result in a net loss of capital.

The economic potential of the proposed system was also assessed by estimating the LCOM. The LCOM is equal to 4.44 €/kg, which is almost 10 times higher than the existing market price of methanol. This shows that such an investment is characterized by a lower return on capital. Therefore, the proposed system is not economically feasible, despite its environmental benefit.

6.2. RECOMMENDATIONS FOR FUTURE RESEARCH

RECOMMENDATIONS for future research and development are made in this chapter. The following list presents the recommendations, which are based on the results and assumptions of this thesis.

- Predictions for the energy yield of the PV panels over a longer time period (e.g. 20 years) should be made. Such predictions should be based on historical data for the weather at the selected location. A better predicted energy input could improve the reliability of the model, because the size of the electrolyzers, methanol converter, auxiliary equipment and buffer tanks could be better estimated/optimized.
- It could be assessed whether or not a combination of two different renewable energy sources could be a better fit for the proposed system. For example, a combination of wind turbines and PV panels could be beneficial for the system. It is well known that PV panels generate power during the day and wind turbines produce more power at night. The combination of both could decrease the intermittency of their combined power generation over the whole day. Therefore, the electrolyzers could follow their power output easier and more efficiently.
- Due to the dynamic operation of the electrolyzers, a detailed assessment of its consequences to the electrolyzers should be made. The dynamic operation of the electrolyzers means that the electrolyzers follow the intermittent power output of the PVs, by adjusting the number of their stacks, which are in operation, every hour. Therefore, it should be assessed what consequences could the hourly switching on/off of their stacks have, in terms of overall cell structure, cell stability, membrane stability, membrane degradation, damage on the catalyst, damage on the electrodes, gas permeation etc. This assessment should be related to the selected electrolysis technologies (i.e. alkaline water electrolysis and alkaline polymer electrolyte membrane for CO₂ electrolysis).
- The possibility of increasing the operating pressure of the electrolyzers should be assessed. According to Tables 3.5 and 3.6, the operating pressure of both electrolyzers is 10 bar. But, the electrolysis products (i.e. H₂ and CO) must be fed into the methanol reactor at a pressure of 69.7 bar (see Table 3.10). It should be assessed if the selected AEL water electrolyzer and PEM CO₂ electrolyzer can operate more efficiently at higher pressures. If yes, this could reduce the power demand for further compression of H₂ and CO. Therefore, smaller compressors would be required and subsequently the capital and operational expenditures of the system would be reduced.

- The implementation of a battery bank in the system may eliminate the dumped energy and increase the mean operating efficiency of the electrolyzers. Also, a battery bank could affect the selected efficiency ranges of operation for each electrolyzer. It has been decided that the CO₂ electrolyzer operates in the energy efficiency range of 45-55% and the H₂O electrolyzer in the energy efficiency range of 75.83-81.90% (see Tables 3.5 and 3.6, respectively). According to Tables 4.4 and 4.5, the mean operating efficiency of the CO₂ electrolyzer is equal to 50.86% and 76.52% for the H₂O electrolyzer. Also, the dumped energy of the system was equal to 121.20 MWh/year. For example, a potential scenario would be that a battery bank may result in narrower selected efficiency ranges (like 50-55% and 78-81.90% for the CO₂ and H₂O electrolyzers, respectively), subsequently higher mean operating efficiencies and zero dumped energy. Therefore, the benefit of a battery bank should be assessed, in terms of the aforementioned parameters and the economic feasibility of the system.
- Another recommendation would be the optimization of the operating energy efficiency ranges for both electrolyzers. It should be estimated what are the optimal energy efficiency ranges for the electrolyzers, in terms of capital and operational costs of the system. For example, a range of 40-55% for the CO₂ electrolyzer might be more beneficial, compared to the selected range of 45-55%, because more PVs energy yield will be exploited and not dumped. This recommendation is related to the implemented system, without the use of a battery bank.
- As far as the buffer tanks are concerned, their design and size have been based on the fact that, the H₂ and CO gases have been treated by this thesis in accordance with the ideal gas law (for simplicity). As it can be seen in Table 3.7, the average compressibility factors of CO (z_{CO}) and H₂ (z_{H_2}) are equal to 0.99964 and 1.0006, respectively. Since these factors are not equal to 1, these gases cannot be considered as ideal gases. So, H₂ is more compressible than ideal gases ($z_{H_2} > 1$) and CO is less compressible than ideal gases ($z_{CO} < 1$). Since real gases have the property of attraction or repulsion between different molecules, their molecules can vary their size by being combined/stuck with other molecules (forming one thing) or being repelled. This property affects the compressibility of H₂ and CO in reality and subsequently their injection times from and to the buffer tanks. Therefore, a detailed assessment of how such real gases must be treated and handled should be done, taking into the aforementioned parameters and safety aspects.
- The sizing of the proposed system was done according to an empirical analysis of the various system parameters (e.g. amount of methanol reactor's tubes, buffer tanks capacity, feeding rates of H₂ and CO to the methanol reactor, etc.). Therefore, the system size should be optimized using a solver for mixed-integer linear programming (including a sensitivity analysis). An optimized system size may result in lower capital and operational expenditures (making this investment more attractive).
- The last recommendation is related to the equipment prices, which affect strongly the capital expenditures of the proposed system. It could be assessed what would

the influence of future equipment prices be on the system's economic feasibility. For example, what would the NPV and LCOM projections be, if the system lifetime was from 2030 to 2050? It is expected that the prices of various system's components will be reduced by 2030 (e.g. PV panels, H₂O and CO₂ electrolyzers). So, based on future reduction of the capital investment, this proposed system might be attractive.

BIBLIOGRAPHY

- [1] NASA, *Overview: Weather, Global Warming and Climate Change*, [Accessed: 24.05.2021]. [Online]. Available: <https://climate.nasa.gov/resources/global-warming-vs-climate-change/>.
- [2] European Union, *Causes of climate change*, [Accessed: 24.05.2021]. [Online]. Available: https://ec.europa.eu/clima/change/causes_en.
- [3] United Nations Framework Convention on Climate Change (UNFCCC secretariat), *Key aspects of the Paris Agreement*, [Accessed: 24.05.2021]. [Online]. Available: <https://unfccc.int/process-and-meetings/the-paris-agreement/the-paris-agreement/key-aspects-of-the-paris-agreement>.
- [4] —, *Paris Agreement - Status of Ratification*, [Accessed: 24.05.2021]. [Online]. Available: <https://unfccc.int/process/the-paris-agreement/status-of-ratification>.
- [5] European Union, *2030 climate energy framework*, [Accessed: 24.05.2021]. [Online]. Available: https://ec.europa.eu/clima/policies/strategies/2030_en.
- [6] —, “Energy roadmap 2050,” Publications Office of the European Union, 2012. DOI: 10.2833/10759. [Online]. Available: https://ec.europa.eu/energy/sites/ener/files/documents/2012_energy_roadmap_2050_en_0.pdf.
- [7] —, “The potential for ccs and ccu in europe,” May 2019. [Online]. Available: https://ec.europa.eu/info/sites/default/files/iogp_-_report_-_ccs_ccu.pdf.
- [8] M. Pérez-Fortes, J. C. Schöneberger, A. Boulamanti, and E. Tzimas, “Methanol synthesis using captured co₂ as raw material: Techno-economic and environmental assessment,” *Applied Energy*, vol. 161, Jan. 2016, ISSN: 03062619. DOI: 10.1016/j.apenergy.2015.07.067. [Online]. Available: [https://www.sciencedirect-com.tudelft.idm.oclc.org/science/article/pii/S0306261915009071#b0025](https://www.sciencedirect.com.tudelft.idm.oclc.org/science/article/pii/S0306261915009071#b0025).
- [9] N. von der Assen, P. Voll, M. Peters, and A. Bardow, “Life cycle assessment of co₂ capture and utilization: A tutorial review,” *Chem. Soc. Rev.*, vol. 43, 23 Jan. 2014, ISSN: 0306-0012. DOI: 10.1039/C3CS60373C. [Online]. Available: <https://pubs-rsc-org.tudelft.idm.oclc.org/en/content/articlelanding/2014/CS/C3CS60373C#divAbstract>.
- [10] G. Buffo, P. Marocco, D. Ferrero, A. Lanzini, and M. Santarelli, *Power-to-x and power-to-power routes*, 2019. DOI: 10.1016/B978-0-12-814853-2.00015-1. [Online]. Available: <https://www.sciencedirect-com.tudelft.idm.oclc.org/science/article/pii/B9780128148532000151#s0040>.

- [11] SAPEA, Science Advice for Policy by European Academies, “Novel carbon capture and utilisation technologies: Research and climate aspects,” 2018, p. 50. DOI: [10.26356/CARBONCAPTURE](https://doi.org/10.26356/CARBONCAPTURE). [Online]. Available: <https://www.sapea.info/topics/carboncaptureandutilisation/>.
- [12] W. A. Smith, T. Burdyny, D. A. Vermaas, and H. Geerlings, “Pathways to industrial-scale fuel out of thin air from co₂ electrolysis,” *Joule*, vol. 3, 8 Aug. 2019, ISSN: 25424351. DOI: [10.1016/j.joule.2019.07.009](https://doi.org/10.1016/j.joule.2019.07.009). [Online]. Available: <https://www-sciencedirect-com.tudelft.idm.oclc.org/science/article/pii/S2542435119303538>.
- [13] R. Andika, A. B. D. Nandiyanto, Z. A. Putra, M. R. Bilad, Y. Kim, C. M. Yun, and M. Lee, *Co-electrolysis for power-to-methanol applications*, Nov. 2018. DOI: [10.1016/j.rser.2018.07.030](https://doi.org/10.1016/j.rser.2018.07.030). [Online]. Available: <https://www-sciencedirect-com.tudelft.idm.oclc.org/science/article/pii/S1364032118305380?via%5C%3Dihub>.
- [14] A. A. Tountas, X. Peng, A. V. Tavasoli, P. N. Duchesne, T. L. Dingle, Y. Dong, L. Hurtado, A. Mohan, W. Sun, U. Ulmer, L. Wang, T. E. Wood, C. T. Maravelias, M. M. Sain, and G. A. Ozin, *Towards solar methanol: Past, present, and future*, 2019. DOI: [10.1002/advs.201801903](https://doi.org/10.1002/advs.201801903). [Online]. Available: <https://onlinelibrary-wiley-com.tudelft.idm.oclc.org/doi/full/10.1002/advs.201801903>.
- [15] H. R. M. Jhong, S. Ma, and P. J. Kenis, *Electrochemical conversion of co₂ to useful chemicals: Current status, remaining challenges, and future opportunities*, May 2013. DOI: [10.1016/j.coche.2013.03.005](https://doi.org/10.1016/j.coche.2013.03.005). [Online]. Available: <https://www-sciencedirect-com.tudelft.idm.oclc.org/science/article/pii/S2211339813000294#bib0070>.
- [16] B. R. de Vasconcelos and J. M. Lavoie, *Recent advances in power-to-X technology for the production of fuels and chemicals*, 2019. DOI: [10.3389/fchem.2019.00392](https://doi.org/10.3389/fchem.2019.00392). [Online]. Available: <https://www.frontiersin.org/articles/10.3389/fchem.2019.00392/full>.
- [17] Carbon Recycling International (CRI), *George olah renewable methanol plant; first production of fuel from co₂ at industrial scale*, [Accessed: 17.01.2021]. [Online]. Available: <https://www.carbonrecycling.is/projects>.
- [18] —, *First minister of scotland visits cri*, [Accessed: 17.01.2021], Oct. 2017. [Online]. Available: <https://www.carbonrecycling.is/news-media/tag/George+Olah+Plant>.
- [19] Methanol Institute, *The marine fuel of the future*, [Accessed: 20.12.2020], Jul. 2020. [Online]. Available: <https://www.methanol.org/marine-fuel/>.
- [20] S. Verhelst, J. W. Turner, L. Sileghem, and J. Vancoillie, “Methanol as a fuel for internal combustion engines,” *Progress in Energy and Combustion Science*, vol. 70, 2019, ISSN: 03601285. DOI: [10.1016/j.pecs.2018.10.001](https://doi.org/10.1016/j.pecs.2018.10.001). [Online]. Available: <https://www-sciencedirect-com.tudelft.idm.oclc.org/science/article/pii/S036012851830042X>.

- [21] Methanol Institute, *Overview of global methanol fuel blending*, [Accessed: 02.01.2021], Jan. 2019. [Online]. Available: <https://www.methanol.org/wp-content/uploads/2019/02/4.-Greg-Dolan-Overview-of-Global-Methanol-Fuel-Blending.pdf>.
- [22] Q. I. Roode-Gutzmer, D. Kaiser, and M. Bertau, "Renewable methanol synthesis," *ChemBioEng Reviews*, vol. 6, 6 2019, ISSN: 21969744. DOI: 10.1002/cben.201900012. [Online]. Available: <https://onlinelibrary-wiley-com.tudelft.idm.oclc.org/doi/full/10.1002/cben.201900012>.
- [23] DNV-GL, *Methanol as a potential alternative fuel for shipping: A brief talk with chris chatterton of the methanol institute*, [Accessed: 28.12.2020], May 2020. [Online]. Available: <https://www.dnvgl.com/maritime/advisory/afi-update/Methanol-as-a-potential-alternative-fuel-for-shipping-A-brief-talk-with-Chris-Chatterton.html>.
- [24] Methanol Institute, *Methanol gasoline blends - alternative fuel for today's automobiles and cleaner burning octane for today's oil refinery*, [Accessed: 02.01.2021], 2016. [Online]. Available: <http://www.methanol.org/wp-content/uploads/2016/06/Blenders-Product-Bulletin-Final.pdf>.
- [25] N. Monnerie, P. G. Gan, M. Roeb, and C. Sattler, "Methanol production using hydrogen from concentrated solar energy," *International Journal of Hydrogen Energy*, vol. 45, 49 2020, ISSN: 03603199. DOI: 10.1016/j.ijhydene.2019.12.200. [Online]. Available: <https://www-sciencedirect-com.tudelft.idm.oclc.org/science/article/pii/S0360319920300033>.
- [26] Linde, *Safety data sheet Methane, compressed*, [Accessed: 07.01.2021], Jan. 2005. [Online]. Available: http://hiq.linde-gas.com/en/images/Methane%5C%20SDS%5C%20Linde%5C%20EU%5C%20format%5C%20HiQ%5C%20Jan%5C%202011_tcm899-92363.pdf.
- [27] —, *Safety Data Sheet Ethylene*, [Accessed: 13.01.2021], Jan. 2013. [Online]. Available: https://produkte.linde-gas.at/sdb_konform/C2H4_10021778EN.pdf.
- [28] Y.-T. Hung, P. Kajitvichyanukul, and L. K. Wang, *Advances in anaerobic systems for organic pollution removal from food processing wastewater*, 2008. DOI: 10.1533/9781845694678.5.755.
- [29] S. Rönsch, J. Schneider, S. Matthischke, M. Schlüter, M. Götz, J. Lefebvre, P. Prabhakaran, and S. Bajohr, "Review on methanation – from fundamentals to current projects," *Fuel*, vol. 166, Feb. 2016, ISSN: 00162361. DOI: 10.1016/j.fuel.2015.10.111. [Online]. Available: <https://www-sciencedirect-com.tudelft.idm.oclc.org/science/article/pii/S0016236115011254?via%3Dihub#b0025>.
- [30] M. Bailera, P. Lisbona, L. M. Romeo, and S. Espatolero, "Power to gas projects review: Lab, pilot and demo plants for storing renewable energy and co₂," *Renewable and Sustainable Energy Reviews*, vol. 69, pp. 292–312, Mar. 2017, ISSN: 18790690. DOI: 10.1016/j.rser.2016.11.130. [Online]. Available: <https://www-sciencedirect-com.tudelft.idm.oclc.org/science/article/pii/S1364026716300000>.

- [//www-sciencedirect-com.tudelft.idm.oclc.org/science/article/pii/S1364032116307833](https://www-sciencedirect-com.tudelft.idm.oclc.org/science/article/pii/S1364032116307833).
- [31] J. Gorre, F. Ortloff, and C. van Leeuwen, "Production costs for synthetic methane in 2030 and 2050 of an optimized power-to-gas plant with intermediate hydrogen storage," *Applied Energy*, vol. 253, Nov. 2019, ISSN: 03062619. DOI: [10.1016/j.apenergy.2019.113594](https://doi.org/10.1016/j.apenergy.2019.113594). [Online]. Available: <https://www-sciencedirect-com.tudelft.idm.oclc.org/science/article/pii/S0306261919312681#b0005>.
- [32] S. Faramawy, T. Zaki, and A. A. Sakr, "Natural gas origin, composition, and processing: A review," *Journal of Natural Gas Science and Engineering*, vol. 34, pp. 34–54, Aug. 2016, ISSN: 18755100. DOI: [10.1016/j.jngse.2016.06.030](https://doi.org/10.1016/j.jngse.2016.06.030). [Online]. Available: <https://www-sciencedirect-com.tudelft.idm.oclc.org/science/article/pii/S1875510016304139>.
- [33] Gas Infrastructure Europe (GIE), * *press release* * *existing gas storage capacity in europe exceeded one petawatthour in 2018, shrunked against 2016*, [Accessed: 06.01.2021], Dec. 2018. [Online]. Available: <https://www.gie.eu/index.php/gie-media/press-releases/13-news/gie/379-press-release-existing-gas-storage-capacity-in-europe-exceeded-one-petawatthour-in-2018-shrunked-against-2016>.
- [34] H. Al-Megren and T. Xiao, *Petrochemical Catalyst Materials, Processes, and Emerging Technologies*, H. Al-Megren and T. Xiao, Eds. IGI Global, 2016, pp. 82, 90–92, 105, ISBN: 9781466699755. DOI: [10.4018/978-1-4666-9975-5](https://doi.org/10.4018/978-1-4666-9975-5). [Online]. Available: <https://app.knovel.com/hotlink/toc/id:kpPCMPETOP/petrochemical-catalyst/petrochemical-catalyst>.
- [35] I. Rossetti, A. Tripodi, and G. Ramis, "Hydrogen, ethylene and power production from bioethanol: Ready for the renewable market?" *International Journal of Hydrogen Energy*, vol. 45, pp. 10 292–10 303, 17 Mar. 2020, ISSN: 03603199. DOI: [10.1016/j.ijhydene.2019.07.201](https://doi.org/10.1016/j.ijhydene.2019.07.201). [Online]. Available: <https://www-sciencedirect-com.tudelft.idm.oclc.org/science/article/pii/S036031991932837X>.
- [36] J. Althoff, K. Biesheuvel, A. D. Kok, H. Pelt, M. Ruitenbeek, G. Spork, J. Tange, and R. Wevers, "Economic feasibility of the sugar beet-to-ethylene value chain," *ChemSusChem*, vol. 6, 9 Sep. 2013, ISSN: 18645631. DOI: [10.1002/cssc.201300478](https://doi.org/10.1002/cssc.201300478). [Online]. Available: <https://chemistry-europe-onlinelibrary-wiley-com.tudelft.idm.oclc.org/doi/full/10.1002/cssc.201300478>.
- [37] M. Chu, C. Chen, Y. Wu, X. Yan, S. Jia, R. Feng, H. Wu, M. He, and B. Han, "Enhanced co₂ electroreduction to ethylene via strong metal-support interaction," *Green Energy Environment*, Dec. 2020, ISSN: 24680257. DOI: [10.1016/j.gee.2020.12.001](https://doi.org/10.1016/j.gee.2020.12.001). [Online]. Available: <https://www-sciencedirect-com.tudelft.idm.oclc.org/science/article/pii/S2468025720302223>.

- [38] Gulf Petrochemicals Chemicals Association (GPCA), *Ethylene: A litmus test for the chemical industry*, [Accessed: 14.01.2021], Nov. 2019. [Online]. Available: https://www.gpca.org.ae/wp-content/uploads/2020/04/Ethylene-A-Litmus-Test-for-the-Chemical-Industry_ES.pdf.
- [39] G. Bozzano and F. Manenti, "Efficient methanol synthesis: Perspectives, technologies and optimization strategies," *Progress in Energy and Combustion Science*, vol. 56, Sep. 2016, ISSN: 03601285. DOI: 10.1016/j.pecs.2016.06.001. [Online]. Available: <https://www.sciencedirect.com.tudelft.idm.oclc.org/science/article/pii/S0360128515300484#bib0130>.
- [40] S. G. Jadhav, P. D. Vaidya, B. M. Bhanage, and J. B. Joshi, "Catalytic carbon dioxide hydrogenation to methanol: A review of recent studies," *Chemical Engineering Research and Design*, vol. 92, 11 Nov. 2014, ISSN: 02638762. DOI: 10.1016/j.cherd.2014.03.005. [Online]. Available: <https://www.sciencedirect.com/science/article/pii/S0263876214001282>.
- [41] J. Albo, M. Alvarez-Guerra, P. Castaño, and A. Irabien, "Towards the electrochemical conversion of carbon dioxide into methanol," *Green Chemistry*, vol. 17, 4 2015, ISSN: 1463-9262. DOI: 10.1039/C4GC02453B. [Online]. Available: <https://pubs-rsc-org.tudelft.idm.oclc.org/en/content/articlelanding/2015/GC/C4GC02453B!divAbstract>.
- [42] D. Bellotti, M. Rivarolo, L. Magistri, and A. Massardo, "Feasibility study of methanol production plant from hydrogen and captured carbon dioxide," *Journal of CO2 Utilization*, vol. 21, Oct. 2017, ISSN: 22129820. DOI: 10.1016/j.jcou.2017.07.001. [Online]. Available: <https://www.sciencedirect.com/science/article/pii/S2212982017302007?via%5C%3Dihub#bib0055>.
- [43] V. Palma, E. Meloni, C. Ruocco, M. Martino, and A. Ricca, *State of the art of conventional reactors for methanol production*, 2018. DOI: 10.1016/B978-0-444-63903-5.00002-9. [Online]. Available: <https://www.sciencedirect.com.tudelft.idm.oclc.org/science/article/pii/B9780444639035000029#s0080>.
- [44] H.-J. Wernicke, L. Plass, and F. Schmidt, *Methanol: The Basic Chemical and Energy Feedstock of the Future*, M. Bertau, H. Offermanns, L. Plass, F. Schmidt, and H.-J. Wernicke, Eds. Springer Berlin Heidelberg, 2014, pp. 234–266, ISBN: 978-3-642-39708-0. DOI: 10.1007/978-3-642-39709-7. [Online]. Available: <https://link-springer-com.tudelft.idm.oclc.org/book/10.1007%5C%2F978-3-642-39709-7#about>.
- [45] R. J. Dry, "Possibilities for the development of large-capacity methanol synthesis reactors for synfuel production," *Industrial Engineering Chemistry Research*, vol. 27, 4 Apr. 1988, ISSN: 0888-5885. DOI: 10.1021/ie00076a015. [Online]. Available: <https://pubs-acsc-org.tudelft.idm.oclc.org/doi/abs/10.1021/ie00076a015>.

- [46] D. Milani, R. Khalilpour, G. Zahedi, and A. Abbas, "A model-based analysis of CO₂ utilization in methanol synthesis plant," *Journal of CO₂ Utilization*, vol. 10, Jun. 2015, ISSN: 22129820. DOI: 10.1016/j.jcou.2015.02.003. [Online]. Available: <https://www-sciencedirect-com.tudelft.idm.oclc.org/science/article/pii/S2212982015000189>.
- [47] A. Ursua, L. M. Gandia, and P. Sanchis, "Hydrogen Production From Water Electrolysis: Current Status and Future Trends," *Proceedings of the IEEE*, vol. 100, no. 2, pp. 410–426, Feb. 2012, ISSN: 0018-9219. DOI: 10.1109/JPROC.2011.2156750. [Online]. Available: <http://ieeexplore.ieee.org/document/5898382/>.
- [48] O. Schmidt, A. Gambhir, I. Staffell, A. Hawkes, J. Nelson, and S. Few, "Future cost and performance of water electrolysis: An expert elicitation study," *International Journal of Hydrogen Energy*, vol. 42, pp. 30 470–30 492, 52 Dec. 2017, ISSN: 03603199. DOI: 10.1016/j.ijhydene.2017.10.045. [Online]. Available: <https://www-sciencedirect-com.tudelft.idm.oclc.org/science/article/pii/S0360319917339435>.
- [49] J. Chi and H. Yu, *Water electrolysis based on renewable energy for hydrogen production*, Mar. 2018. DOI: 10.1016/S1872-2067(17)62949-8. [Online]. Available: <https://www-sciencedirect-com.tudelft.idm.oclc.org/science/article/pii/S1872206717629498>.
- [50] J. D. Holladay, J. Hu, D. L. King, and Y. Wang, *An overview of hydrogen production technologies*, Jan. 2009. DOI: 10.1016/j.cattod.2008.08.039. [Online]. Available: <https://www-sciencedirect-com.tudelft.idm.oclc.org/science/article/pii/S0920586108004100>.
- [51] Air Liquide, *Air Liquide inaugurates the world's largest low-carbon hydrogen membrane-based production unit in Canada*, [Accessed: 03.02.2021], Jan. 2021. [Online]. Available: <https://www.airliquide.ca/en/air-liquide-inaugurates-the-worlds-largest-low-carbon-hydrogen-membrane-based-production-unit-in-canada/product/News-2021-01-26>.
- [52] R. Kungas, "Review—Electrochemical CO₂ Reduction for CO Production: Comparison of Low- and High-Temperature Electrolysis Technologies," *Journal of The Electrochemical Society*, vol. 167, 4 Feb. 2020, ISSN: 1945-7111. DOI: 10.1149/1945-7111/ab7099. [Online]. Available: <https://iopscience-iop-org.tudelft.idm.oclc.org/article/10.1149/1945-7111/ab7099>.
- [53] S. Hernandez-Aldave and E. Andreoli, "Fundamentals of gas diffusion electrodes and electrolyzers for carbon dioxide utilisation: Challenges and opportunities," *Catalysts*, vol. 10, 6 Jun. 2020, ISSN: 2073-4344. DOI: 10.3390/catal10060713. [Online]. Available: <https://www.mdpi.com/2073-4344/10/6/713/htm>.
- [54] B. Endrődi, G. Bencsik, F. Darvas, R. Jones, K. Rajeshwar, and C. Janáky, *Continuous-flow electroreduction of carbon dioxide*, Sep. 2017. DOI: 10.1016/j.pecs.2017.05.005. [Online]. Available: <https://www-sciencedirect-com.tudelft.idm.oclc.org/science/article/pii/S0360128517300333?via%3Dihub>.

- [55] D. M. Weekes, D. A. Salvatore, A. Reyes, A. Huang, and C. P. Berlinguette, "Electrolytic co₂ reduction in a flow cell," *Accounts of Chemical Research*, vol. 51, 4 Apr. 2018, ISSN: 0001-4842. DOI: 10.1021/acs.accounts.8b00010. [Online]. Available: <https://pubs-acrs-org.tudelft.idm.oclc.org/doi/full/10.1021/acs.accounts.8b00010>.
- [56] L. Zhang, S. Hu, X. Zhu, and W. Yang, *Electrochemical reduction of co₂ in solid oxide electrolysis cells*, Jul. 2017. DOI: 10.1016/j.jechem.2017.04.004. [Online]. Available: <https://www-sciencedirect-com.tudelft.idm.oclc.org/science/article/pii/S2095495617301870>.
- [57] G. Kaur, A. P. Kulkarni, and S. Giddey, "Co₂ reduction in a solid oxide electrolysis cell with a ceramic composite cathode: Effect of load and thermal cycling," *International Journal of Hydrogen Energy*, vol. 43, pp. 21 769–21 776, 48 Nov. 2018, ISSN: 03603199. DOI: 10.1016/j.ijhydene.2018.10.014. [Online]. Available: <https://www-sciencedirect-com.tudelft.idm.oclc.org/science/article/pii/S036031991833163X>.
- [58] J. Hartvigsen, S. Elangovan, J. Elwell, and D. Larsen, "Oxygen production from mars atmosphere carbon dioxide using solid oxide electrolysis," *ECS Transactions*, vol. 78, 1 May 2017, ISSN: 1938-6737. DOI: 10.1149/07801.2953ecst. [Online]. Available: <https://iopscience-iop-org.tudelft.idm.oclc.org/article/10.1149/07801.2953ecst/meta>.
- [59] A. P. Kulkarni, S. Giddey, and S. P. Badwal, "Efficient conversion of co₂ in solid oxide electrolytic cells with pd doped perovskite cathode on ceria nanofilm interlayer," *Journal of CO₂ Utilization*, vol. 17, pp. 180–187, Jan. 2017, ISSN: 22129820. DOI: 10.1016/j.jcou.2016.11.014. [Online]. Available: <https://www-sciencedirect-com.tudelft.idm.oclc.org/science/article/pii/S2212982016302621>.
- [60] V. Kaplan, E. Wachtel, K. Gartsman, Y. Feldman, and I. Lubomirsky, "Conversion of co₂ to co by electrolysis of molten lithium carbonate," *Journal of The Electrochemical Society*, vol. 157, 4 2010, ISSN: 00134651. DOI: 10.1149/1.3308596. [Online]. Available: <https://iopscience-iop-org.tudelft.idm.oclc.org/article/10.1149/1.3308596/meta>.
- [61] L. Hu, G. Lindbergh, and C. Lagergren, "Performance and durability of the molten carbonate electrolysis cell and the reversible molten carbonate fuel cell," *The Journal of Physical Chemistry C*, vol. 120, 25 Jun. 2016, ISSN: 1932-7447. DOI: 10.1021/acs.jpcc.6b04417. [Online]. Available: https://www.researchgate.net/publication/303890565_Performance_and_Durability_of_the_Molten_Carbonate_Electrolysis_Cell_MCEC_and_the_Reversible_Molten_Carbonate_Fuel_Cell_RMFCF.
- [62] S. Liang, N. Altaf, L. Huang, Y. Gao, and Q. Wang, *Electrolytic cell design for electrochemical co₂ reduction*, Jan. 2020. DOI: 10.1016/j.jcou.2019.09.007. [Online]. Available: <https://www-sciencedirect-com.tudelft.idm.oclc.org/science/article/pii/S2212982019308261>.

- [63] T. Burdyny and W. A. Smith, "Co₂ reduction on gas-diffusion electrodes and why catalytic performance must be assessed at commercially-relevant conditions," *Energy Environmental Science*, vol. 12, 5 2019, ISSN: 1754-5692. DOI: [10.1039/C8EE03134G](https://doi.org/10.1039/C8EE03134G). [Online]. Available: <https://pubs-rsc-org.tudelft.idm.oclc.org/en/content/articlelanding/2019/EE/C8EE03134G#!divAbstract>.
- [64] C. Delacourt, P. L. Ridgway, J. B. Kerr, and J. Newman, "Design of an electrochemical cell making syngas (co+h₂) from co₂ and h₂o reduction at room temperature," *Journal of The Electrochemical Society*, vol. 155, 1 2008, ISSN: 00134651. DOI: [10.1149/1.2801871](https://doi.org/10.1149/1.2801871). [Online]. Available: <https://iopscience-iop-org.tudelft.idm.oclc.org/article/10.1149/1.2801871/meta>.
- [65] U. O. Nwabara, E. R. Cofell, S. Verma, E. Negro, and P. J. A. Kenis, "Durable cathodes and electrolyzers for the efficient aqueous electrochemical reduction of co₂," *ChemSusChem*, vol. 13, 5 Mar. 2020, ISSN: 1864-5631. DOI: [10.1002/cssc.201902933](https://doi.org/10.1002/cssc.201902933). [Online]. Available: <https://chemistry-europe-onlinelibrary-wiley-com.tudelft.idm.oclc.org/doi/full/10.1002/cssc.201902933>.
- [66] Y. C. Li, D. Zhou, Z. Yan, R. H. Gonçalves, D. A. Salvatore, C. P. Berlinguette, and T. E. Mallouk, "Electrolysis of co₂ to syngas in bipolar membrane-based electrochemical cells," *ACS Energy Letters*, vol. 1, 6 Dec. 2016, ISSN: 2380-8195. DOI: [10.1021/acsenenergylett.6b00475](https://doi.org/10.1021/acsenenergylett.6b00475). [Online]. Available: <https://pubs-acscs-org.tudelft.idm.oclc.org/doi/full/10.1021/acsenenergylett.6b00475>.
- [67] J. Koponen, V. Ruuskanen, A. Kosonen, M. Niemela, and J. Ahola, "Effect of converter topology on the specific energy consumption of alkaline water electrolyzers," *IEEE Transactions on Power Electronics*, vol. 34, 7 Jul. 2019, ISSN: 0885-8993. DOI: [10.1109/TPEL.2018.2876636](https://doi.org/10.1109/TPEL.2018.2876636). [Online]. Available: <https://ieeexplore.ieee.org/document/8494794>.
- [68] Z. Dobó and Á. B. Palotás, "Impact of the current fluctuation on the efficiency of alkaline water electrolysis," *International Journal of Hydrogen Energy*, vol. 42, 9 Mar. 2017, ISSN: 03603199. DOI: [10.1016/j.ijhydene.2016.11.142](https://doi.org/10.1016/j.ijhydene.2016.11.142). [Online]. Available: <https://www.sciencedirect.com/science/article/pii/S0360319916334310>.
- [69] F-W. Speckmann, S. Bintz, and K. P. Birke, "Influence of rectifiers on the energy demand and gas quality of alkaline electrolysis systems in dynamic operation," *Applied Energy*, vol. 250, Sep. 2019, ISSN: 03062619. DOI: [10.1016/j.apenergy.2019.05.014](https://doi.org/10.1016/j.apenergy.2019.05.014). [Online]. Available: <https://www.sciencedirect.com/science/article/pii/S0306261919308694>.
- [70] A. Ursúa, L. Marroyo, E. Gubía, L. M. Gandía, P. M. Diéguez, and P. Sanchis, "Influence of the power supply on the energy efficiency of an alkaline water electrolyser," *International Journal of Hydrogen Energy*, vol. 34, 8 May 2009, ISSN: 03603199. DOI: [10.1016/j.ijhydene.2009.02.017](https://doi.org/10.1016/j.ijhydene.2009.02.017). [Online]. Available: <https://www.sciencedirect.com/science/article/pii/S036031990900216X>.
- [71] Methanol Institute, *Renewable methanol report*, [Accessed: 18.05.2021], Jan. 2019. [Online]. Available: <https://www.methanol.org/wp-content/uploads/2019/01/MethanolReport.pdf>.

- [72] ICIS Chemical Business, *Europe chemical profile: Methanol*, [Accessed: 18.05.2021], Jun. 2012. [Online]. Available: <https://www.icis.com/explore/resources/news/2012/06/25/9571858/europechemical-profile-methanol/>.
- [73] Methanol Institute, *Methanol technical data sheet*, [Accessed: 18.05.2021]. [Online]. Available: <http://www.methanol.org/wp-content/uploads/2016/06/Methanol-Technical-Data-Sheet.pdf>.
- [74] E. S. Sanz-Pérez, C. R. Murdock, S. A. Didas, and C. W. Jones, "Direct Capture of CO₂ from Ambient Air," *Chemical Reviews*, vol. 116, 19 Oct. 2016, ISSN: 0009-2665. DOI: 10.1021/acs.chemrev.6b00173. [Online]. Available: <https://pubs.acs.org.tudelft.idm.oclc.org/doi/10.1021/acs.chemrev.6b00173>.
- [75] G. A. Olah, "Beyond oil and gas: The methanol economy," *Angewandte Chemie International Edition*, vol. 44, 18 Apr. 2005, ISSN: 1433-7851. DOI: 10.1002/anie.200462121. [Online]. Available: <https://onlinelibrary-wiley-com.tudelft.idm.oclc.org/doi/full/10.1002/anie.200462121>.
- [76] Global CCS Institute, "Global status report 2019," 2018, pp. 21, 57, 63. [Online]. Available: https://www.globalccsinstitute.com/wp-content/uploads/2019/12/GCC_GLOBAL_STATUS_REPORT_2019.pdf.
- [77] X. Wang and C. Song, "Carbon capture from flue gas and the atmosphere: A perspective," *Frontiers in Energy Research*, vol. 8, Dec. 2020, ISSN: 2296-598X. DOI: 10.3389/fenrg.2020.560849. [Online]. Available: <https://www.frontiersin.org/articles/10.3389/fenrg.2020.560849/full>.
- [78] M. G. Plaza, S. Martínez, and F. Rubiera, "CO₂ Capture, Use, and Storage in the Cement Industry: State of the Art and Expectations," *Energies*, vol. 13, 21 Oct. 2020, ISSN: 1996-1073. DOI: 10.3390/en13215692. [Online]. Available: <https://www.mdpi.com/1996-1073/13/21/5692/htm>.
- [79] M. Voldsund, S. O. Gardarsdottir, E. D. Lena, J.-F. Pérez-Calvo, A. Jamali, D. Berstad, C. Fu, M. Romano, S. Roussanaly, R. Anantharaman, H. Hoppe, D. Sutter, M. Mazzotti, M. Gazzani, G. Cinti, and K. Jordal, "Comparison of technologies for CO₂ capture from cement production-part 1: Technical evaluation," vol. 12, p. 559, 2019. DOI: 10.3390/en12030559. [Online]. Available: <https://www.mdpi.com/1996-1073/12/3/559/htm>.
- [80] S. O. Gardarsdottir, E. D. Lena, M. Romano, S. Roussanaly, M. Voldsund, J.-F. Pérez-Calvo, D. Berstad, C. Fu, R. Anantharaman, D. Sutter, M. Gazzani, M. Mazzotti, and G. Cinti, "Comparison of Technologies for CO₂ Capture from Cement Production-Part 2: Cost Analysis," 2019. DOI: 10.3390/en12030542. [Online]. Available: <https://www.mdpi.com/1996-1073/12/3/542>.
- [81] D. Kourkoumpas, E. Papadimou, K. Atsonios, S. Karellas, P. Grammelis, and E. Kakaras, "Implementation of the power to methanol concept by using CO₂ from lignite power plants: Techno-economic investigation," *International Journal of Hydrogen Energy*, vol. 41, 38 Oct. 2016, ISSN: 03603199. DOI: 10.1016/j.ijhydene.2016.07.100. [Online]. Available: <https://www.sciencedirect-com.tudelft.idm.oclc.org/science/article/pii/S0360319916301239#sec6>.

- [82] L. Jiang, A. Gonzalez-Diaz, J. Ling-Chin, A. Roskilly, and A. Smallbone, "Post-combustion CO₂ capture from a natural gas combined cycle power plant using activated carbon adsorption," *Applied Energy*, vol. 245, Jul. 2019, ISSN: 03062619. DOI: [10.1016/j.apenergy.2019.04.006](https://doi.org/10.1016/j.apenergy.2019.04.006). [Online]. Available: [https://www.sciencedirect-com.tudelft.idm.oclc.org/science/article/pii/S0306261919306300#s0065](https://www.sciencedirect.com/tudelft.idm.oclc.org/science/article/pii/S0306261919306300#s0065).
- [83] M. Vaccarelli, R. Carapellucci, and L. Giordano, "Energy and economic analysis of the CO₂ capture from flue gas of combined cycle power plants," *Energy Procedia*, vol. 45, 2014, ISSN: 18766102. DOI: [10.1016/j.egypro.2014.01.122](https://doi.org/10.1016/j.egypro.2014.01.122). [Online]. Available: [https://www-sciencedirect-com.tudelft.idm.oclc.org/science/article/pii/S1876610214001234](https://www.sciencedirect.com/tudelft.idm.oclc.org/science/article/pii/S1876610214001234).
- [84] E. HASANEN, V. POHJOLA, M. HAHKALA, R. ZILLIACUS, and K. WICKSTROM, "Emissions from power plants fueled by peat, coal, natural gas and oil," *Science of The Total Environment*, vol. 54, Oct. 1986, ISSN: 00489697. DOI: [10.1016/0048-9697\(86\)90254-8](https://doi.org/10.1016/0048-9697(86)90254-8). [Online]. Available: [https://www-sciencedirect-com.tudelft.idm.oclc.org/science/article/pii/0048969786902548](https://www.sciencedirect-com.tudelft.idm.oclc.org/science/article/pii/0048969786902548).
- [85] Innovation Combustion Technologies, *Natural gas fired boilers*, [Accessed: 19.05.2021]. [Online]. Available: <https://www.innovativecombustion.com/natural-gas-fired-boilers/>.
- [86] B. H. Ko, B. Hasa, H. Shin, E. Jeng, S. Overa, W. Chen, and F. Jiao, "The impact of nitrogen oxides on electrochemical carbon dioxide reduction," *Nature Communications*, vol. 11, 1 Dec. 2020, ISSN: 2041-1723. DOI: [10.1038/s41467-020-19731-8](https://doi.org/10.1038/s41467-020-19731-8). [Online]. Available: <https://www-nature-com.tudelft.idm.oclc.org/articles/s41467-020-19731-8>.
- [87] W. Luc, B. H. Ko, S. Kattel, S. Li, D. Su, J. G. Chen, and F. Jiao, "So₂-induced selectivity change in CO₂ electroreduction," *Journal of the American Chemical Society*, vol. 141, 25 Jun. 2019, ISSN: 0002-7863. DOI: [10.1021/jacs.9b03215](https://doi.org/10.1021/jacs.9b03215). [Online]. Available: <https://pubs-acsc-org.tudelft.idm.oclc.org/doi/abs/10.1021/jacs.9b03215>.
- [88] Conch, *Conch Group's First Batch of Industrial Grade Carbon Dioxide Products Were Successfully Dispatched for Sale*, [Accessed: 18.05.2021], Oct. 2018. [Online]. Available: <http://www.conch.cn/en/News/info.aspx?itemid=166511>.
- [89] CarbonClean, *Solvents*, [Accessed: 18.05.2021]. [Online]. Available: <https://www.carbonclean.com/solvents>.
- [90] TITAN Cement Group, "Integrated Annual Report 2020," 2021, p. 87. [Online]. Available: https://www.titan-cement.com/TITAN_Cement_Group_IAR_2020_EN.pdf.
- [91] IndustryAbout, *Titan - Kamari Cement Plant*, [Accessed: 24.05.2021], Apr. 2019. [Online]. Available: <https://www.industryabout.com/country-territories-3/364-greece/cement-industry/1836-titan-kamari-cement-plant>.
- [92] Global Solar Atlas, *Global Solar Atlas online application website*, [Accessed: 29.05.2021], 2021. [Online]. Available: <https://globalsolaratlas.info/map>.

- [93] —, *Global Photovoltaic Power Potential by Country*, [Accessed: 29.05.2021], 2021. [Online]. Available: <https://globalsolaratlas.info/global-pv-potential-study>.
- [94] EU Science Hub, *Photovoltaic Geographical Information System*, [Accessed: 22.05.2021], Oct. 2019. [Online]. Available: https://re.jrc.ec.europa.eu/pvg_tools/en/#MR.
- [95] —, *PVGIS users manual*, [Accessed: 22.05.2021], Sep. 2020. [Online]. Available: <https://ec.europa.eu/jrc/en/PVGIS/docs/usermanual>.
- [96] Z. Yin, H. Peng, X. Wei, H. Zhou, J. Gong, M. Huai, L. Xiao, G. Wang, J. Lu, and L. Zhuang, "An alkaline polymer electrolyte CO₂ electrolyzer operated with pure water," *Energy Environmental Science*, vol. 12, 8 2019, ISSN: 1754-5692. DOI: 10.1039/C9EE01204D. [Online]. Available: <https://pubs-rsc-org.tudelft.idm.oclc.org/en/content/articlelanding/2019/ee/c9ee01204d#!divAbstract>.
- [97] Hydrogenics, *HySTAT® HYDROGEN GENERATORS*, [Accessed: 21.04.2021]. [Online]. Available: <https://www.h2gentec.com/pdf/generators-hystat-10.pdf>.
- [98] Clean Energy Manufacturing Analysis Center (CEMAC), *Manufacturing Competitiveness Analysis for PEM and Alkaline Water Electrolysis Systems*, [Accessed: 21.04.2021], Aug. 2017. [Online]. Available: <https://www.nrel.gov/docs/fy19osti/70380.pdf>.
- [99] Hydrogenics, *HySTAT®-A Hydrogen Plants*, [Accessed: 21.04.2021]. [Online]. Available: <https://pdf.directindustry.com/pdf/hydrogenics/hystat-a-hydrogen-generator-plant/33492-75126.html>.
- [100] A. Ursúa, I. S. Martín, E. L. Barrios, and P. Sanchis, "Stand-alone operation of an alkaline water electrolyser fed by wind and photovoltaic systems," *International Journal of Hydrogen Energy*, vol. 38, 35 Nov. 2013, ISSN: 03603199. DOI: 10.1016/j.ijhydene.2013.09.085. [Online]. Available: <https://www.sciencedirect-com.tudelft.idm.oclc.org/science/article/pii/S0360319913023082>.
- [101] D. V. Rosato, D. V. Rosato, and M. G. Rosato, *Auxiliary equipment and secondary operations*, 2000. DOI: 10.1007/978-1-4615-4597-2_10. [Online]. Available: https://link-springer-com.tudelft.idm.oclc.org/chapter/10.1007/978-1-4615-4597-2_10.
- [102] P. Castello, E. Tzimas and P. Moretto, "Techno-economic assessment of hydrogen transmission distribution systems in europe in the medium and long term," Institute for Energy and Transport (Joint Research Centre), Dec. 2006. [Online]. Available: <https://op.europa.eu/en/publication-detail/-/publication/08331a6f-05a4-4aed-89fe-fb92840b8cc5>.

- [103] N. D. Díez, S. van der Meer, J. Bonetto and A. Herwijn, “Technical assessment of hydrogen transport, compression, processing offshore,” North Sea Energy, Jun. 2020. [Online]. Available: <https://north-sea-energy.eu/static/7ffd23ec%5C-69b9d82a7a982b828be04c50/FINAL-NSE3-D3.1-Final-report-techni%5C-cal-assessment-of-Hydrogen-transport-compression-processing-offshore.pdf>.
- [104] Ohio University, *Properties of Various Ideal Gases (at 300 K)*, [Accessed: 20.05.2021]. [Online]. Available: https://www.ohio.edu/mechanical/thermo/property_tables/gas/idealGas.html.
- [105] Air Liquide, *Gas Encyclopedia*, [Accessed: 20.05.2021], 2021. [Online]. Available: <https://encyclopedia.airliquide.com/carbon-monoxide>.
- [106] Engineering ToolBox, *Ideal gas law*, [Accessed: 22.06.2021], 2003. [Online]. Available: https://www.engineeringtoolbox.com/ideal-gas-law-d_157.html.
- [107] —, *Compression and expansion of gases*, [Accessed: 22.06.2021], 2003. [Online]. Available: https://www.engineeringtoolbox.com/compression-expansion-gases-d_605.html.
- [108] —, *Heat capacity*, [Accessed: 22.06.2021], 2003. [Online]. Available: https://www.engineeringtoolbox.com/heat-capacity-d_338.html.
- [109] National Institute of Standards and Technology (NIST), *Carbon monoxide, Gas Phase Heat Capacity (Shomate Equation)*, [Accessed: 22.06.2021], 2018. [Online]. Available: <https://webbook.nist.gov/cgi/cbook.cgi?ID=C630080&Type=JANAFG&Table=on>.
- [110] —, *Hydrogen, Gas Phase Heat Capacity (Shomate Equation)*, [Accessed: 22.06.2021], 2018. [Online]. Available: <https://webbook.nist.gov/cgi/cbook.cgi?ID=C1333740&Mask=1&Type=JANAFG&Table=on>.
- [111] Engineering ToolBox, *Cooling Load - Convert kW/ton to COP or EER*, [Accessed: 22.06.2021], 2003. [Online]. Available: https://www.engineeringtoolbox.com/cop-eer-d_409.html.
- [112] Carrier Corporation, “Heating, ventilation and air conditioning catalogue 2018/2019,” Apr. 2018, pp. 141, 142, 154, 163, 176–178. [Online]. Available: <https://www.shareddocs.com/hvac/docs/1001/Public/0A/Carrier-Catalogue-2018-2019/1/Carrier-Catalogue-2018-2019.pdf>.
- [113] M. Tvrdý, S. Havel, L. Hyspecká, and K. Mazanec, “Hydrogen embrittlement of crmo and crmov pressure vessel steels,” *International Journal of Pressure Vessels and Piping*, vol. 9, 5 Sep. 1981, ISSN: 03080161. DOI: [10.1016/0308-0161\(81\)90008-9](https://doi.org/10.1016/0308-0161(81)90008-9). [Online]. Available: <https://www.sciencedirect.com.tudelft.idm.oclc.org/science/article/pii/0308016181900089>.
- [114] Engineering ToolBox, *Critical Temperatures and Pressures for some Common Substances*, [Accessed: 22.06.2021], 2003. [Online]. Available: https://www.engineeringtoolbox.com/gas-critical-temperature-pressure-d_161.html.

- [115] Z. Andreas, "Hydrogen storage methods," *Naturwissenschaften*, vol. 91, 4 Apr. 2004, ISSN: 0028-1042. DOI: [10.1007/s00114-004-0516-x](https://doi.org/10.1007/s00114-004-0516-x). [Online]. Available: https://www.researchgate.net/publication/8618603_Hydrogen_storage_methods.
- [116] G. Ortiz, J. Biela, D. Bortis, and J. W. Kolar, "1 megawatt, 20 khz, isolated, bidirectional 12kv to 1.2kv dc-dc converter for renewable energy applications," IEEE, Jun. 2010, ISBN: 978-1-4244-5394-8. DOI: [10.1109/IPEC.2010.5542018](https://doi.org/10.1109/IPEC.2010.5542018). [Online]. Available: <https://ieeexplore-ieee-org.tudelft.idm.oclc.org/document/5542018/figures#figures>.
- [117] P. L. Spath and D. C. Dayton, "Preliminary screening – technical and economic assessment of synthesis gas to fuels and chemicals with emphasis on the potential for biomass-derived syngas," National Renewable Energy Laboratory (NREL), Dec. 2003. DOI: [10.2172/15006100](https://doi.org/10.2172/15006100). [Online]. Available: https://www.researchgate.net/publication/235015112_Preliminary_Screening_-_Technical_and_Economic_Assessment_of_Synthesis_Gas_to_Fuels_and_Chemicals_With_Emphasis_on_the_Potential_for_Biomass-Derived_Syngas.
- [118] B. A. B. T. Walid, B. Hassiba, H. Boumediene, and S. Weifeng, "Improved design of the lurgi reactor for methanol synthesis industry," *Chemical Engineering Technology*, vol. 41, 10 Oct. 2018, ISSN: 09307516. DOI: [10.1002/ceat.201700551](https://doi.org/10.1002/ceat.201700551). [Online]. Available: <https://onlinelibrary-wiley-com.tudelft.idm.oclc.org/doi/full/10.1002/ceat.201700551#ceat201700551-bib-0013>.
- [119] V. Dieterich, A. Buttler, A. Hanel, H. Spliethoff, and S. Fendt, "Power-to-liquid via synthesis of methanol, dme or fischer-tropsch-fuels: A review," *Energy Environmental Science*, vol. 13, 10 2020, ISSN: 1754-5692. DOI: [10.1039/DOEE01187H](https://doi.org/10.1039/DOEE01187H). [Online]. Available: <https://pubs-rsc-org.tudelft.idm.oclc.org/en/content/articlehtml/2020/ee/d0ee01187h>.
- [120] I. Wender, "Reactions of synthesis gas," *Fuel Processing Technology*, vol. 48, 3 Sep. 1996, ISSN: 03783820. DOI: [10.1016/S0378-3820\(96\)01048-X](https://doi.org/10.1016/S0378-3820(96)01048-X). [Online]. Available: <https://www-sciencedirect-com.tudelft.idm.oclc.org/science/article/pii/S037838209601048X>.
- [121] S. S. Iyer, T. Renganathan, S. Pushpavanam, M. V. Kumar, and N. Kaisare, "Generalized thermodynamic analysis of methanol synthesis: Effect of feed composition," *Journal of CO2 Utilization*, vol. 10, Jun. 2015, ISSN: 22129820. DOI: [10.1016/j.jcou.2015.01.006](https://doi.org/10.1016/j.jcou.2015.01.006). [Online]. Available: <https://www-sciencedirect-com.tudelft.idm.oclc.org/science/article/pii/S2212982015000086?via%5C%3Dihub>.
- [122] K. Bussche and G. Froment, "A steady-state kinetic model for methanol synthesis and the water gas shift reaction on a commercial cu/zno/al2o3catalyst," *Journal of Catalysis*, vol. 161, 1 Jun. 1996, ISSN: 00219517. DOI: [10.1006/jcat.1996.0156](https://doi.org/10.1006/jcat.1996.0156). [Online]. Available: <https://www-sciencedirect-com.tudelft.idm.oclc.org/science/article/pii/S0021951796901566>.

- [123] L. Chen, Q. Jiang, Z. Song, and D. Posarac, "Optimization of methanol yield from a lurgi reactor," *Chemical Engineering Technology*, vol. 34, 5 May 2011, ISSN: 09307516. DOI: [10.1002/ceat.201000282](https://doi.org/10.1002/ceat.201000282). [Online]. Available: <https://onlinelibrary-wiley-com.tudelft.idm.oclc.org/doi/abs/10.1002/ceat.201000282>.
- [124] PV Magazine, *Module price index*, [Accessed: 07.09.2021], Jan. 2021. [Online]. Available: <https://www.pv-magazine.com/module-price-index/>.
- [125] E. Vartiainen, G. Masson, C. Breyer, D. Moser, and E. R. Medina, "Impact of weighted average cost of capital, capital expenditure, and other parameters on future utility-scale pv levelised cost of electricity," *Progress in Photovoltaics: Research and Applications*, vol. 28, 6 Jun. 2020, ISSN: 1062-7995. DOI: [10.1002/pip.3189](https://doi.org/10.1002/pip.3189). [Online]. Available: <https://onlinelibrary-wiley-com.tudelft.idm.oclc.org/doi/10.1002/pip.3189>.
- [126] H. Shin, K. U. Hansen, and F. Jiao, "Techno-economic assessment of low-temperature carbon dioxide electrolysis," *Nature Sustainability*, Jul. 2021, ISSN: 2398-9629. DOI: [10.1038/s41893-021-00739-x](https://doi.org/10.1038/s41893-021-00739-x). [Online]. Available: <https://www-nature-com.tudelft.idm.oclc.org/articles/s41893-021-00739-x?proof=tr>.
- [127] European Central Bank, *Euro foreign exchange reference rates, US dollar (USD)*, [Accessed: 07.09.2021], 2021. [Online]. Available: https://www.ecb.europa.eu/stats/policy_and_exchange_rates/euro_reference_exchange_rates/html/eurofxref-graph-usd.en.html.
- [128] I. Dikschas and T. Smolinka, "Wasserelektrolyse an der schwelle zur großskaligen industrialisierung - trends und herausforderungen bis 2030," Fraunhofer Institute, May 2019, p. 10. [Online]. Available: https://publica.fraunhofer.de/eprints/urn_nbn_de_0011-n-5782492.pdf.
- [129] L. Bertuccioli, A. Chan, D. Hart, F. Lehner, B. Madden, and E. Standen, "Development of water electrolysis in the european union," Fuel Cells and Hydrogen Joint Undertaking, Feb. 2014, p. 64. [Online]. Available: <https://www.fch.europa.eu/node/783>.
- [130] S. Brynolf, M. Taljegard, M. Grahn, and J. Hansson, "Electrofuels for the transport sector: A review of production costs," *Renewable and Sustainable Energy Reviews*, vol. 81, Jan. 2018, ISSN: 13640321. DOI: [10.1016/j.rser.2017.05.288](https://doi.org/10.1016/j.rser.2017.05.288). [Online]. Available: <https://www-sciencedirect-com.tudelft.idm.oclc.org/science/article/pii/S1364032117309358#bib78>.
- [131] H. Zhang, L. Wang, J. V. herle, F. Maréchal, and U. Desideri, "Techno-economic optimization of co2-to-methanol with solid-oxide electrolyzer," *Energies*, vol. 12, 19 Sep. 2019, ISSN: 1996-1073. DOI: [10.3390/en12193742](https://doi.org/10.3390/en12193742). [Online]. Available: <https://www.mdpi.com/1996-1073/12/19/3742/htm>.
- [132] E. C. D. Tan, M. Talmadge, A. Dutta, J. Hensley, J. Schaidle, M. Bidy, D. Humbird, L. J. Snowden-Swan, J. Ross, D. Sexton, R. Yap, and J. Lukas, "Process design and economics for the conversion of lignocellulosic biomass to hydrocarbons via indirect liquefaction. thermochemical research pathway to high-octane gasoline blendstock through methanol/dimethyl ether intermediates," National Renewable Energy Laboratory (NREL), Mar. 2015, p. 66. DOI: [10.2172/1215006](https://doi.org/10.2172/1215006). [On-

- line]. Available: <https://www.osti.gov/biblio/1215006-process-design-economics-conversion-lignocellulosic-biomass-hydrocarbons-via-indirect-liquefaction-thermochemical-research-pathway-high-octane-gasoline-blendstock-through-methanol-dimethyl-ether-intermediates>.
- [133] W. D. Seider, D. R. Lewin, J. D. Seader, S. Widagdo, R. Gani, and K. M. Ng, *Product and Process Design Principles: Synthesis, Analysis and Evaluation*, Third edi. John Wiley Sons Inc., 2009, p. 595, ISBN: 978-0470-04895-5.
- [134] M. Shamoushaki, P. H. Niknam, L. Talluri, G. Manfrida, and D. Fiaschi, "Development of cost correlations for the economic assessment of power plant equipment," *Energies*, vol. 14, 9 May 2021, ISSN: 1996-1073. DOI: 10.3390/en14092665. [Online]. Available: <https://www.mdpi.com/1996-1073/14/9/2665/htm#B28-energies-14-02665>.
- [135] C. Jepma, G.-J. Kok, M. Renz, M. van Schot, and K. Wouters, "Towards sustainable energy production on the North Sea - Green hydrogen production and CO2 storage: onshore or offshore?" TNO, Mar. 2018, p. 43. [Online]. Available: [https://cdn.change.inc/download/759/North%5C%20Sea%5C%20Energy%5C%20I%5C%20-%5C%20D3.1.2-3.1.4,%5C%20D3.1.6%5C%20Towards%5C%20sustainable%5C%20energy%5C%20production%5C%20on%5C%20the%5C%20North%5C%20Sea_final-public\(1\).pdf](https://cdn.change.inc/download/759/North%5C%20Sea%5C%20Energy%5C%20I%5C%20-%5C%20D3.1.2-3.1.4,%5C%20D3.1.6%5C%20Towards%5C%20sustainable%5C%20energy%5C%20production%5C%20on%5C%20the%5C%20North%5C%20Sea_final-public(1).pdf).
- [136] Florida Power Light Company (FPL), *Air-Cooled Chillers*, pp. 1, 4. [Online]. Available: <https://infpl.fpl.com/business/pdf/air-cooled-chillers-primer.pdf>.
- [137] Methanex, *Methanex posts regional contract methanol prices for North America, Europe and Asia*. [Accessed: 07.09.2021], 2021. [Online]. Available: <https://www.methanex.com/our-business/pricing>.
- [138] Federal Reserve Economic Data (FRED), *Producer Price Index by Industry: Industrial Gas Manufacturing: Oxygen*, [Accessed: 07.09.2021], 2021. [Online]. Available: <https://fred.stlouisfed.org/series/PCU325120325120A#0>.
- [139] Athens Water Supply and Sewerage Company (EYDAP S.A.), *TARIFF*, [Accessed: 07.09.2021], 2021. [Online]. Available: <https://www.eydap.gr/en/CustomerSupport/normalrates/>.
- [140] A. Jaeger-Waldau, "PV Status Report 2019," Publications Office of the European Union, 2019, p. 22. DOI: 10.2760/326629. [Online]. Available: <https://publications.jrc.ec.europa.eu/repository/handle/JRC118058>.
- [141] M. S. Peters, K. D. Timmerhaus, and R. E. West, *Plant design and economics for chemical engineers*, Fifth edition. McGraw-Hill, 2003, pp. 232, 233, 244, 248, 250, 251, 254, ISBN: 0-07-239266-5.
- [142] Jason Fernando, *Net Present Value (NPV)*, Investopedia, [Accessed: 14.09.2021], Aug. 2021. [Online]. Available: <https://www.investopedia.com/terms/n/npv.asp>.

- [143] M. Jouny, W. Luc, and F. Jiao, "General techno-economic analysis of co ₂ electrolysis systems," *Industrial Engineering Chemistry Research*, vol. 57, 6 Feb. 2018, ISSN: 0888-5885. DOI: [10.1021/acs.iecr.7b03514](https://doi.org/10.1021/acs.iecr.7b03514). [Online]. Available: <https://pubs-acsc-org.tudelft.idm.oclc.org/doi/full/10.1021/acs.iecr.7b03514>.
- [144] Will Kenton, *Salvage Value*, Investopedia, [Accessed: 14.09.2021], Sep. 2020. [Online]. Available: <https://www.investopedia.com/terms/s/salvagevalue.asp>.
- [145] PricewaterhouseCoopers (PWC), *Corporate - Taxes on corporate income*, [Accessed: 14.09.2021], Aug. 2021. [Online]. Available: <https://taxsummaries.pwc.com/greece/corporate/taxes-on-corporate-income>.
- [146] Julia Kagan, *Earnings Before Tax (EBT)*, Investopedia, [Accessed: 14.09.2021], Dec. 2020. [Online]. Available: <https://www.investopedia.com/terms/e/ebt.asp>.
- [147] Chris B. Murphy, *Is It Possible to Have Positive Cash Flow and Negative Net Income?* Investopedia, [Accessed: 14.09.2021], Apr. 2021. [Online]. Available: <https://www.investopedia.com/ask/answers/05/060105.asp>.
- [148] S. Ghose and M. J. Franchetti, *Economic aspects of food waste-to-energy system deployment*, 2018. DOI: [10.1016/B978-0-12-811157-4.00011-5](https://doi.org/10.1016/B978-0-12-811157-4.00011-5). [Online]. Available: <https://www-sciencedirect-com.tudelft.idm.oclc.org/science/article/pii/B9780128111574000115>.
- [149] S. Raikar and S. Adamson, *Renewable energy finance in the international context*, 2020. DOI: [10.1016/B978-0-12-816441-9.00013-1](https://doi.org/10.1016/B978-0-12-816441-9.00013-1). [Online]. Available: <https://www-sciencedirect-com.tudelft.idm.oclc.org/science/article/pii/B9780128164419000131>.
- [150] World Bank, *CO2 emissions (metric tons per capita) - European Union*, [Accessed: 26.09.2021], 2021. [Online]. Available: <https://data.worldbank.org/indicator/EN.ATM.CO2E.PC?locations=EU>.
- [151] U.S. Environmental Protection Agency (EPA), *Greenhouse Gas Emissions from a Typical Passenger Vehicle*, [Accessed: 26.09.2021], Jul. 2021. [Online]. Available: <https://www.epa.gov/greenvehicles/greenhouse-gas-emissions-typical-passenger-vehicle>.
- [152] EU Science Hub, *Data sources and calculation methods*, [Accessed: 22.05.2021], Oct. 2020. [Online]. Available: <https://ec.europa.eu/jrc/en/PVGIS/docs/methods>.
- [153] K. Shukla, S. Rangnekar, and K. Sudhakar, "Comparative study of isotropic and anisotropic sky models to estimate solar radiation incident on tilted surface: A case study for bhopal, india," *Energy Reports*, vol. 1, Nov. 2015, ISSN: 23524847. DOI: [10.1016/j.egyr.2015.03.003](https://doi.org/10.1016/j.egyr.2015.03.003). [Online]. Available: <https://www-sciencedirect-com.tudelft.idm.oclc.org/science/article/pii/S2352484715000177>.

- [154] A. Amillo, T. Huld, and R. Müller, “A new database of global and direct solar radiation using the eastern meteosat satellite, models and validation,” *Remote Sensing*, vol. 6, 9 Aug. 2014, ISSN: 2072-4292. DOI: [10 . 3390 / rs6098165](https://doi.org/10.3390/rs6098165). [Online]. Available: <https://www.mdpi.com/2072-4292/6/9/8165/htm>.

A

DATA ON PLANT LOCATION

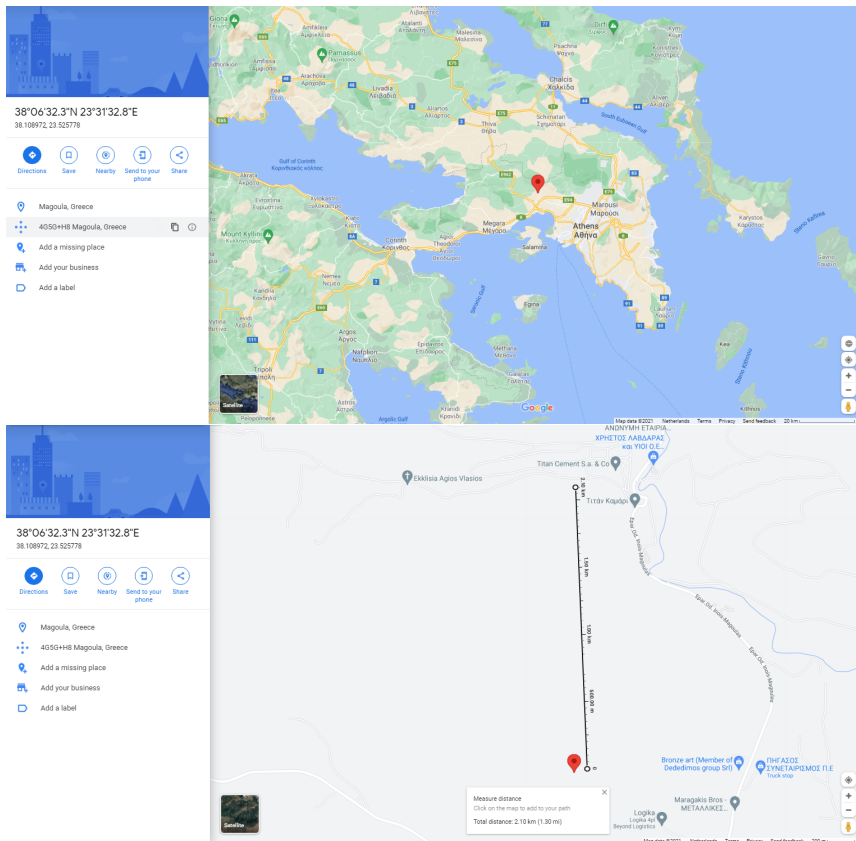


Figure A.1: Plant location on Google Maps

The screenshot displays the PVGIS web application interface. At the top, it features the European Commission logo and the title 'PHOTOVOLTAIC GEOGRAPHICAL INFORMATION SYSTEM'. Below the header, there is a navigation menu with options like 'Home', 'Tools', 'Downloads', 'Documentation', and 'Contact us'. The main area is divided into a map on the left and a control panel on the right. The map shows a geographical area with a blue location pin. The control panel includes a 'Cursor' section with 'Selected' coordinates (38.109, 23.526) and 'Elevation (m): 205'. It also has a 'Use terrain shadows' section with a checked 'Calculated horizon' option. The 'HOURLY RADIATION DATA' panel is expanded, showing a 'Solar radiation database' dropdown set to 'PVGIS-SARAH', 'Start year' and 'End year' both set to '2018', and a 'Mounting type' section with 'Fixed' selected. Other options include 'Slope [°]' (0-90), 'Azimuth [°]' (-180-180), 'PV power' (checked), 'PV technology' (Crystalline silicon), 'Installed peak PV power [kWp]' (5000), and 'System loss [%]' (0). There are 'Go!' buttons for the address and coordinates, and 'csv' and 'json' download buttons at the bottom of the panel. The status bar at the bottom indicates 'Last update: 15/10/2019 Top'.

Figure A.2: Screenshot of the platform PVGIS

B

METHODS USED FOR THE PVGIS CALCULATIONS

According to the PVGIS documentation, the solar radiation and PV power output are calculated as follows [152]:

1. Calculation of solar radiation on **an horizontal plane** from satellite, taking into account the cloud albedo and the clear-sky irradiance.
 - (a) An *effective cloud albedo* is calculated, using images from the METEOSAT satellites, for the estimation of the influence of clouds on the solar radiation.
 - (b) The *clear-sky irradiance* is calculated at clear sky conditions (i.e. no clouds), using the theory of radiative transfer in the atmosphere. Also, the concentrations of ozone, water vapor and aerosols (e.g. dust and particles) in the atmosphere are taken into account, because they absorb radiation at particular wavelengths.

The method described above produces the global horizontal irradiance (G) and beam horizontal irradiance (G_b), measured in W/m^2 . Also, the following equation shows that G is the sum of G_b and diffuse horizontal irradiance (G_d) [153]:

$$G = G_b + G_d \quad (\text{B.1})$$

In terms of data validation, the estimated solar radiation by the data-set PVGIS-SARAH has been compared with ground station measurements in various locations by a number of scientific papers. For example, it was found that the estimated solar radiation by PVGIS-SARAH was 3.6% higher than the ground station measurements for 2005 in Thessaloniki, Greece [154].

2. Calculation of solar radiation on **an inclined plane**

PVGIS estimates the global in-plane irradiance (G_i) as the sum of beam in-plane irradiance ($G_{b,i}$), diffuse in-plane irradiance ($G_{d,i}$) and reflected in-plane irradiance ($G_{r,i}$). The following equation represents the aforementioned mathematical statement [153]:

$$G_i = G_{b,i} + G_{d,i} + G_{r,i} \quad (\text{B.2})$$

- (a) $G_{b,i}$ is estimated by PVGIS as a function of G_b and the slope of the tilted surface.
- (b) $G_{r,i}$ is estimated by PVGIS as a function of G , ground reflectance and the slope of the tilted surface.
- (c) $G_{d,i}$ is estimated by PVGIS, using an anisotropic model of two components.

As far as the horizon profile is concerned, PVGIS uses built-in information (with a resolution of 3 arc-seconds, about 90 m), for calculating the times when hills or mountains block the sun light. In these cases, the radiation is based only on $G_{d,i}$. However, this approach does not take into account shadows from shorter objects, such as houses or trees.

3. Calculation of real PV power output

The following factors are taken into account by PVGIS for the calculation of real PV power output:

- (a) The *shallow-angle reflection* describes the amount of sunlight that will be reflected away without being absorbed by the PV modules. For fixed plane PV modules, the sunlight is reflected away by 2-4% due to this effect.
- (b) The *changes in the spectrum of the sunlight* affect the PV power output and the PV modules response, because the PV modules are sensitive to only a specific range of wavelengths of light. These effects are included in the PVGIS calculations for c-Si modules.
- (c) The *irradiance and module temperature* affect the efficiency and power output of the PV modules. The PVGIS uses these factors as follows:

$$P = G'_i \times A \times \eta_{nom} \times \eta_{rel}(G'_i, T'_m) \quad (\text{B.3})$$

where A is the surface area of the PV modules and η_{nom} is the nominal conversion efficiency of the PV modules. The normalized global in-plane irradiance (G'_i) is given by the following equation:

$$G'_i = \frac{G_i}{G_{i,STC}} \quad (\text{B.4})$$

where $G_{i,STC}$ is equal to 1000 W/m^2 at standard test conditions. The relative conversion efficiency of the PV modules (η_{rel}) is given by the following equation:

$$\eta_{rel}(G'_i, T'_m) = 1 + k_1 \ln(G'_i) + k_2 \ln(G'_i)^2 + k_3 T'_m + k_4 T'_m \ln(G'_i) + k_5 T'_m \ln(G'_i)^2 + k_6 T'^2_m \quad (\text{B.5})$$

where the coefficients k_1 to k_6 for the c-Si PV modules have been estimated by the European Solar Test Installation lab (ESTI) and are given in the following table:

Coefficient	Value for c-Si modules
k_1	-0.017237
k_2	-0.040465
k_3	-0.004702
k_4	0.000149
k_5	0.000170
k_6	0.000005

The normalized module temperature (T_m') is given by the following equation:

$$T_m' = T_m - T_{m,STC} \quad (B.6)$$

where T_m is the module temperature and $T_{m,STC}$ is the module temperature at standard test conditions (25°C).

- (d) *System losses* such as losses in cables, power inverters, dirt on the PV modules etc. are taken into account by PVGIS for estimating the delivered PV power. It is recommended by PVGIS that the system losses are equal to 14%. But, in our case the system losses were equal to 0% (see section 3.5).

C

MATLAB SCRIPT

Contents

- [Download hourly radiation data](#)
- [DC-DC Converter](#)
- [CO2 Electrolyzer](#)
- [H2O Electrolyzer](#)
- [Compression](#)
- [Cooling Units](#)
- [Methanol Converter](#)
- [Estimation of average efficiencies of the CO2 and H2O electrolyzers,](#)

```
clear all
clc
format compact
```

Download hourly radiation data

```
% Import hourly radiation data

Data_Radiation_v1 = ...
    readtable(...
        'Timeseries_38.109_23.526_SA_18000kWp_crystSi_0_32deg_-2deg'...
        '2016_2016.csv','Range', 'A11:I8795');
Data_Radiation_v2 = table2array(Data_Radiation_v1(:,[2:9]));
Data_Radiation_v11 = ...
    readtable('Timeseries_38.109_23.526_SA_18000kWp_crystSi_0_32deg'...
        '-2deg_2016_2016_NO_RADIATION_COMPONENTS.csv','Range', 'A11:C8795');
Data_Radiation_v21 = table2array(Data_Radiation_v11(:,3));
Data_Radiation_v3 = zeros(8784,10);
for i =1:8784
    Data_Radiation_v3(i,1)=i; % Hours in a year [h]
end
Data_Radiation_v3(:,[2:8])= Data_Radiation_v2(:,[1:7]);
Data_Radiation_v3(:,9)= Data_Radiation_v21(:,1);
% Column 1: Hours in a year [h]
% Column 2: PV power output [W]
% Column 3: Gb(i) - Direct in-plane irradiance [W/m^2]
% Column 4: Gd(i) - Diffuse in-plane irradiance [W/m^2]
% Column 5: Gr(i) - Reflected in-plane irradiance [W/m^2]
% Column 6: H_sun - Sun height [°]
% Column 7: T2m - Air temperature [°C]
% Column 8: WS10m - Wind speed at 10m [m/s]
% Column 9: G(i) - Global in-plane irradiance [W/m2]
% Column 10: PV current [A]

P_PV_out = Data_Radiation_v3(:,[1:2]); % PV power output [W]
P_PV_out_MAX = max(Data_Radiation_v3(:,2)); % MAX PV power output [W]
P_PV_peak = ceil((P_PV_out_MAX/(10^6))); % ROUNDEDN UP PV power output [MW]
```

DC-DC Converter

```
Data_DC_DC_Eff = table2array(readtable...
    ('Efficiency_curve_of_DC_DC_converter.csv'));
```

CO2 Electrolyzer

```
A_CO2_cell = 1000;      % Cell area [cm^2]
n_CO2_cells = 199;     % number of cells per stack [pieces]
n_CO2_stacks = 40;     % number of stacks [pieces]
n_CO2_stacks_MAX = 40; % maximum number of stacks [pieces]
A_CO2_stack = A_CO2_cell * n_CO2_cells; % Stack area [cm^2]
%for at least energy efficiency of 45%
    P_density_CO2_MAX = 578.84; % Power density MAX [mW/cm^2]
    P_density_CO2_MIN = 27.25; % Power density MIN [mW/cm^2]

Data_CO2_COFE = table2array(readtable (...
    'CO2_electrolyzer_Voltage_COFE.csv'));
Data_CO2_H2FE = table2array(readtable (...
    'CO2_electrolyzer_Voltage_H2FE.csv'));
Data_CO2_JV = table2array(readtable ('CO2_electrolyzer_I_V_curve.csv'));
Data_CO2_EE = table2array(readtable ('CO2_electrolyzer_Voltage_EE.csv'));
```

H2O Electrolyzer

```
A_H2O_cell = 1000;      % Cell area [cm^2]
n_H2O_cells = 199;     % number of cells per stack [pieces]
n_H2O_stacks = 1;      % number of stacks [pieces]
n_H2O_stacks_MAX = 100; % maximum number of stacks [pieces]
A_H2O_stack = A_H2O_cell * n_H2O_cells; % Stack area [cm^2]
%for energy efficiency around 81%
    P_density_H2O_MAX=681; % Power density MAX [mW/cm^2]
    P_density_H2O_MIN=30; % Power density MIN [mW/cm^2]

Data_H2O_IV = table2array(readtable ('H2O_electrolyzer_I_V_curve.csv'));
Data_H2O_JV(:,1) = (Data_H2O_IV(:,1)/300)*1000; % Current density [mA/cm^2]
Data_H2O_JV(:,2) = Data_H2O_IV(:,2)/22; % Cell voltage [V]
Data_H2O_JV(:,3) = Data_H2O_IV(:,1).*...
    Data_H2O_IV(:,2); % Power density [mW/cm^2]
Data_H2O_EE = table2array(readtable (...
    'H2O_electrolyzer_Current_EE_curve.csv'));
Data_H2O_EE(:,1) = (Data_H2O_EE(:,1)/300)*1000; % Current density [mA/cm^2]
```

Compression

```
eff_a_comp = 0.8; % Adiabatic (isentropic) efficiency of the compressor
eff_mech_comp = 0.98; % Mechanical efficiency of the compressor
R = 8.3145; % Universal gas constant [J/K*mol]

% CO

T1_CO = 333.15; % Inlet temperature of CO,
% based on operating temperature of CO2 electrolyzer [K]
Z_CO = 0.99964; % Compressibility factor of CO at 25 Celcius
k_CO = 1.4013; % Specific heat ratio (or adiabatic coefficient) of CO
P1_CO = 10; % Inlet pressure of CO,
% based on operating pressure of CO2 electrolyzer [bar]
P2_CO = 69.7; % Outlet pressure of CO,
% based on feed pressure of Lurgi reactor [bar]
E_comp_CO = ((R*T1_CO*k_CO*Z_CO)/...
    ((k_CO-1)*eff_a_comp*eff_mech_comp))*...
    (((P2_CO/P1_CO)^(k_CO-1)/k_CO)-1); % Specific energy
% for compression of CO [J/mol]
```

```

% H2

T1_H2_1= 333.15; % Inlet temperature of H2,
                % based on operating temperature of CO2 electrolyzer [K]
Z_H2 = 1.0006; % Compressibility factor of H2 at 25 Celcius
k_H2 = 1.4054; % Specific heat ratio (or adiabatic coefficient) of H2
P1_H2 = 10; % Inlet pressure of H2,
            % based on operating pressure of CO2 and
            % H2O electrolyzers [bar]
P2_H2 = 69.7; % Outlet pressure of H2,
              % based on feed pressure of Lurgi reactor [bar]

E_comp_H2_1 = ((R*T1_H2_1*k_H2*Z_H2)/...
              ((k_H2-1)*eff_a_comp*eff_mech_comp))*...
              (((P2_H2/P1_H2)^(k_H2-1)/k_H2))-1); % Specific energy for
                                                    % compression of H2 from CO2
                                                    % electrolyzer [J/mol]

T1_H2_2= 338.15; % Inlet temperature of H2,
                 % based on operating temperature of H2O electrolyzer [K]
E_comp_H2_2 = ((R*T1_H2_2*k_H2*Z_H2)/...
              ((k_H2-1)*eff_a_comp*eff_mech_comp))*...
              (((P2_H2/P1_H2)^(k_H2-1)/k_H2))-1); % Specific energy for compression
                                                    % of H2 from H2O
                                                    % electrolyzer [J/mol]

```

Cooling Units

```

Cp_CO = 30.47; % Molar heat capacity of CO at 600 K, [J/mol*K]

Cp_H2 = 29.32; % Molar heat capacity of H2 at 600 K, [J/mol*K]

EER = 3; % Energy efficiency ratio of Air-Cooled chiller from Carrier, [-]

```

Methanol Converter

```

T3 = 498.15; % Inlet temperature of syngas,
             % based on methanol converter specs [K]
P3 = 69.7; % Inlet pressure of syngas,
           % based on methanol converter specs [bar]

```

Estimation of average efficiencies of the CO2 and H2O electrolyzers,

based on simulation results

```

% CO2 electrolyzers

% Faradaic efficiency for CO

Sim_Data_CO2_COFE_v1=out.Sim_CO2_COFE.Data;
j=1;
for i=1:8784
    if Sim_Data_CO2_COFE_v1(i,1)>0
        Sim_Data_CO2_COFE_v2(j,1)=Sim_Data_CO2_COFE_v1(i,1);
        j=j+1;
    end
end

% Energy efficiency of the CO2 electrolyzer

```

```

Sim_Data_CO2_EE_v1=out.Sim_CO2_EE.Data;
j=1;
for i=1:8784
    if Sim_Data_CO2_EE_v1(i,1)>0
        Sim_Data_CO2_EE_v2(j,1)=Sim_Data_CO2_EE_v1(i,1);
        j=j+1;
    end
end

% Energy efficiency of the cell reaction (CO2 = CO + 0.5O2)

Sim_Data_CO2_EE_cell_v1=out.Sim_CO2_EE_cell.Data;
j=1;
for i=1:8784
    if Sim_Data_CO2_EE_cell_v1(i,1)>0
        Sim_Data_CO2_EE_cell_v2(j,1)=Sim_Data_CO2_EE_cell_v1(i,1);
        j=j+1;
    end
end

% H2O electrolyzers
% Faradaic efficiency

Sim_Data_H2O_FE_v1=out.Sim_H2O_FE.Data;
j=1;
for i=1:8784
    if Sim_Data_H2O_FE_v1(i,1)>0
        Sim_Data_H2O_FE_v2(j,1)=Sim_Data_H2O_FE_v1(i,1);
        j=j+1;
    end
end

% Energy efficiency of the H2O electrolyzer

Sim_Data_H2O_EE_v1=out.Sim_H2O_EE.Data;
j=1;
for i=1:8784
    if Sim_Data_H2O_EE_v1(i,1)>0
        Sim_Data_H2O_EE_v2(j,1)=Sim_Data_H2O_EE_v1(i,1);
        j=j+1;
    end
end

% Energy efficiency of the cell reaction (H2O = H2 + 0.5O2)

Sim_Data_H2O_EE_cell_v1=out.Sim_H2O_EE_cell.Data;
j=1;
for i=1:8784
    if Sim_Data_H2O_EE_cell_v1(i,1)>0
        Sim_Data_H2O_EE_cell_v2(j,1)=Sim_Data_H2O_EE_cell_v1(i,1);
        j=j+1;
    end
end

```


D

SIMULINK MODELS

D

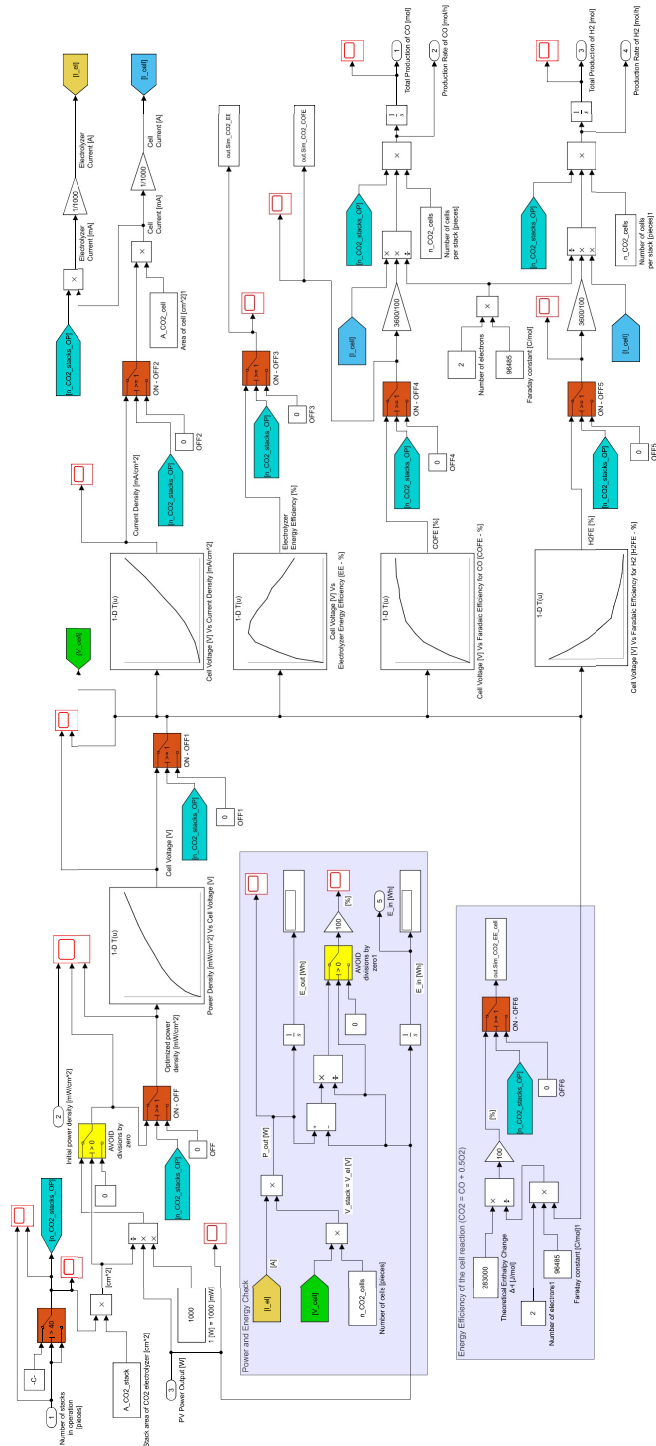
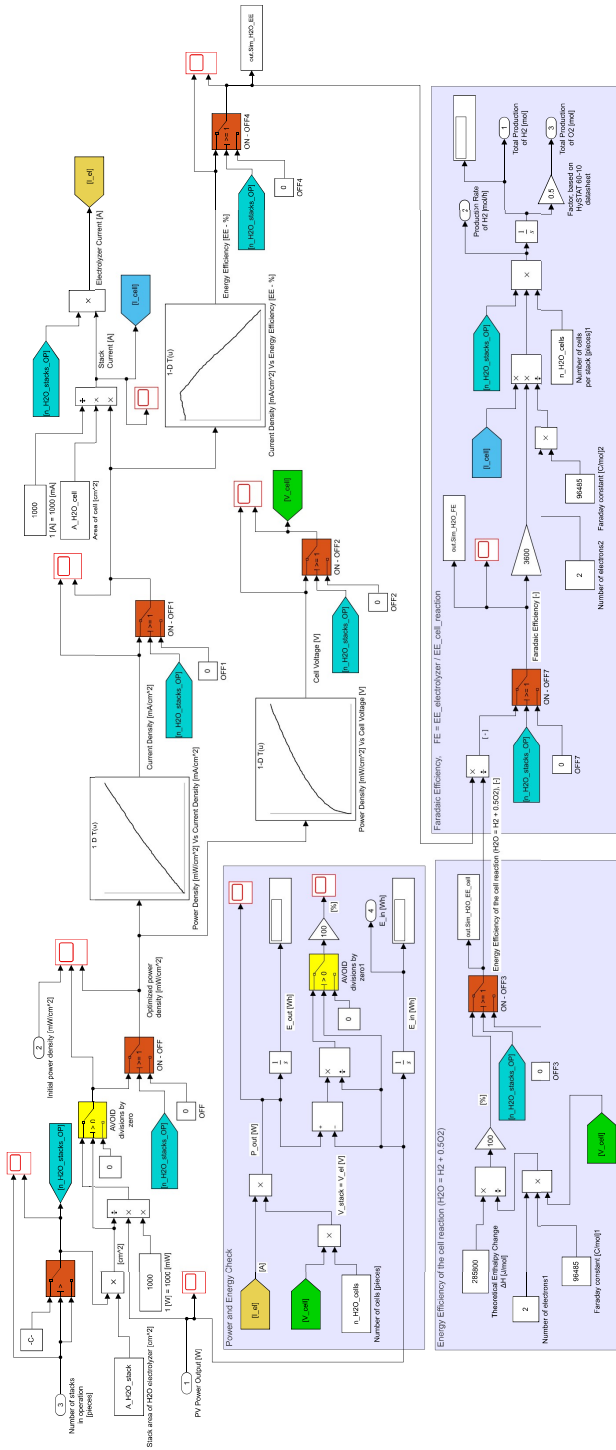


Figure D.1: Model of APE CO₂ electrolyzer in Simulink



D

Figure D.2: Model of AEL H₂O electrolyzer in Simulink

D

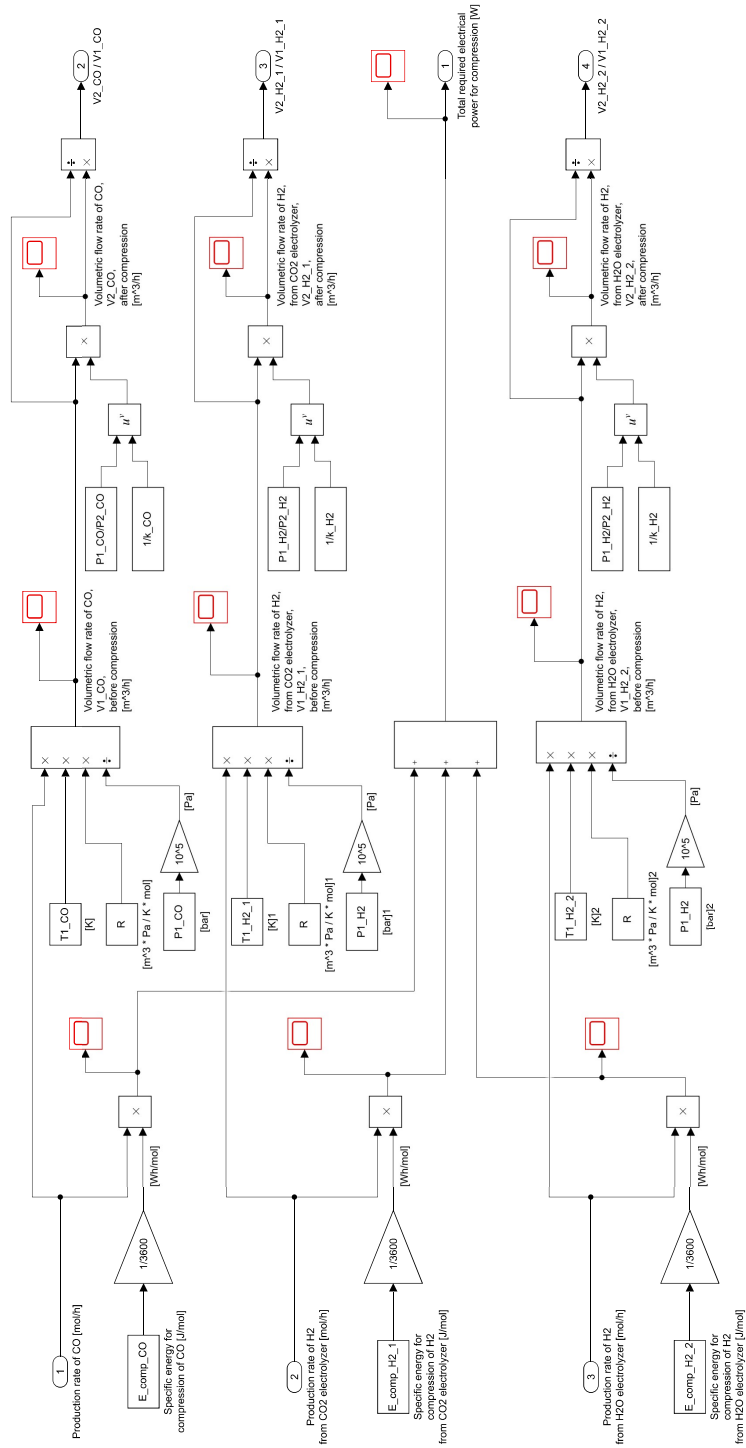


Figure D.3: Model of Compressor in Simulink

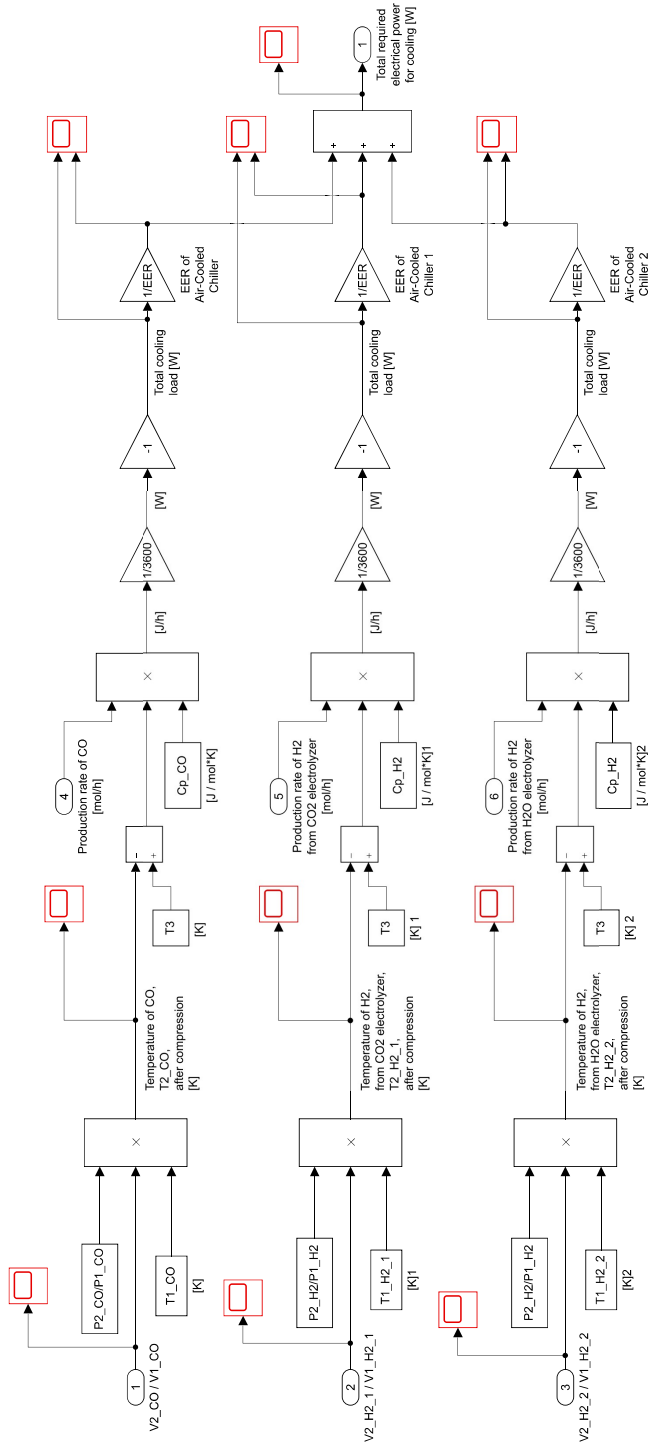


Figure D.4: Model of Cooling Units in Simulink

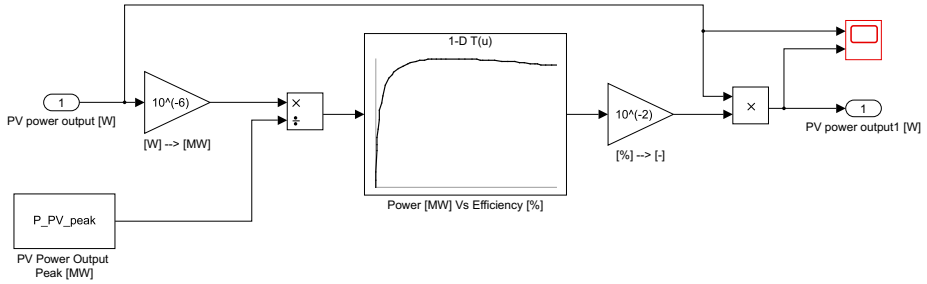


Figure D.5: Model of DC-DC Converter in Simulink

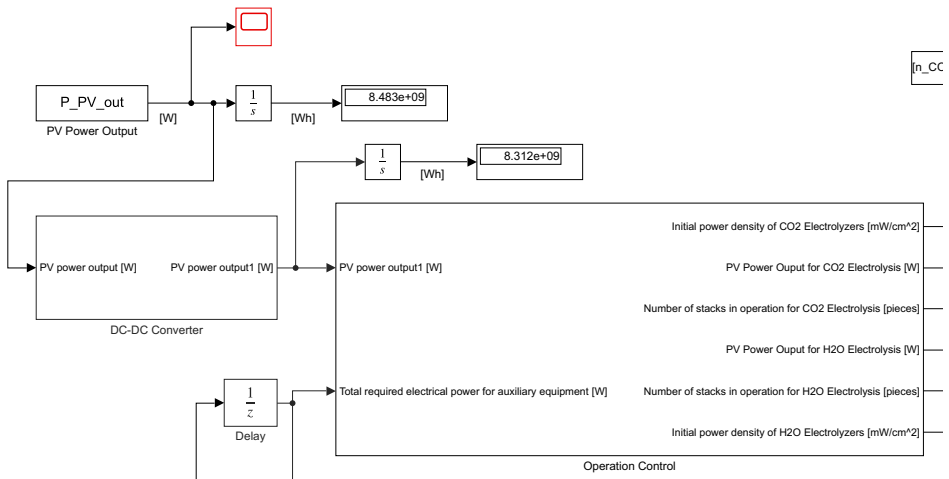


Figure D.6: Model of Power Supply to Auxiliary Equipment in Simulink

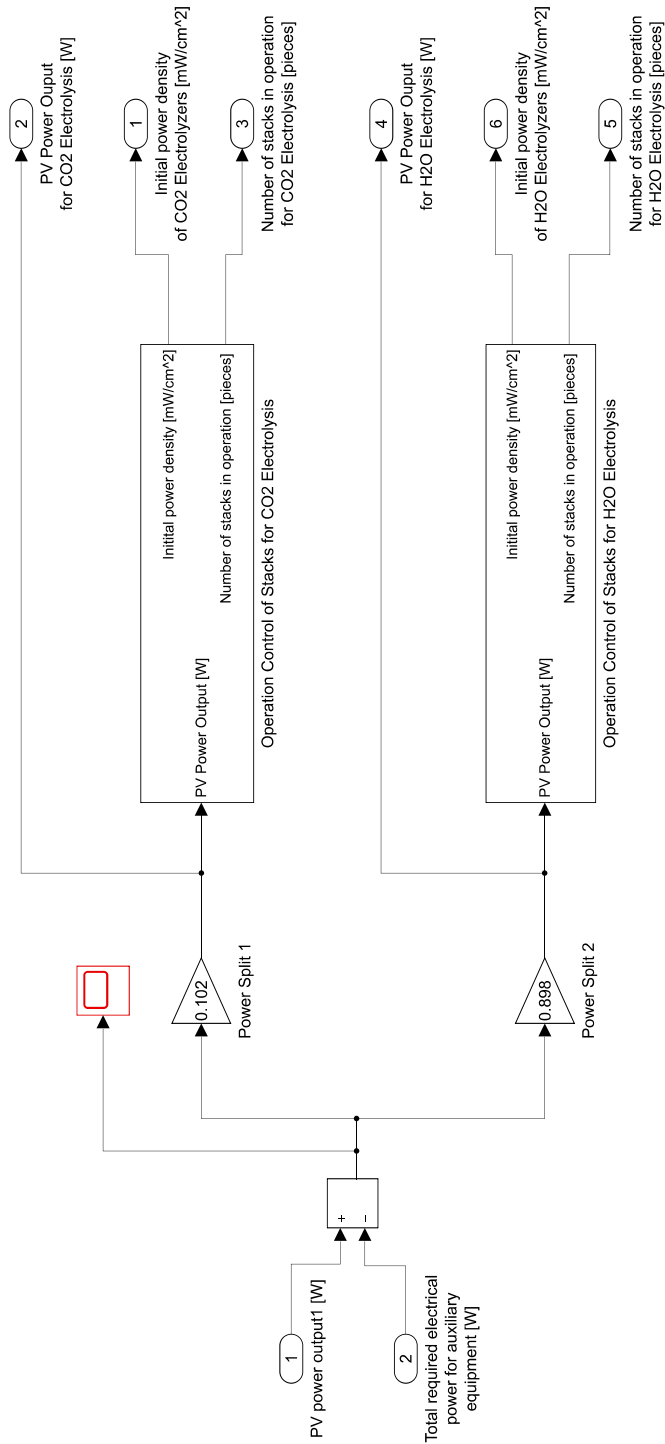
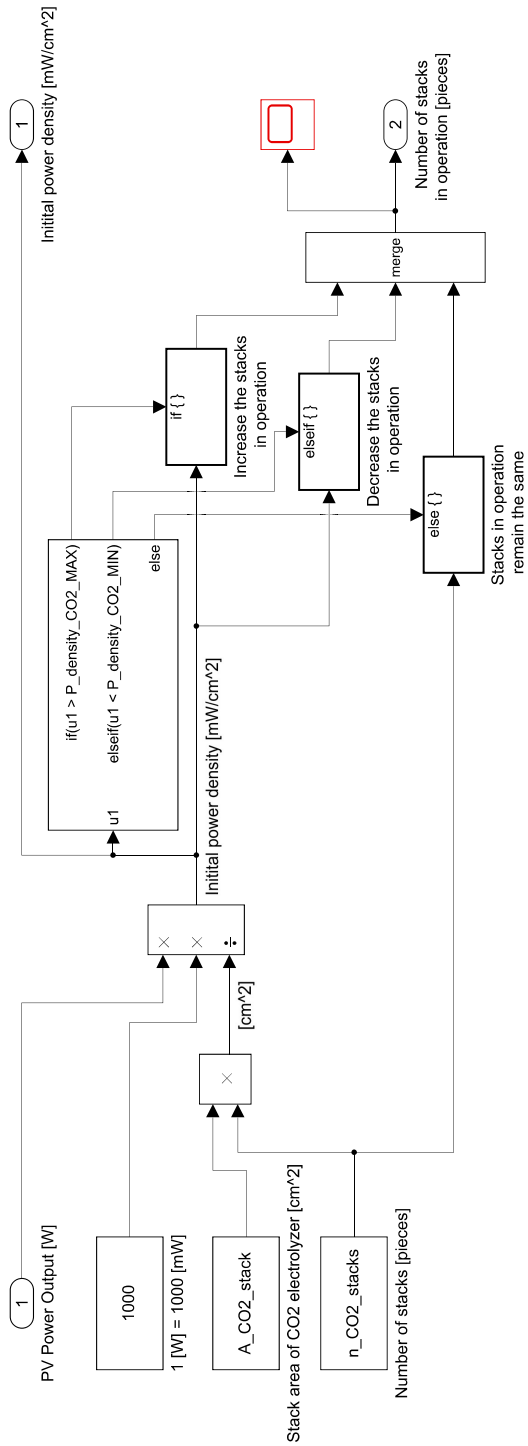
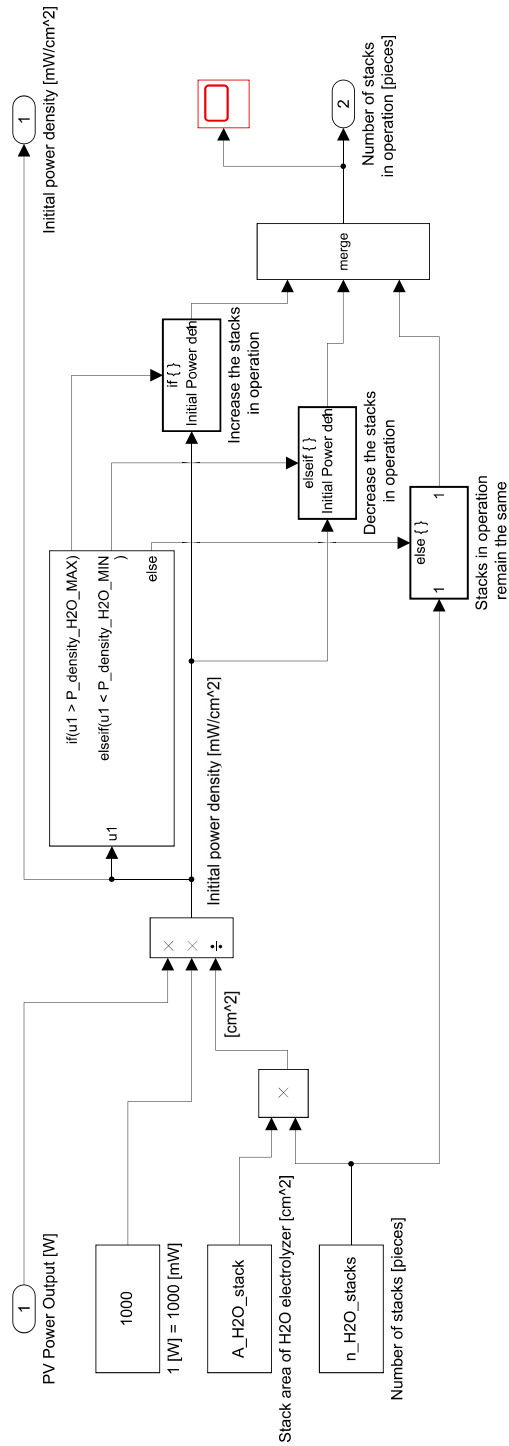


Figure D.7: Model of Control Logic in Simulink

D

Figure D.8: Model of Control Logic for the CO₂ electrolyzer in Simulink

Figure D.9: Model of Control Logic for the H₂O electrolyzer in Simulink

E

REACTION KINETICS OF THE LURGI QUASI-ISOTHERMAL METHANOL REACTOR

The simulation study of Chen et al. [123] is based on the steady-state kinetic model of Bussche and Froment [122]. The reaction kinetics that take place in the reactor simulation of Chen et al. [123] are presented below.

The rates of reactions 2.4 (i.e. CO₂ hydrogenation) and 2.5 (i.e WGS reaction) are presented by the following equations [123]:

$$r_{2.4} = \frac{k_1 P_{\text{CO}_2} P_{\text{H}_2} \left(1 - \frac{1}{K_{e,1}} \frac{P_{\text{H}_2\text{O}} P_{\text{CH}_3\text{OH}}}{P_{\text{H}_2}^3 P_{\text{CO}_2}} \right)}{\left(1 + K_1 P_{\text{H}_2}^{0.5} + K_2 P_{\text{H}_2\text{O}} + K_3 \frac{P_{\text{H}_2\text{O}}}{P_{\text{H}_2}} \right)^3} \left(\frac{\text{mol}}{\text{skg}_{\text{cat}}} \right) \quad (\text{E.1})$$

$$r_{2.5} = \frac{k_2 P_{\text{CO}_2} \left(1 - \frac{1}{K_{e,2}} \frac{P_{\text{H}_2\text{O}} P_{\text{CO}}}{P_{\text{H}_2} P_{\text{CO}_2}} \right)}{\left(1 + K_1 P_{\text{H}_2}^{0.5} + K_2 P_{\text{H}_2\text{O}} + K_3 \frac{P_{\text{H}_2\text{O}}}{P_{\text{H}_2}} \right)} \left(\frac{\text{mol}}{\text{skg}_{\text{cat}}} \right) \quad (\text{E.2})$$

In Table E.1, the parameters values and descriptions of the equations E.1 and E.2 are presented.

In this synthesis process, there are some impurities that are also generated as side products, based on the reactions E.3, E.4 and E.5, i.e. ethanol (CH₂CH₃OH), propanol (C₃H₇OH) and methyl formate (HCOOCH₃) [123]. Based on the same simulation study, it is assumed that these reactions are second order and independent of temperature [123]. Their reaction constants are as follows: $r_{E.3} = 9.88 \times 10^{-10}$, $r_{E.4} = 1.2 \times 10^{-9}$ and $r_{E.5} = 5.714 \times 10^{-12}$ [123].

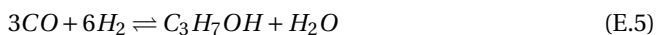
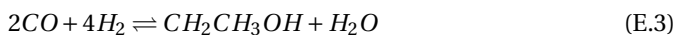


Table E.1: Parameters values and descriptions for equations E.1 and E.2 (obtained from [123])

Parameter	Value
Reaction rate constants, k_i	$k_1 = 1.07 \times \exp\left(\frac{36696 \text{ kJ kmol}^{-1}}{KT}\right)$ $k_2 = 1.22 \times \exp\left(\frac{-94765 \text{ k/kmol}^{-1}}{hT}\right)$
Equilibrium constants, $K_{e,i}$	$\log_{10}(K_{e,1}) = \frac{3066}{T} - 10.592$ $\log_{10}(K_{e,2}) = \frac{-2073}{T} + 2.029$
Adsorption constants, K_i	$K_2 = 6.62 \times 10^{-11} \exp\left(\frac{124119 \text{ kJ kmol}^{-1}}{RT}\right)$ $K_3 = 3453.8$
Partial pressures, P_i	$P_{H_2O} = -bar$ $P_{H_2} = -bar$ $P_{CO_2} = -bar$ $P_{CO} = -bar$ $P_{CH_3OH} = -bar$

F

ECONOMIC ANALYSIS

Table F1: MACRS depreciation scheme over 10 years [143]

Year	Percentage
1	10.00%
2	18.00%
3	14.40%
4	11.52%
5	9.22%
6	7.37%
7	6.55%
8	6.55%
9	6.56%
10	6.55%
11	3.28%

Table F.2: Cash Flow Analysis

Year	Fixed Capital Investment (FCI)	Working Capital (WC)	Depreciation	Gross Revenues (GR)	Gross Earnings (GE)	Earnings Before Tax (EBT)	Net Earnings (Net Income)	Undiscounted Cash Flow, R_t	Cash (Present Value)	Flow	Cumulative Present Value
0	-166,333,745 €	-29,372,427 €	0 €	0 €	0 €	0 €	0 €	-195,706,172 €	-195,706,172 €		-195,706,172 €
1			-16,633,375 €	2,905,705 €	855,535 €	-15,777,839 €	-15,777,839 €	855,535 €	777,759 €		-194,928,413 €
2			-29,940,074 €	2,905,705 €	855,535 €	-29,084,539 €	-29,084,539 €	855,535 €	707,054 €		-194,221,359 €
3			-23,952,059 €	2,905,705 €	855,535 €	-23,096,524 €	-23,096,524 €	855,535 €	642,776 €		-193,578,583 €
4			-19,161,647 €	2,905,705 €	855,535 €	-18,306,112 €	-18,306,112 €	855,535 €	584,342 €		-192,994,241 €
5			-15,335,971 €	2,905,705 €	855,535 €	-14,480,436 €	-14,480,436 €	855,535 €	531,220 €		-192,463,021 €
6			-12,258,797 €	2,905,705 €	855,535 €	-11,403,262 €	-11,403,262 €	855,535 €	482,927 €		-191,980,093 €
7			-10,894,860 €	2,905,705 €	855,535 €	-10,039,325 €	-10,039,325 €	855,535 €	439,025 €		-191,541,068 €
8			-10,894,860 €	2,905,705 €	855,535 €	-10,039,325 €	-10,039,325 €	855,535 €	399,113 €		-191,141,955 €
9			-10,911,494 €	2,905,705 €	855,535 €	-10,055,958 €	-10,055,958 €	855,535 €	362,830 €		-190,779,124 €
10			-10,894,860 €	2,905,705 €	855,535 €	-10,039,325 €	-10,039,325 €	855,535 €	329,846 €		-190,449,279 €
11			-5,455,747 €	2,905,705 €	855,535 €	-4,600,212 €	-4,600,212 €	855,535 €	299,860 €		-190,149,419 €
12			0 €	2,905,705 €	855,535 €	855,535 €	667,317 €	667,317 €	212,628 €		-189,936,791 €
13			0 €	2,905,705 €	855,535 €	855,535 €	667,317 €	667,317 €	193,298 €		-189,743,493 €
14			0 €	2,905,705 €	855,535 €	855,535 €	667,317 €	667,317 €	175,726 €		-189,567,767 €
15			0 €	2,905,705 €	855,535 €	855,535 €	667,317 €	667,317 €	159,750 €		-189,408,017 €
16			0 €	2,905,705 €	855,535 €	855,535 €	667,317 €	667,317 €	145,228 €		-189,262,789 €
17			0 €	2,905,705 €	855,535 €	855,535 €	667,317 €	667,317 €	132,025 €		-189,130,764 €
18			0 €	2,905,705 €	855,535 €	855,535 €	667,317 €	667,317 €	120,023 €		-189,010,741 €
19			0 €	2,905,705 €	855,535 €	855,535 €	667,317 €	667,317 €	109,112 €		-188,901,629 €
20		62,639,176 €	0 €	2,905,705 €	855,535 €	855,535 €	667,317 €	63,306,494 €	9,410,107 €		-179,491,522 €